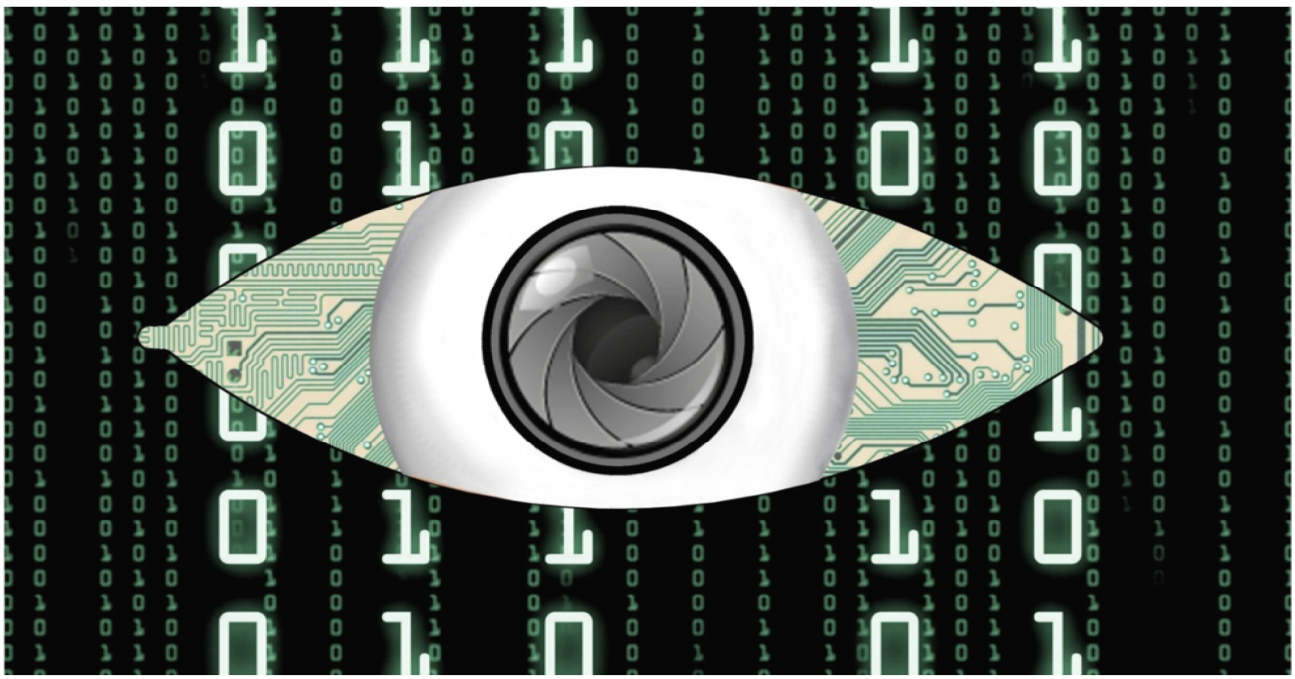

Theory and Model of the Hyperacuity in the Human Eye

upna Universidad Pública de Navarra Nafarroako Unibertsitate Publikoa

Theory and Model of the Hyperacuity in the Human Eye

A thesis by

Oier Dominguez Lopez de Lacalle

Under the supervision of

Dr. Carlos del Río Bocio

Submitted in fulfilment of the requirements for the degree of Doctor of Philosophy

Public University of Navarre

Department of Electrical and Electronic Engineering

Pamplona, 2015

(Page left intentionally blank)

ABSTRACT

The hyperacuity of the human eye may be defined as its known capacity to see small details far away from the limitations set by the number and size of the detectors it has.

Basically, the problem consists in the fact that the image projected on the retina is blurred by the effect of diffraction, but instead of getting an image at poor detail the Human Visual System handles to obtain very fine details. In this sense, we consider the blurring prior to the detection stage a key for the hyperacuity in the human eye.

This way, we could assume some blurring mechanism prior to the signal detection stage, knowing that afterwards, we may be able to restore the information just by reversing the intentionally introduced known blur at the detection process. Under certain conditions this blur may be compensated solving the appropriate inverse problem, and so, a much higher resolution image can be obtained.

In addition to the explanation of the hyperacuity, we propose ideas on how this could leverage diverse applications. As a result of applying this paradigm, the angular resolution can be increased by even a magnitude and therefore enhancing the acuity on applications like imaging devices, radar systems, Terahertz technology…

RESUMEN

La hiperagudeza del ojo humano puede definirse como la capacidad que tiene para poder ver pequeños detalles lejos de las limitaciones impuestas por el número y tamaño de los detectores que posee.

Básicamente, el problema consiste en el hecho de que la imagen proyectada en la retina es borrosa por el efecto de difracción, pero en lugar de obtener una imagen pobre en detalle el sistema visual humano se las arregla para obtener detalles muy finos. En este sentido, consideramos que el emborronado anterior a la etapa de detección es clave para la hiperagudeza en el ojo humano.

De esta manera, podríamos suponer algún mecanismo de emborronado previo a la etapa de detección de la señal, sabiendo que después podremos restaurar la información simplemente invirtiendo dicho emborronado conocido el cual ha sido introducido deliberadamente en el proceso de detección. Bajo ciertas condiciones este emborronado puede ser compensado resolviendo el problema inverso de modo apropiado, y conseguir así una imagen de resolución mucho mayor.

Además de la explicación de la hiperagudeza, proponemos ideas sobre cómo se podrían aprovechar diversas aplicaciones. Como resultado de la aplicación de este paradigma, la resolución angular puede aumentarse incluso en una magnitud y por lo tanto así la mejora de la agudeza en aplicaciones como dispositivos de imágenes, sistemas de radar, tecnología de terahercios...

Table of Contents

Table of figures

Index of tables

Acknowledgments

I would like first to acknowledge all the support from those who have direct and indirectly contributed to this research, including friends and acquaintances.

Due to the multidisciplinary nature of the subject of this dissertation, one of the additional challenges I had to face was to communicate results efficiently so as to understand and be understood by different scientific communities. In this sense, I had valuable help from Susana Martinez Conde and Stephen L. Macnick, whose comments on different aspects I dealt with during my stay at the Barrow Neurobiology Institute at St. Joseph's Hospital in Phoenix (AZ, USA) were very helpful.

My gratitude also, to Zbynek Raida, Petr Kadlec and other colleagues from the VUT for their patience and comments on the work I carried out using different signal processing tools during my stay at the Technical University of Brno (Czech Republic).

Thank you also to my colleague from our university Adur Lagunas Tabar for all his comments and personal efforts for his major contribution to the achievements of this research which would not have been possible without the myriad of different tests on inverse filters, deconvolution techniques he has performed.

I wish to specially thank my mentor Carlos del Rio Bocio who has greatly contributed and strongly supported my work developed at the Public University of Navarre. He has played a decisive role regarding the research strands I had to deal with. Additionally, he has active and uninterruptedly assisted to my research even during his hospitalisation –now fortunately satisfactorily recovered–.

At last but not least, this work goes in memory of my family, including past and future relatives.

Eskerrik asko guztioi.

Oier Dominguez Lopez de Lacalle

Begia noraino, gogoa haraino

[One's mind goes as far as his eyes see. Old Basque proverb]

Prologue

For the last five years I have been involved in this research with great enthusiasm.

This thesis is intended to give an overview to our findings and hypothesis to the questions up to now at some extent unexplained about the resolving capabilities of the human eye.

One of the greatest motivations that encourage me writing this thesis, is the large amount of questions I have often be asked by relatives, friends or acquaintances. Therefore, an important goal of this document is to transmit the results of this work to the non-scientific community, which is why I intersperse scientific data and deep technical details with light, common and simple descriptions.

I wish to apologize if the reader finds any phrase misleading, inexact or incomplete or if I might have left out any detail the reader considers important. Anyway, I have faith that regarding the main aspects intended to be shown about this research few were omitted.

On a personal basis, during this time, I have dealt in all senses with peaks and lobes. Some of them were theoretical, some practical, and some others personal. In this way, I have had a chance to metaphorically climb mountains – hundreds of tests and hours with matlab – as well as physically – a nice one in the South Mountain Park (AZ, USA) –. I have walked through valleys – a good one in Czesky Krumlov (CZ Rep.) – and faced up challenging questions and papers, which led me to meet nice and interesting people and at the same time live emotional hills and canyons. I should confess that this doctoral thesis has provided me skills and a point of view that I did not expect to develop, that is, I am totally sure of not being the same person as I was at the beginning of this long way. In this sense, I feel really grateful for the opportunity I have been granted with this PhD program as it has illustrated me by the people, work, values and a path I did not expect to discover.

In the recent years we have come along with the Terahertz technology in the Antenna Group of the Department of Electrical and Electronics Engineering at the Public University of Navarre. From this, it arises that Terahertz Imaging is a field of rising interest due to the properties of waves interacting materials at these frequencies.

In this regard, there are a variety of community-wide efforts pursuing to overcome the existing challenges with antenna imaging technologies which most important is the actual limit of resolution, related in turn to different bottlenecks: available maximum number, size and density of sensors, lack of efficient electronic sweeping,…

In a more general perspective, one of the most important requirements of all antenna systems is the angular resolution achievable; that is, to distinguish two punctual sources placed quite close to each other in far field. The angular resolution is determined by the possibility of having high-directivity beams quite close, in angle, to each other.

In connection with this, an interesting antenna system can be found in the human eye, which itself conforms an imaging system showing impressive performances. It is capable of focusing near and far objects automatically, it can see under low-light conditions (scotopic vision), it can control the entrance of light to prevent possible saturation of photoreceptors; and finally, the most impressive feature, the really high resolution of the images captured. Some facts in numbers are the resolution and Vernier acuity of about 5 seconds of an arc and/or the equivalent antenna directivity of approximately 100 dB – 550nm wavelength – which correspondent circular waveguide antenna aperture would require an area with a diameter of at least 25.6 mm, definitely much more extensive than the surface of an eye.

So, with this thesis we intend to draw an outline of the eye's working scheme and provide the antenna community a new approach to a possible solution already existing in nature.

Chapter I. The Hyperacuity on the Human Eye

A. Introduction

Natural evolution has provided living creatures advanced sensing mechanisms aiming to seek or be aware. Thereby, the visual system appears as a highly evolved detection system adapted in each species to its particular conditions.

Genetic algorithms have reached particular solutions for living beings' visual system matching the needs of each. Below are shown some, which illustrate the case for different animals, such as amphibians, fish and vertebrates. These all are visual systems in different grades of evolution which can be found in nature.

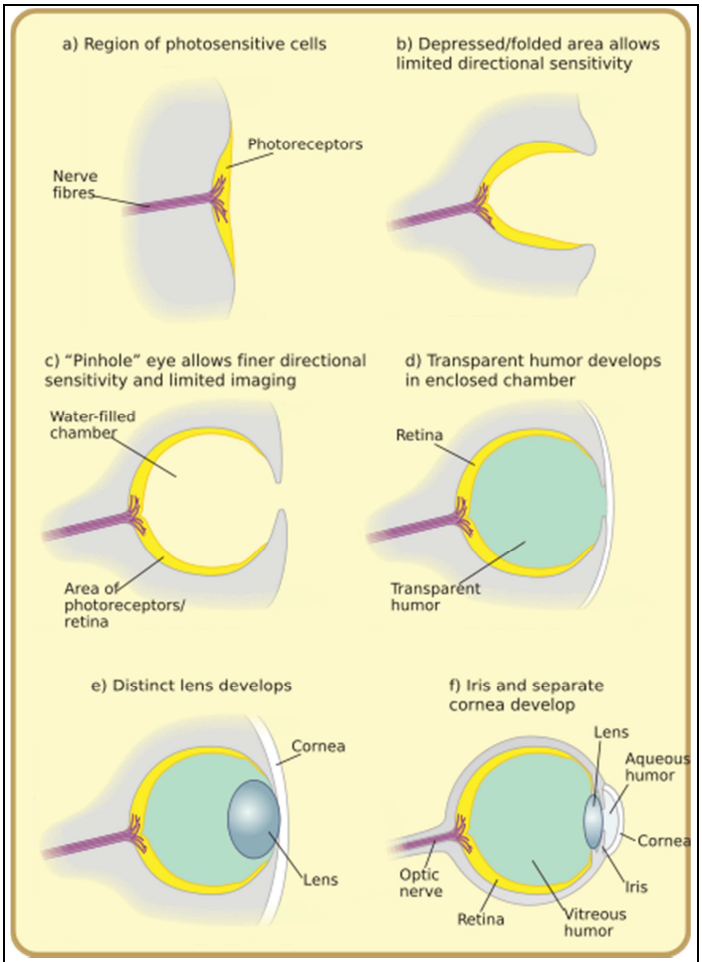

Figure I.1. Evolution of vertebrates' eye.

The illustration from the bottom right of Figure I.1 represents the vertebrates' eye, which has gone through several levels of natural evolution. Thus, at an early stage was extremely basic, and consisted in the simple detection of light. In later stages a cavity or chamber was created which permitted more directivity and continued to improve until today. There, we may witness what we experience with of our eyes, and in a rough view at its configuration, appears to be more complex than some of its homologous shown aside, such as the pinhole eye or open cavities.

In this context, there are many visual systems among wild life species showing interesting or even impressive properties surpassing in some aspects our capacities, such as the so called falcon's eye or night predators' which acuity surpass the humans' – like the nocturnal raptors' or some felids' – which can obtain images at high details even of very poorly illuminated scenes. In a more popular sense, it is said from the biological and optical point of view that the human vision is one of the most complex and sharpest visual system existing in nature.

In this regard, if we somehow compare the human *imaging system* to an artificial imaging device, we may notice that in addition to being outperforming, it is at some extent fail proof. Science fiction films have in some cases emulated robotic eyes (Figure

I.2) where data processing apparently makes it outperforming the humans'. Although the way the image is captured by the eye resembles greatly that of a regular camera, the real fact is that any artificial imaging device is nowadays very far from achieving capabilities that vertebrates' visual system show.

Figure I.2. Human eyes have for long been object of study and fictional recreation.
Credits: Hemdale, Pacific Western

The physiology of the human eye could provide very interesting data when comparing to digital cameras. In these terms, the resolution of the human eye is a parameter difficult to measure, since the sensors are not uniformly distributed over the retina ("a plane or an array of sensors"), but there is a special area called fovea centralis, which is responsible for a vision of such a high resolution – located in the retina, in the bottom of the eye – in the direction spotted by the gaze. The size of this area is approximately 1 mm diameter, which is notably less than the full frame sensor size of a camera, but even smaller than the typical sensor size of compact digital cameras (approx. 5x4mm). This could be understood as the limitation of the human eye to perceive focused only a small angle around the pointing direction, while cameras get the whole image at its maximal resolution in a single shot. Thus, the capability of seeing so well in all directions can be attributed to the brain; on one hand, it is able to move the eye in the desired direction as fast as to perceive a perfectly focused and stabilized image. On the other hand, it is capable to construct a uniform image with a non-uniform sampling in all our visual range, which allows seeing movements or objects in all directions. Maybe natural evolution has provided species with particular visual capabilities adapted to the particular needs of each, but that is another discussion.

The actual fact is that the human eye presents capabilities still unbeaten by any artificial imaging device but before doing any comparison, it might be interesting some breakdown of this human biology, so along the first part of this chapter we deal with some aspects of the biology of the human eye, more specifically on the opto-mechanical layout of the eye, the signal capturing mechanism, and the transmitting mechanism as well. Next, we present the human eye from the point of view of artificial imaging devices, analysing some of its extraordinary capabilities such as the resolution and its resolving capacity, focusing on the hyperacuity at last.

B. An overview of the biology of the human eye

1. Definition and framework

The human eye is the organ that the human body uses to capture images from the environment. It is more or less spherical shaped and connected to the neural and circulatory systems. In addition, the eyes can be moved – gaze – to point in a desired direction, which is controlled by the extraocular muscles.

Regarding the optical process, light enters the human eye through the cornea and the lens (8, 6 and 1 from Figure I.3), which refractive index is changed so that objects at different distances can be projected on the retina (the average value (Kaufman, Alm et al. 2003) for this index is thought to be 62). This refractive index of the lens is modified by the pulling and pushing of the ciliary muscles, and controlled from the brain. In order to adjust the amount of incoming light, the iris is opened or closed by non-reflexive movements, by means of the sphincter and a set of dilator muscles.

Thereby, electromagnetic waves must traverse the rest of the eye globe containing the vitreous humour and optic nerves before they arrive in the retina. Thus, before light arrives in the retina (Figure I.6, Figure I.3–part 19), it encounters obstacles such as optic nerves and vitreous humour which may contribute to getting the right refraction index and focus the image on the retina.

The retina is the layer of tissue of the back side of the eye, considered part of the brain and in charge of light sensing, where the light sensors – photoreceptors – are located. So light is captured by the photoreceptors in the retina, also known in biology as *cones* and *rods*, which are the two general types of sensors.

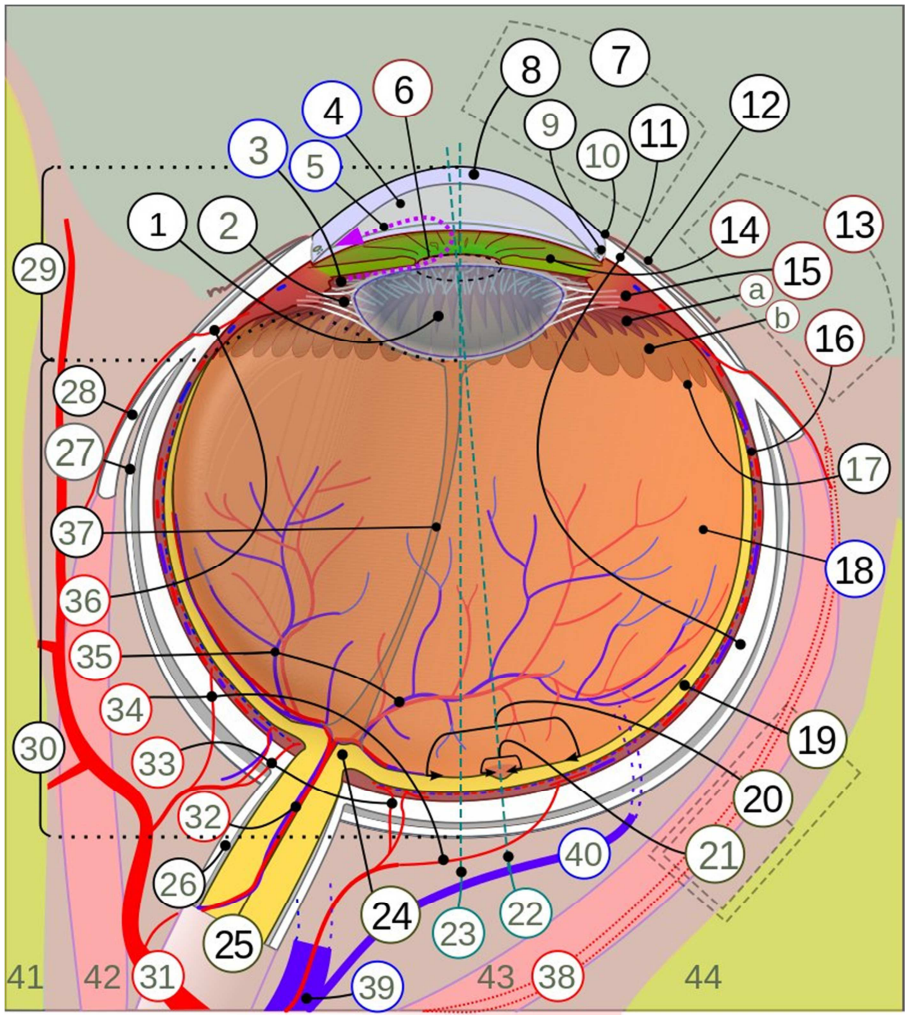

1. Lens
2. Ciliary zonule
3. Posterior chamber
4. Anterior chamber
5. Aqueous humour
6. Pupil
7. Corneosclera
8. Cornea
9. Trabecular meshwork
10. Corneal limbus
11. Sclera
12. Conjunctiva
13. Uvea
14. Iris
15. Ciliary body (with a: pars plicata and b: pars plana)
16. Choroid
17. Ora serrata
18. Vitreous humour
19. Retina
20. Macula
21. Fovea centralis
22. Optical axis
23. Axis of the eye
24. Optic disc,blind spot
25. Optic nerve
26. Dural sheath
27. Bulbar sheath
28. Tendon
29. Anterior segment
30. Posterior segment
31. Ophtalmic artery
32. Artery and central retinal vein
33. Posterior short ciliary arteries
34. Posterior long ciliary arteries
35. Blood vessels of the retina
36. Anterior long ciliary arteries
37. Hyaloid canal
38. Lacrimal artery
39. Ophtalmic vein
40. Vorticose vein
41. Ethmoid bone
42. Medial rectus muscle
43. Lateral rectus muscle
44. Sphenoid bone

Figure I.3. Illustration of the anatomy of the human eye. Source: J. March i Nogué

A curious design fact is the “inverse” layout of the optic nerve in the retina. Some scientists call it the “backwards retina” which relates to how the optic nerves are connected to the photoreceptors in the retina. This is fairly represented by Figure I.4.

There are speculations on this particularity claiming that there wouldn't be any other way of developing such design unless optic nerves weren't connected so, due to lack of space on the rear side of the ocular globe where blood vessels are located and supply the retina. In the contrary, cephalopods' eyes are "designed forwards", which means that the nerve fibres are attached to the retina from the rear side and in consequence, they do not have a blind spot. The explanation for this could be that at an early stage of evolution the visual system in cephalopods developed as an invagination of the head surface whereas in vertebrates went towards an extension of the brain.

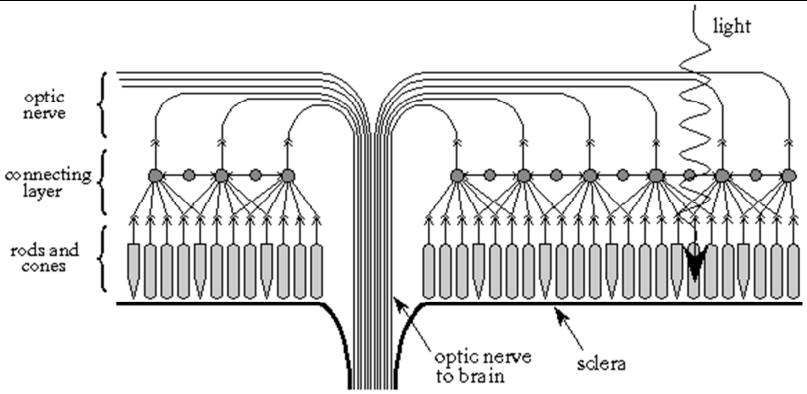

Figure I.4. "Backwards retina". Optic nerve is connected to photoreceptors from the "front" side.

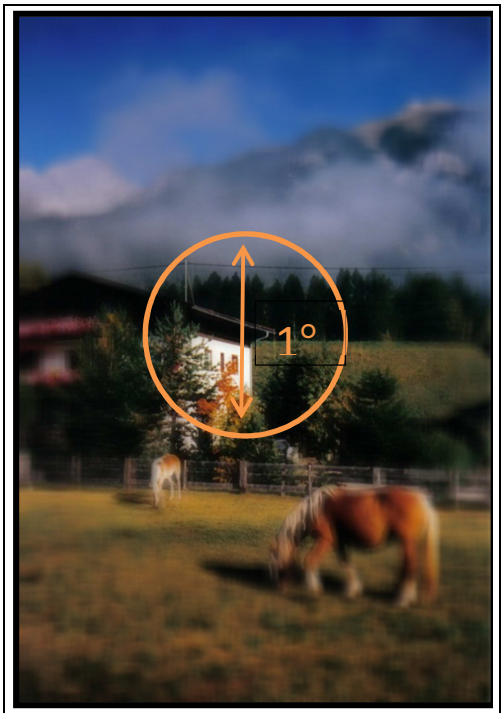

Figure I.5. Image representing a field of view of 1º

Anyway, photoreceptors in vertebrates' eyes are attached and oriented towards the reflective surface of the retina, which makes reception of light rather optimal.

At this point, it can be understood that the way the photoreceptors are connected to the optic nerves require a "passage" through the eye globe, which as depicted earlier, is located in the retina. This area contains no photoreceptors and in consequence there is a blind spot in the field of view, although we are not aware of it because the HVS (Human Visual System) fills that space. Moreover, the field of view of the eye is one degree – where the gaze is fixed – meaning that focused vision is basically reduced to this angle. The corresponding image is captured in an area called fovea, which is the inner depression of the area known as macula (Figure I.6). In this retinal zone nerve fibres are somehow pushed aside so that the maximum amount of light is projected.

Beyond central vision (one degree), away from the optical axis, vision is considered peripheral (Figure I.5), where in contrast to central vision the image perceived is blurry.

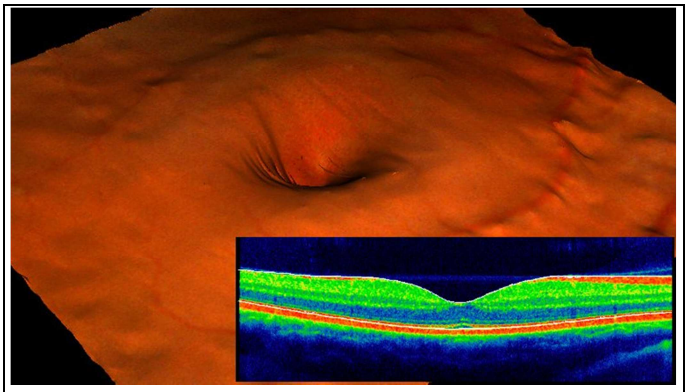

Figure I.6. Extracted tomogram of the Macula in a human retina.

The central part of the picture is projected on the retina, as just commented (which is processed later by brain); more specifically on the *fovea* where this particular bend of the topology of the retina contributes to a natural augmentation of the density of cones per angle of view, thanks to its approximately conical shape. Here, a great concentration of cones of different colours may be found. This high concentration of photon detectors may be just of few hundred thousand of elements, and there's where the controversy of hyperacuity might be found because this low number of elements does not by itself seemingly explain it.

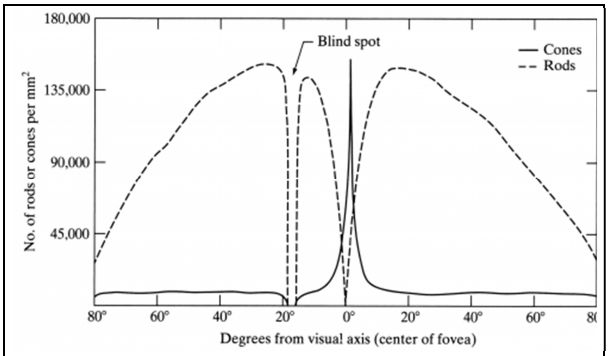

Figure I.7. Distribution of cones and rods on the retina

Unlike in artificial imaging devices, photoreceptors in the human eye are not distributed in a regular or homogeneous manner and as said, the highest density is precisely located in the fovea. This can be observed in Figure I.7. Depending on different reports the concentration of cones varies, but the fact is that the highest acuity is reached where this high concentration of cones is located, in the macular area. Rods though, are widespread all over the retina except in the fovea. Maybe in part due to lack of space, and maybe also because they are not so necessary given that they do not provide any high visual acuity, but they enable scotopic – low light – vision, as in comparison are much more sensitive to light.

As earlier stated, the lens power in the eye is adjusted to project images focused on the retina. This is known as accommodation, and such operation is performed as in a camera's layout, as depicted in Figure I.8. This procedure is carried out mainly by the cornea, which itself has a refractive power of 43 dioptres, but the lens of the relaxed eye provides 19 additional dioptres. In all, the relaxed eye has a total refractive power of 62 dioptres.

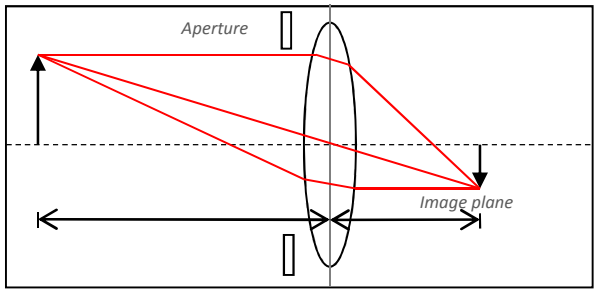

Figure I.8. An optical model of the eye

When accommodation is needed in nearby objects the ciliary muscles exert force and increase the strength of the lens up to 33 dioptres, providing the eye a total strength of 76 dioptres or a focal length of 13 mm.

2. Movements of the eye

With the purpose of better understanding the act of "seeing" in the HVS, the mechanics of the eye are either in a popular or a scientific context ascribed certain importance among the different mechanisms herein involved. In the next lines we try to give an outline of the different movements existing in our visual system.

Scientists today agree on the occurrence of three main types of eye movements during visual fixation in humans: tremor, drifts and microsaccades (Yarbus 1967, Carpenter 1977). Martinez-Conde smartly discusses on her publication about the role of fixational eye movements, purporting that tremor is an aperiodic, wave-like motion of the eyes (Riggs, Ratliff et al. 1953), with a frequency of about 90 Hz (Carpenter 1977). References on this document point them out as the smallest of all eye movements (tremor amplitudes are about the diameter of a cone in the fovea (Yarbus 1967, Carpenter 1977, Ratliff, Riggs 1950)). Actually, visual tremor is difficult to record accurately. Tremor is generally thought to be independent in the two eyes. This imposes a physical limit on the ability of the visual system to match corresponding points in the retinas during stereovision (Spauschus, Marsden et al. 1999, Riggs, Ratliff 1951).

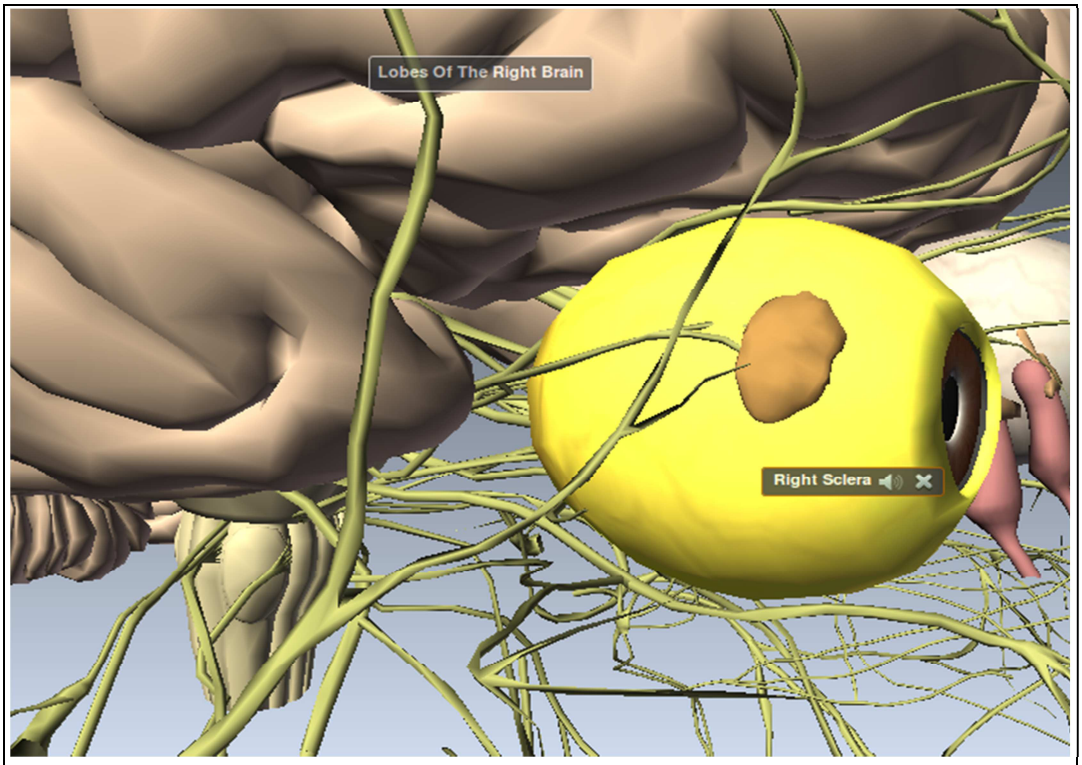

Figure I.9. Screen capture showing the Human Visual System. Credits: Biodigital, Inc

In connection with this, two other kinds of eye movements exist: drifts and microsaccades. Drifts occur simultaneously with tremor and are slow motions of the eye that occur during the epochs between microsaccades. During drifts, the image of the object being fixated can move across a dozen photoreceptors (Ratliff, Riggs 1950). – Fixational – microsaccades are small, fast, jerk-like eye movements that occur during voluntary fixation. They carry the retinal image across a range of several dozen (Ratliff, Riggs 1950) to several hundred (Martinez-Conde, Macknik et al. 2000) photoreceptor widths, and are about 25 ms in duration (Ditchburn 1980).

Type	Amplitude	Frequency	Duration	Max speed	Mean speed	Conjugate	Ref
Tremor	20–40 s	70-90 Hz	-	20 min/s	-	-	(Yarbus 1967)
Drift	-	95–97% fixation time	0.3–0.8 s	30 min/s	6 min/s	No	(Yarbus 1967)

Table I.1. Brief relation of characteristics of tremor and drift

Type	Amplitude	Intersaccadic interval/ microsaccadic frequency	Max speed	Mean speed	Conj.	Ref
Micro-saccades	12.7–65.9 min	0.23–0.93 Hz (mean 0.61 Hz)	28–97 deg/s	16–40 deg/s (mean acc. 2,322–6,44 deg/s)	Yes	(Moller, Laursen et al. 2002)

Table I.2. Brief relation of characteristics of microssacades

3. Photoreceptors: the signal capturing mechanism

a) Numbers and biological composition

The photon capturing specific mechanism is another aspect of special interest to analyse. There are nearly 130 million photoreceptors in the retina (rods and cones) that respond with patterns of luminance. Almost all of the photoreceptors in the fovea are cones which are connected to almost the same amount of fibres in the optic nerve. The 120 million rods and remaining 6 million cones share other fibres.

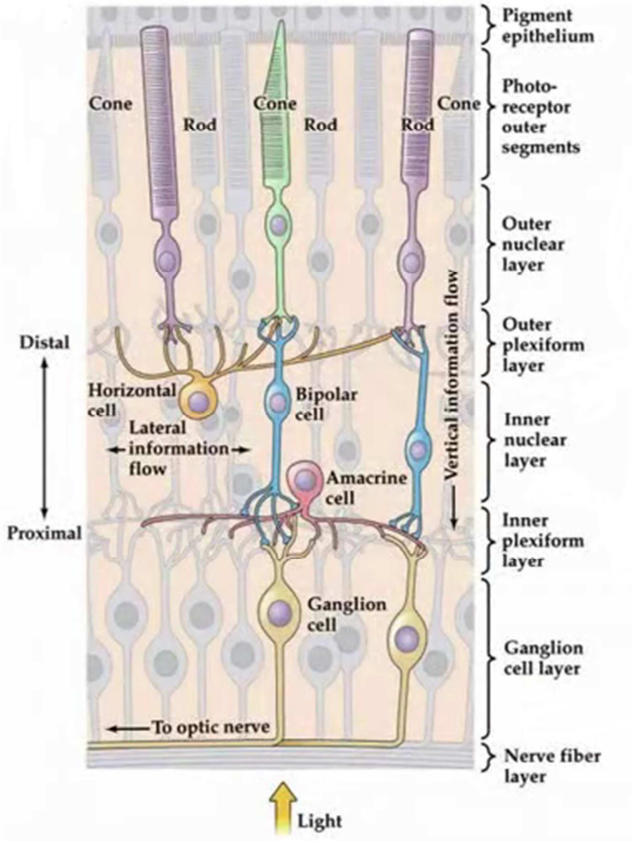

Figure I.10. Layout of the retinal neural system.

Cones are sensitive to colours, actually to 3 different wavelengths, whereas rods respond to the excitation of low levels of light.

Focusing on the signal (image) sensing by the photoreceptors we may find that there are 5 types of cells and 3 layers in the retina. The first of these are the rods and cones submerged in the pigmented retinal epithelium (PRE) which is on the bottom of the retina. Next, bipolar and horizontal cells followed by amacrine cells and finally, we may find ganglion cells.

Cones – and as well rods – are connected to horizontal and bipolar cells. They are called bipolar because at the most distal location they are in contact with the cones, which are

providing the signal input, and in the most proximal area or on the inner plexiform layer may contact retinal ganglion cells on one side and amacrine cells and cones on the other.

In a deeper look at photoreceptors, those close to the sclera contain photopigments that absorb light, creating a series of chemical changes, which ultimately result in transduction of electrical signals that are sent through the optic nerve.

The rods' and cones' photopigment is very similar, consisting of a union of *retinene* at both ends with a protein called *opsin*, which is associated with the membrane. A source of *retinene* is vitamin A, usually found in carrots. At the rods the specific *retinene* is *neoretinene-b* and the protein *scotopsin*. This combination is a molecule called *rhodopsin*, commonly called visual purple.

Apart from the frequency response, cones also have a chemical response reacting to the arrival of photons. Cones have different combinations of the *retinene* protein, called *photopsines*, which can be categorized into three different types of *opsins*. These three pigments absorb different wavelengths; R, G, B, or red, green and yellow, respectively, and therefore have different PSD curves (Power Spectral Density).

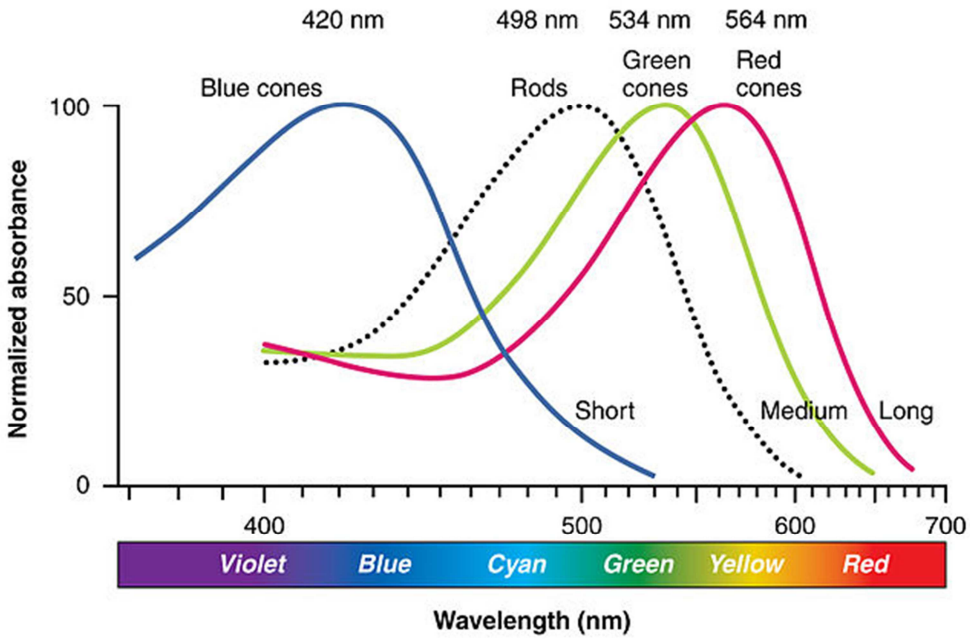

Figure I.11. Absorption spectral curves for each type of photoreceptors. Credits: OpenStax College

We can also say that the maximum absorption of all *opsins* is at 507 nm, which matches just scotopic – half-light – vision and daylight vision. Similarly, we can also say that the sensitivity of the cones is five times less than that of the rods, which is why in low luminance we can hardly see the colour.

b) Wave physics

Generally, antennas are used for transmitting an electrical signal through the space in the form of electromagnetic waves but also for receiving the existing electromagnetic radiation from space and transduce it into an electrical signal. We might notice that

natural evolution has provided species – including the human being – a mechanism to capture these electromagnetic waves, at the wavelengths indicated by Figure I.11. In the case of the human eye, we are referring at cones and rods, which can perfectly be understood as antennas.

From the point of view of antenna theory, cones can be seen as optical waveguides, but an off-the-wall fact is that their size exceeds in several lambdas the frequency is sensing each. To be more specific, for an average 1.5 µm diameter cone (Kolb) tuned at green light (510 nm) we may easily notice this size equals a distance of about three wavelengths (Figure I.12). A major consequence of this natural design is the gain of about 20 dB achieved by the photoreceptors, which involves a beamwidth at the pupil distance of 16 mm, thus covering totally the entrance of light of the human eye.

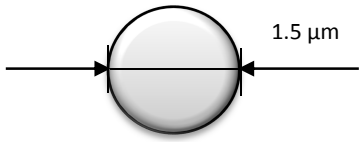

Figure I.12. Illustration of a cone which size equals 3λ

Another aspect of the eye seen from the point of view of antenna imaging systems is that the sensors do not detect the carrier signal, but the modulated.

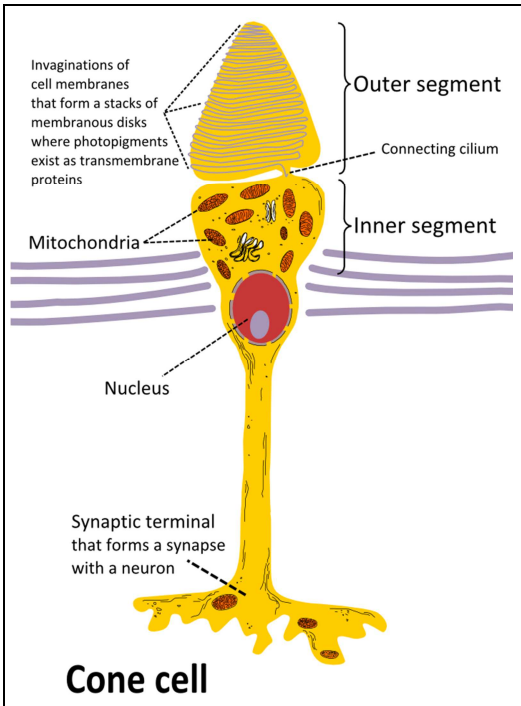

Figure I.13. Illustration of cone cell of the human eye. Credits: I. Kruusamägi – Wikipedia

In the following Figure I.13 a cone cell is depicted, showing its typical parts and composition.

It is to remark the shape of the outer segment which is formed by stacks of membranous disks which is where the name of this cell comes from. Although this illustration shows a nearly perfect cone shape, the top in fact is not tipped and it observes rather a disk shape at its end.

Figure I.14 depicts the simulation of a cone by a regular typical helix antenna where directivity depends on the number of wire turns.

Probably, the antenna paradigm of cones may also be simulated by a circular waveguide type antenna. As they say in their paper (Canbay, Unal 2008) radiant energy can be propagated in human cone outer segments with waveguide modal patterns. One of the questions concerning the antenna paradigm on cones is whether their spectral sensitivity is attributable to only visual pigments, or also to their dimension and geometrical shape. According to the experiment described in that paper they found that the antenna models tested seeking to resemble eye photoreceptor cones had a similar frequency response, confirming the importance of the role played by the geometry and dimensions of the cones, as reported by (Roberts 2006).

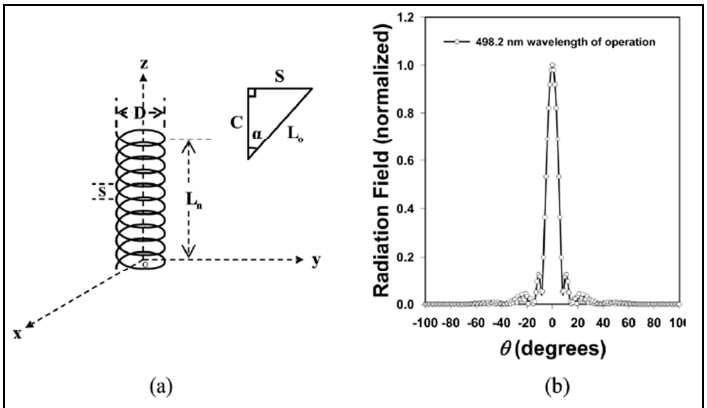

Figure I.14. Modelled helical antenna (a) and corresponding radiation pattern (E-plane). Credits: C. Canbay and İ. Ünal

The conclusion from this section is that cones in the eye seen as antennas do play an essential role in the photo-capturing mechanism, but their antenna design does not explain by itself the level of details the eye is capable to perceive and discern; this is rather an achievement of the hyperacuity model presented in the next chapter.

4. Transmission of signals in the Human Eye

As photoreceptors are excited by incident light, ganglionary cells transmit a signal to the optic nerve. In few words, photoreceptors capture the modulated optical signal of a well-focused (acute or corrected vision) but blurry image and put it in the neural system.

A biological neuron or nerve cell consists of synapses, dendrites, the cell body, and the axon. We may use this paradigm to see photoreceptors as a kind of neurons that have been modified by the natural evolution and as already said, they are connected to and are part of the neural system.

In this regard, synapses are elementary signal processing devices also seen as biochemical devices which convert a pre-synaptic electrical signal into a chemical signal and then back into a post-synaptic electrical signal.

In any case, the information processing occurring through neural pathways is very complex. Without going into very upper levels, photoreceptors are connected to a variety of cells in the retina and its own interface is labyrinthine. So, even today it is not known exactly which processes are going on, although the nature of them is known.

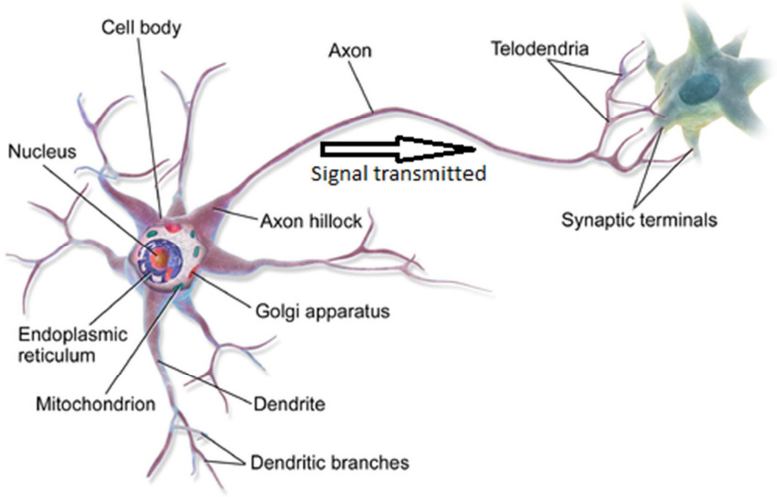

Figure I.15. Transmission of signals in a neuron

Electrical potentials across cell membrane (a layer that separates and protects the interior of the cell from the outside) exhibit spikes called action potentials (Figure I.16). They have a fixed amplitude and time course. Spikes originate in the cell body, travel down the axon of the pre-synaptic neuron, and cause synaptic terminals to release neurotransmitters substances at the synapse, which might or not trigger an action potential at the target neuron(s) – where signals are integrated in time – depending on whether its threshold is exceeded.

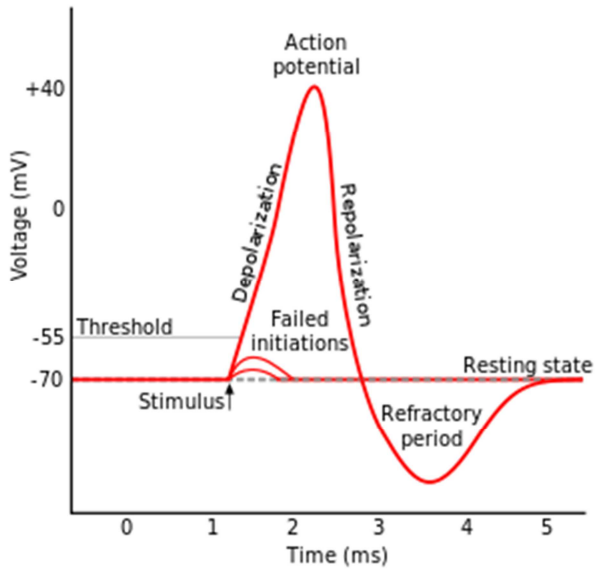

Figure I.16. Transmission of an action potential

Besides, there are other signals such as graded (or gradual) potentials which in contrast to action-potentials, they are not propagated because they are locally transmitted, since they represent changes to the membrane's potential. Graded membrane potentials are particularly important in neurons, where they are produced by synapses.

In the innermost area of the eyeball bipolar cells generate these graded potentials unlike ganglions (Figure I.10), which generate action potentials.

So regarding the transmission of a signal related to the capturing of light, as soon as a photoreceptor is stimulated, it transmits power to nearby bipolar cells and to horizontal cells. The signal passes into the retina until it reaches the ganglion cells. Impulses from

these cells are transmitted to the optic chiasm (part of the brain where the optic nerves partially cross) and travel to the lateral geniculate nucleus (Figure I.18). Then they arrive in the occipital cortex of the brain – notably the cortical layer 4 which is the primary recipient zone of the geniculate input –. This second and third path is much longer than the first path in the retina, so it is transmitted as an electric pulse or action potential of about 0.1 volts amplitude and 0.001 seconds long, until it reaches its target neuron – cells P and K – at the LGN (Lateral Geniculate Nucleus), shown in Figure I.18.

The retina is not greater than 1 mm thick hence the transmission of signals by action potentials is not required. Thus, in the inner and outer layers there will not be any action potential, but graduals. In this sense, ganglions are the only cells performing such conversions, transforming graded potentials in action potentials making it possible to be transmitted to the lateral geniculate nucleus (LGN) i.e. photoreceptors and bipolar cells generate gradual potentials and at short ranges, transmission of action potentials is not necessary.

Two types of ganglion cells exist: on-centre cells and off-centre cells, which might or not be triggered, e.g. depending on whether light is spotted at the centre of our gaze (Figure I.17). The former type is activated with the straight incidence of light but the latter, might be activated through other actions. Therefore receptors are chemically different, allowing us to process the difference of edges in diverse lighting conditions, simply based on the contrast. In this regard, no existing camera can surpass the eye's features. Anyway, it is to be noted that horizontal cells connect several bipolar cells permitting the horizontal flow of the signal. On another level, the known as amacrine cells connect different ganglion cells.

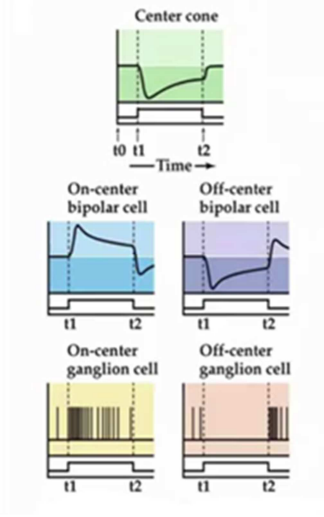

Figure I.17. Off-centre and On-centre ganglion response

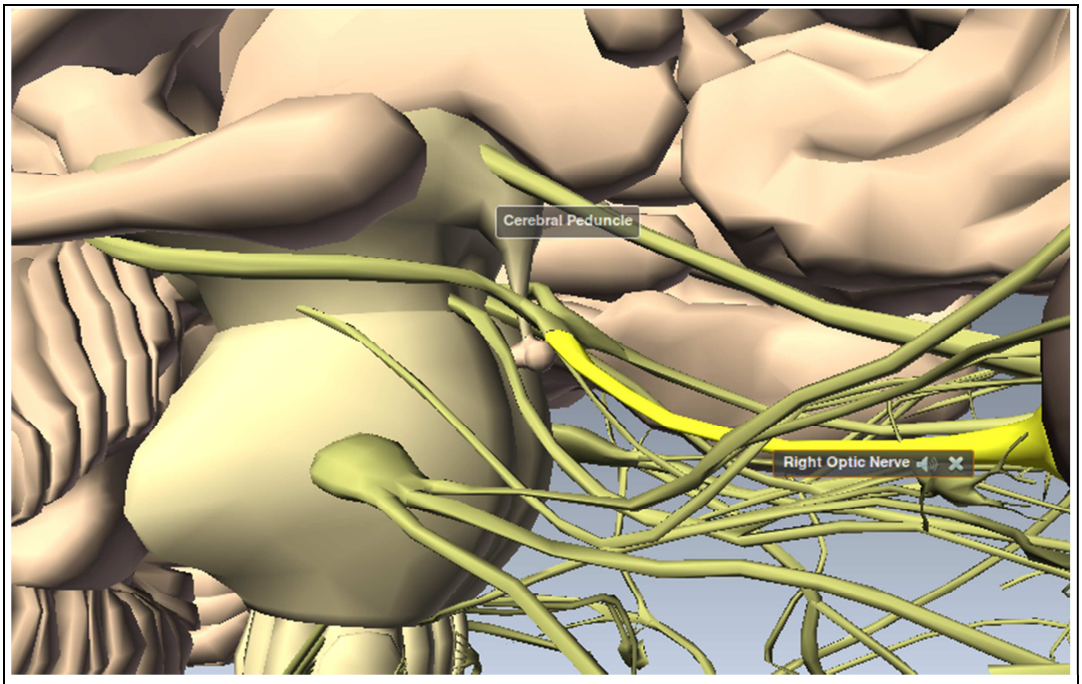

Figure I.18. Screen capture showing the LGN. Credits: Biodigital, Inc.

There is evidence that the rate of electrical pulses in ganglions is increased when the power of stimuli in the retina is increased as well. That is, by logarithmically increasing the luminance in the adjacent photoreceptors. The number of pulses per second is increased by a constant number each time the light is doubled.

The input pulse train has its amplitude modified by parameters stored in the synapse. The nature of this modification depends on the type of the synapse, which can be either inhibitory or excitatory. The postsynaptic signals are aggregated and transferred along the dendrites to the nerve cell body. The cell body generates the output neuronal signal, a spike, which is transferred along the axon to the synaptic terminals of other neurons. The frequency of firing of a neuron is proportional to the total synaptic activities and is controlled by the synaptic parameters (weights).

The pyramidal cell can receive over one hundred synaptic inputs and it can fan-out the output signal to thousands of target cells.

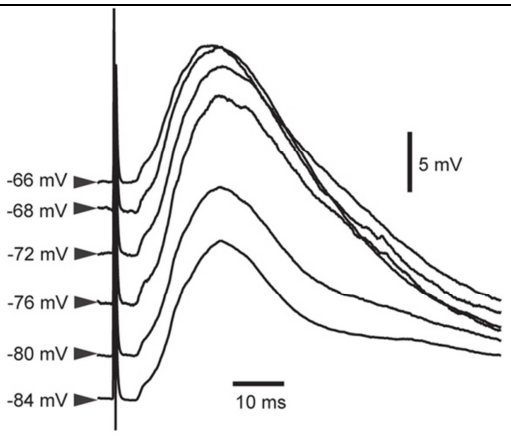

Figure I.19. Properties of Spiny Projection Neurons and cortico-striatal Post-Synaptic Potentials (PSP)[1] (Schulz, Redgrave et al. 2010)**. Dependence of PSP on membrane potential.**

Anyway, the photoreceptors are the very first stage where the electrical/chemical signal is created. These photoreceptors can also be studied as optical waveguides, which confine the light in an efficient manner with the arrival of a stimulus, i.e. light, produces a chemical reaction within the photoreceptor, which causes the emission of sodium at the output of the cell or photoreceptor, therefore hyperpolarising it. The response of a photoreceptor to the arrival of a photon would be not very different from Figure I.19.

It is to be noticed that variability in simultaneously recorded retinal, thalamic, and cortical neurons is shown to be low, as pinpointed by some authors (Kara, Reinagel et al. 2000).

In case of an analogous model for the retinal response, we could understand that neural activity persists for 0.1 seconds when the eye is stimulated with a very short flash light. Therefore if one observes a series of flashes of light shortly spaced in time, the signal can be perceived as a continuous stimulus. The rate at which the trace or flicker trace fades out (called critical fusion frequency) depends on the nature and intensity of the pulse, but it is overall of about 40 flashes per second.

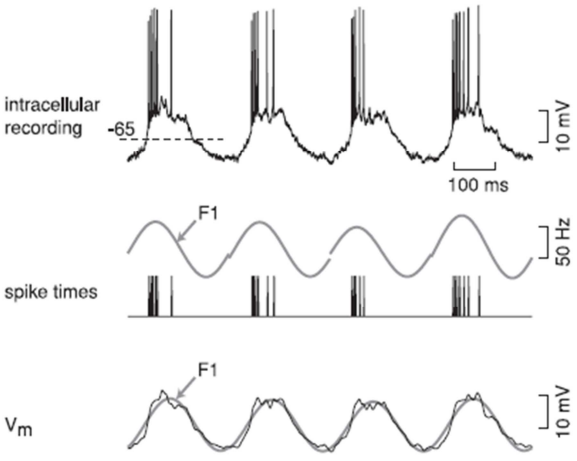

Figure I.20. Intracellular recording from an off brisk-transient (Y) ganglion cell (Demb, Sterling et al. 2004)**.**

It can be seen in Figure I.19 and in Figure I.20 that a flash light generates different responses in the ganglion cells depending on its amplitude, but in terms of the shape of the impulse responses, they resemble in a large degree. Spikes are at a later stage kind of integrated and form more continuous looking signals.

On another hand, the integration behaviour of the HVS does not imply not being able to see in smaller time 'frames' or intervals. It only means that in a continuous process (as it is ongoing in fact) any stimulus has in time the behaviour shown by the graphic itself. The stimulus makes ganglionary cells

[1] A temporary change in membrane potential produced by activation of a synapse by a single graded or action potential is called a postsynaptic potential

form spikes at their output which can be integrated in later stages creating the impression of 'continuous motion'. This can also be understood with the transfer function depicted by Figure I.19.

Retinal ganglion cells respond to the intensity of light (~30 ms) at its frequency band. This means that the cones in the human eye act as integrators, i.e. as photon-counters. Excitation of light is received as a magnitude of power or intensity but not as a function of the phase of the wave front. Thus, the photodetectors measure the amount of captured photons.

Concerning the light adaptation of the eye, the stimulation suffered by photoreceptors causes an inhibitory signal to be created in the horizontally adjacent photoreceptor cells, giving as a result a reduction on the light sensitivity. This process is called lateral inhibition and hence derives the mentioned phenomenon. Equally, *amacrine* cells are rather related to phenomena linked to colour.

Studies in monkeys and cats show that certain cells in the accessible outer layers of the visual cortex receive signals from many optic nerve fibres, and are preferably triggered only when stimulated simultaneous signals are originated by specific spatially related areas in the visual field. Thus there are "line detectors", "corner detectors" which are stimulated when a bright line or bent bright line appears in the image of the retina. Regardless this information is processed at a pre-cognitive or other stage of the HVS – so as the information to be processed exists – it must have been necessarily captured by the photoreceptors.

C. The human eye seen as an imaging system

1. Some aspects of photographic cameras: from paper film to CCD arrays

a) Classical film roll cameras

Interestingly, we may find a parallel between the imaging technology invented by humans and the one derived from natural evolution. First photographic cameras, as well as first eyes in nature (or kind-of) were based on the rudimentary pinhole.

Pinhole cameras used to employ photosensitive paper, decades later substituted by regular film roll. This was the key basis for capturing still scenes where the quality of the image obtained was mainly determined by the properties of the photosensitive material and the time of exposure. All the process was an artwork requiring experience and specific knowledge on the tools and materials used, not only for the photo-shot, but also for the photographic developing process.

Following this parallel, again the next stage in evolution was the featuring of a lens, as happened in the evolution of photographic cameras, which came to be a major achievement; the implementation of the optical lens enhanced the photographic process, as it increased sensitivity, granting the possibility of acquiring an image in a question of few seconds – always depending on the type of photosensitive paper/film –.

More recent film roll cameras have basically used same technology as old fashion cameras but obviously with much greater quality optics and photosensitive film. The resolution of the pictures obtained with these devices has always been limited by the quality of the deposition of chemical layers.

More specifically, the resolution in regular film roll cameras is limited by the density of the granulation of the sensitive film. The bigger the size of the film is, the higher the resolution of the captured image. Something similar happens with digital cameras, and the resolution is conditioned by the size of the sensor frame.

So far, some balancing rules have been established for optimal results in all imaging devices, typically between several parameters such as captured signal power, lens amplification, diffraction distortion, shutter speed... But in all, resolution in these devices is primarily limited by the sensitive paper/film as well as by the aperture, as illustrated in the following Table I.3.

Diffraction is an important phenomenon connected with the aperture of any optics, as it blurs the image projected. The larger the aperture is, the smaller the distortion will be, and vice-versa, but at the same time, if the aperture is too large, the image might be overlapped by the effect of superposition of the image projected, as shown in the following Figure I.21.

Aperture	Diffraction blur	Blur by image overlap
Small	High	None
Medium	Tolerable	Low
Large	Low	High

Table I.3. Influence of the aperture on the image captured by regular digital and film-roll cameras.

Besides the influence of diffraction over the photo-capturing mechanism, the amount of light captured is an important parameter as it is in fact the power of the captured signal and it is controlled by the time of exposure. Thinking of this incoming light as rays, we may notice that for a large aperture, the ray is no longer restricted to just the centre and can wander over the rest of this wider range. This phenomenon can be seen in Figure I.21 and as a consequence a blurry image is captured.

Figure I.21. Superposition of projections in the case of a big circular aperture.

In contrast, when the aperture is very small, diffraction comes to be especially noticed because the diffraction lobes from contiguous pixels are very close from each other.

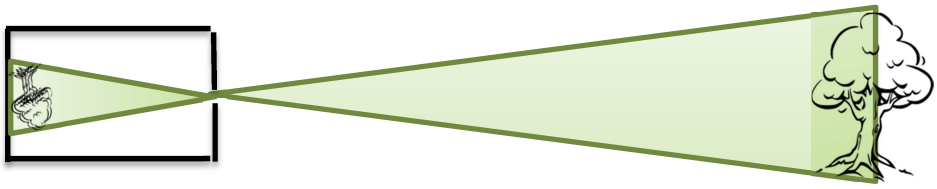

Figure I.22. Illustration of pinhole camera and effects of diffraction

All these explanations are intended to lead to the point that the distortion created by the diffraction has been a major preset condition so far in all imaging devices, as it is generally believed that it has to be avoided as much as possible and at any cost. Optics of cameras are – in a regular basis – designed to capture the information from the main lobe at each pixel with a minor, negligible distortion of secondary lobes.

We may give an example of resolution on 35 mm regular photo film cameras, which typical frame size is 22x16 mm and an average resolution of 50 lp/mm. This gives a value of about 3.5 MPixel and a distance of 10 µm between lines. On photo film cameras the distance between resolving lines (photosensitive granulation) is not necessarily kept as a rule or limit, but the aperture is controlled in relation to the focal distance of the lens, as the resolving angle does matter and the maximum distortion related to diffraction too. The diffraction created by the given pupil aperture will anyway be the bottleneck for an endless magnification or zoom of the photograph taken under the specified parameters, as we will see later.

As a next step in the technological evolution of cameras, the more recent digital ones are in a sense even more similar to the vertebrates' eye since their image capturing sensor consists of a discrete array of sensors emulating at some extent the sensors present in the retina.

b) Digital cameras

During the last years, conventional photographic cameras have progressively been substituted by newer digital versions, within a trend of rapid evolution such as the ability to obtain better and more accurate images. It is not rare to find cameras of resolution over 10 Mpix at conventional photography stores or often integrated in mobile devices such as smart phones and tablets.

It is generally accepted that the higher the number of pixels is, the better the resolution will be, thus more expensive the camera. But the technological limitation, which prevents from getting the resolution endlessly increased, is the size of the detectors, which cannot be smaller than certain feasible dimensions. This could be nowadays of 1 or 2 microns diameter. In addition, from the point of view of the information, sensitivity – defined by ISO – could be understood as the capacity to distinguish the information from noise which is also a limiting factor for the minimum size of the detectors.

In fact, instead of reducing the size of the detectors, the current solution permitting to increase the resolution of the sensors in the camera is to enlarge the total area where the image is captured (full frame, 36x22 mm). This fact pushes engineers to design concepts using bigger lenses in cameras in order to avoid aberrations.

On another hand, certain professional digital cameras' RGB colours are compiled by means of a special crystal prism by splitting the incoming light and drive the different components (Red, Blue and Green) towards the different colour detectors placed below the prism, which are approximately the same diameter size.

As we will specify later, the phenomenon of diffraction creates a distortion pattern with a main lobe and secondary lobes that can affect neighbouring sensor pixels. Therefore, the optimal sampling process for the current industry of photography would be that of a rejection of secondary and other lobes from neighbouring pixels approximately as depicted in Figure I.23 where most of the energy pertaining to each point is captured and represented at its original position by the array of sensors. This paradigm has been used so far almost in all digital photographic cameras.

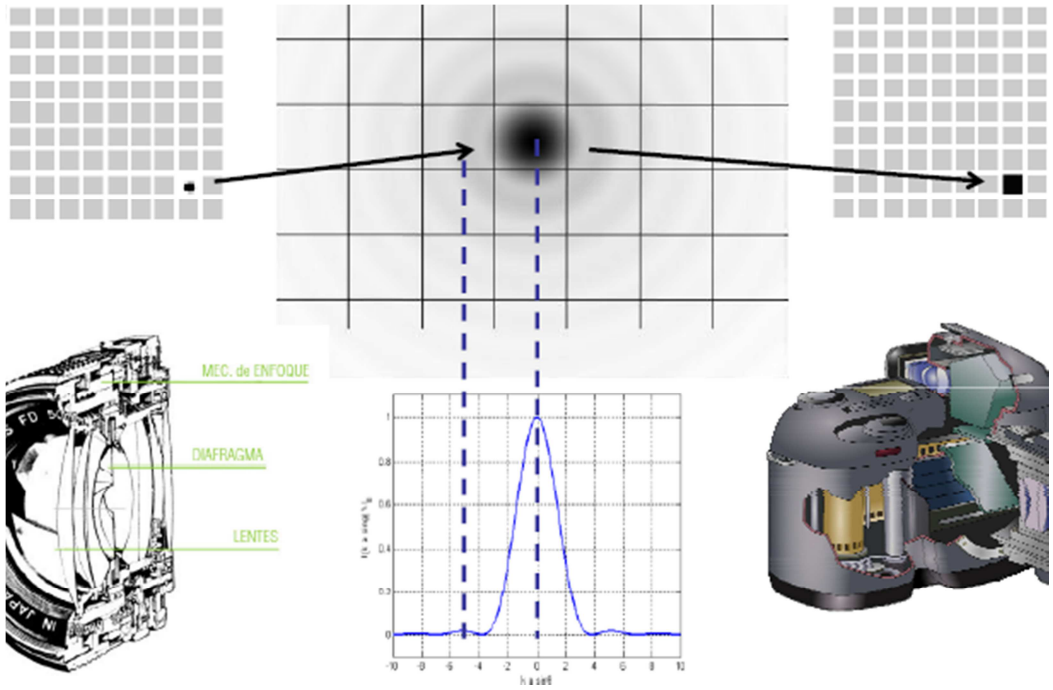

Figure I.23. Pixel captured by CCD camera.

c) Common techniques used to improve the image quality in digital cameras

Digital cameras, in contrast to older classical devices, allow immediate digital processing of the image at stages following to the photo-sensing one. Different techniques exist to improve or denoise an image exposed at low levels of light or even sharpen edges etc. Anyway, in the following lines we provide some notes on a couple of image enhancing procedures just in order to avoid any confusion with the upcoming explanation of our theory.

A rather new technique used to improve the quality of an image is known with the acronym HDR (High Dynamic Range) but it is unrelated to any high resolution processing. Here, several exposures taken at different light sensitivities are combined or mixed together in order to obtain an optimally clear image and avoid dark or burnt areas on the picture. In Figure I.24 shown below, as can be seen at the different stages of the sequence of images, the window is perfectly shown at the lowest illumination sensitivities but the environs are totally dark and nothing can be distinguished.

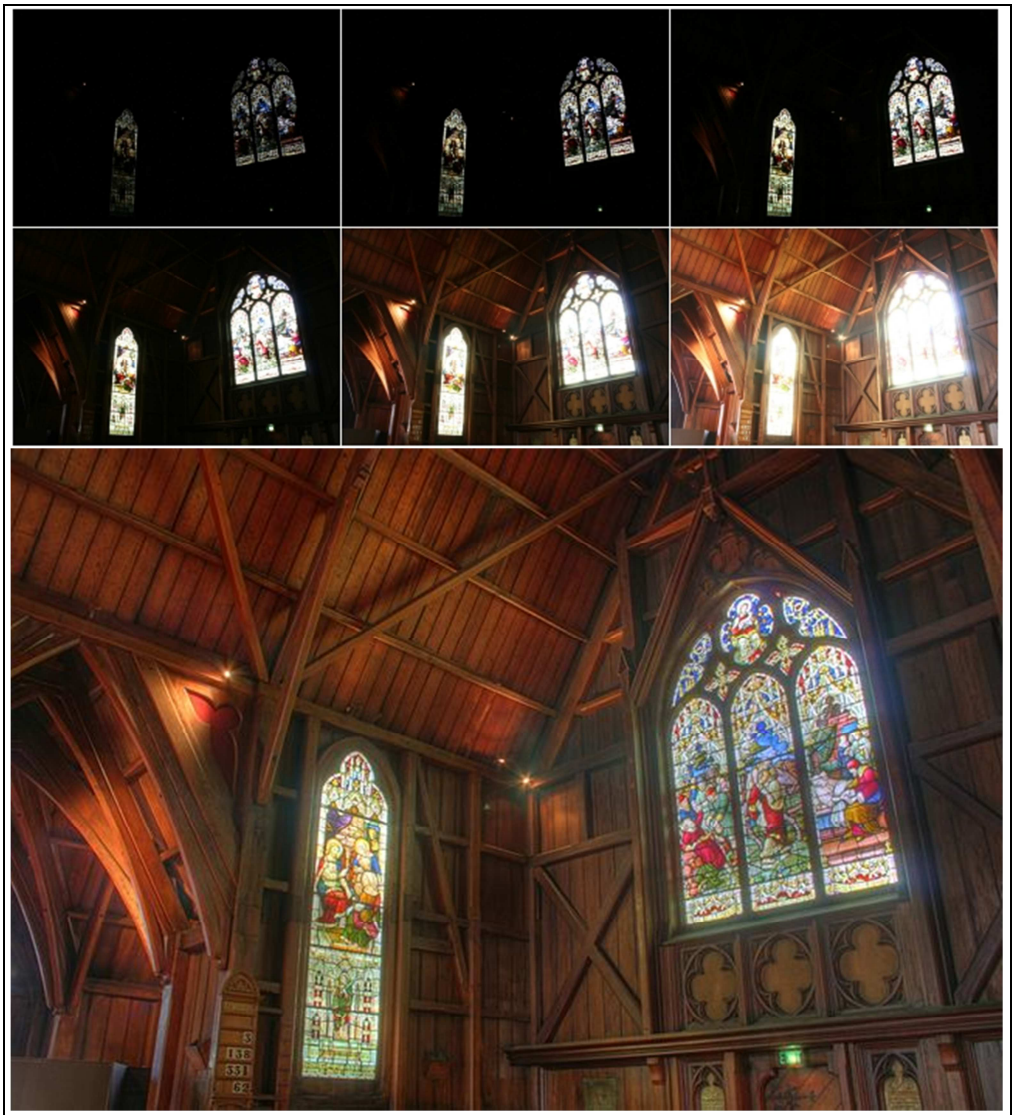

Figure I.24. Process of an HDR image. Credits: Dean S. Pemberton

As a result of the smart combination of the exposures the final image is optimally illuminated in all areas of the picture.

Another technique used to increase the resolution and the acuity as well is known as superresolution (SR) by overlapping of subpixel shifted images, also called resolution enhancement (RE). Here, the degree of the improved acuity depends on many factors but a fact is that along different exposures, the SNR rate is improved due to the Gaussian distribution of the noise.

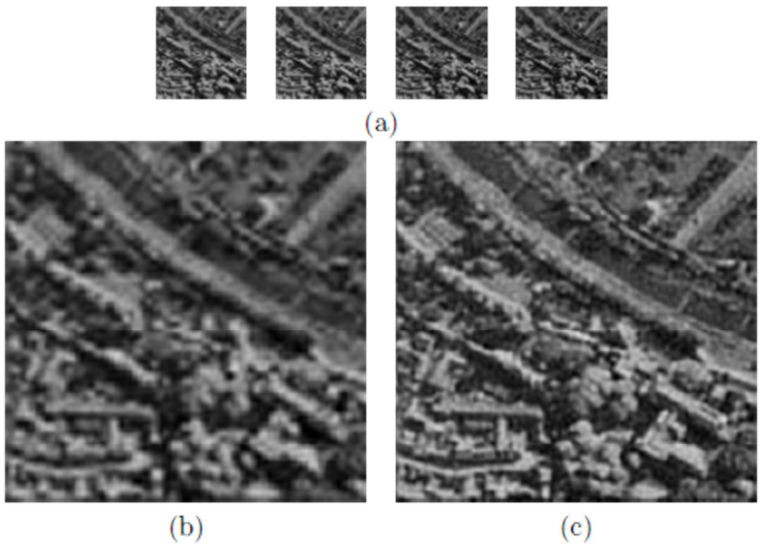

Figure I.25. Captured low-resolution photos (a). Top-left image enlarged for better comparison (b). High resolution image obtained by combining the above. Credits: Javier Mateos – UGR

Besides that, depending on the degree of subpixel displacement, the additional pixels provide new information on the signal. Unlike in a process of interpolation these different subpixels are not derived from neighbouring pixels or points.

All these neighbour pixels are arranged in a new image and form the superresolution image.

As we may notice, these two techniques improve the quality of an image, but the fact is that several expositions need to be combined in order to improve the final resolution of the resulting picture.

The resolution of an image is often a topic of discussion that we will see next.

2. Resolving capacity

As exposed formerly, artificial cameras may give us an idea of an assumed layout of the eye, that is to say, the configuration of the optics, photoreceptors etc. But in the following lines we will see what the truth is about the typical presumptions on these questions, especially about the eye's configuration and capabilities to resolve details.

The eye and its abilities have been in discussion probably for centuries. Resolution is a concept which has different interpretations. Some scientists use it to express the number of pixels or points in an image, some others use it to express the level of detail in an image and some others mix these both concepts.

In the popular culture people are often interested in the question of the resolution of the human eye – probably because the popular knowledge background of resolution is supported on the almost ubiquitous digital embedded-camera smartphones – and would like an answer in terms of megapixels. In this section, we will see that the exact answer to this question is more complex than the usually expected, so in order to understand these concepts and to evaluate the origins of the high resolution, we analyse here some parameters of resolving capabilities.

Benson et al. (Benson, Luke et al. 2009) stated that there are different ways to understand the acuity parameter of the eye, but we prefer to stay with the definition of

the acuity as the capability to distinguish two punctual sources placed close to each other at a certain distance from the observer.

The use of the word *resolution* should carefully be restricted to the definition of the number of points or pixels composing an image, which is totally different from the degree of details present in it. Neuroscientists though, rarely ever misconceive this word and have historically used other terms to accurately describe each magnitude, parameter or capacity and they use different concepts to describe the eye's resolving features. For instance, the angular details and the information about the position of a point are different capacities.

The angular resolution is a measure of the degree of details an imaging device – or an eye – may distinguish. It gives the relation of the separation of two points and the distance to them, i.e. the angle formed respecting to the observer – or imaging device –. This angular resolution can also be understood as the regular acuity.

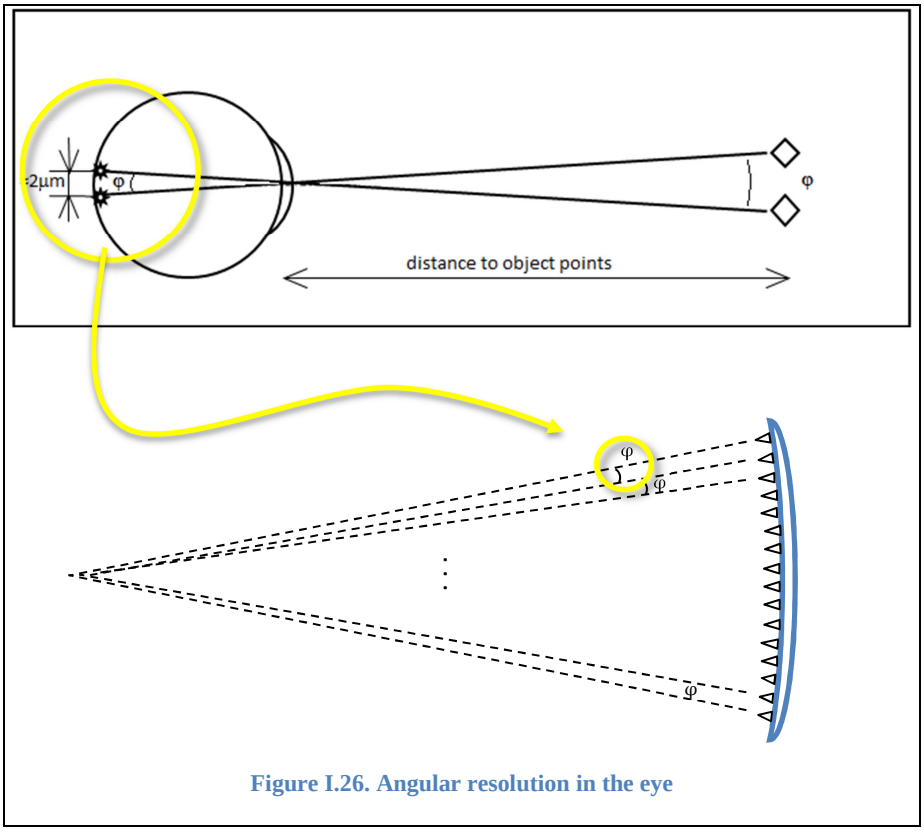

Figure I.26. Angular resolution in the eye

The separation between 2 cones is shown in Figure I.26; although the angle is fixed, the width of the resolved element increases linearly with the distance from the eye, and the acuity decays.

An illustrative example of this may facilitate comprehension: a single human hair (50 µm as an average) would not be seen beyond a distance of just 35 cm (13.78 in) far from an observer; it would be a priori below the necessary sampling frequency threshold, since the required minimum size of the object to be seen should in this case be 87.5 µm width. As a consequence of this the human hair (50 µm) would not be resolved that

distance, but only perceived – at most its pattern –. Despite all, it is a common and undeniable fact that in this example, the human hair is undoubtedly seen with great detail at distances of even meters and furthermore, it is resolved.

At the beginning of the XXth century Hartridge (Hartridge 1922) explained – probably for the first time in history – the resolving power of the human eye. Schober (Schober 1938) later emphasized the human eye as an optical instrument and remarked its resolution.

The resolving power is a very similar concept to that of the angular resolution. In the eye, it is a magnitude of the capacity to distinguish two subsequent points which means that an observer resolving details on an image should do so at that degree of detail. In this sense, it is assumed by the scientific community that the acuity or resolving capacity of the human eye is about a minute of arc; this value is known as the MAR (*Minimum Angle of Resolution*). Thus, considering that the focal distance of the human eye is about 16 mm, we could easily calculate the MAR, just by dividing the distance between two non-consecutive photodetectors – 4 microns – and the focal distance, which yields an angle of 0.25 mrad or 50 seconds of arc.

Nevertheless, the human eye can see even below that resolving scheme, that is to say, the capability to see despite not being able to distinguish subsequent multiple points.

All these parameters commented so far are magnitudes used in imaging systems used – sometimes accurately, sometimes inappropriately – to define at some extent the quality or sharpness of detail of the images it may obtain.

The resolving power and these parameters used to measure the acuteness of an image capturing mechanism generally limited by many factors that create distortion on the captured image. This distortion might come from different sources; mainly optics and noise. Nevertheless the optical lay-out of any image capturing device is usually conditioned by the natural phenomenon of diffraction.

The phenomenon of diffraction creates distortion in the image captured by the eye too. The diffraction pattern is shown in Figure I.27, to better understand its implications. This is in fact a phenomenon that cannot be eliminated, but only controlled. Thus, light undergoes the phenomenon of diffraction when it goes through any aperture or slit; there, the Airy disk given by an angle $\alpha = 1{,}22\lambda/d$ matches the Rayleigh criterion for resolution as it defines the necessary minimum angle in radians so that both disks can be visible i.e. the distance between the centre of the two circles, if we take two adjacent main lobes.

So as we say, diffraction exists in all optical devices without exception – including the eye – and it is originated due to the transmission of waves through a slit or the aperture of an object. Unlike in the eye, in artificial imaging systems, the dimensions of the optics and the image capturing sensors are designed such that 99% of the energy coming from an area is contained mainly in its corresponding pixel, and as a result of this, the distortion does not affect neighbouring pixels as depicted by Figure I.27.

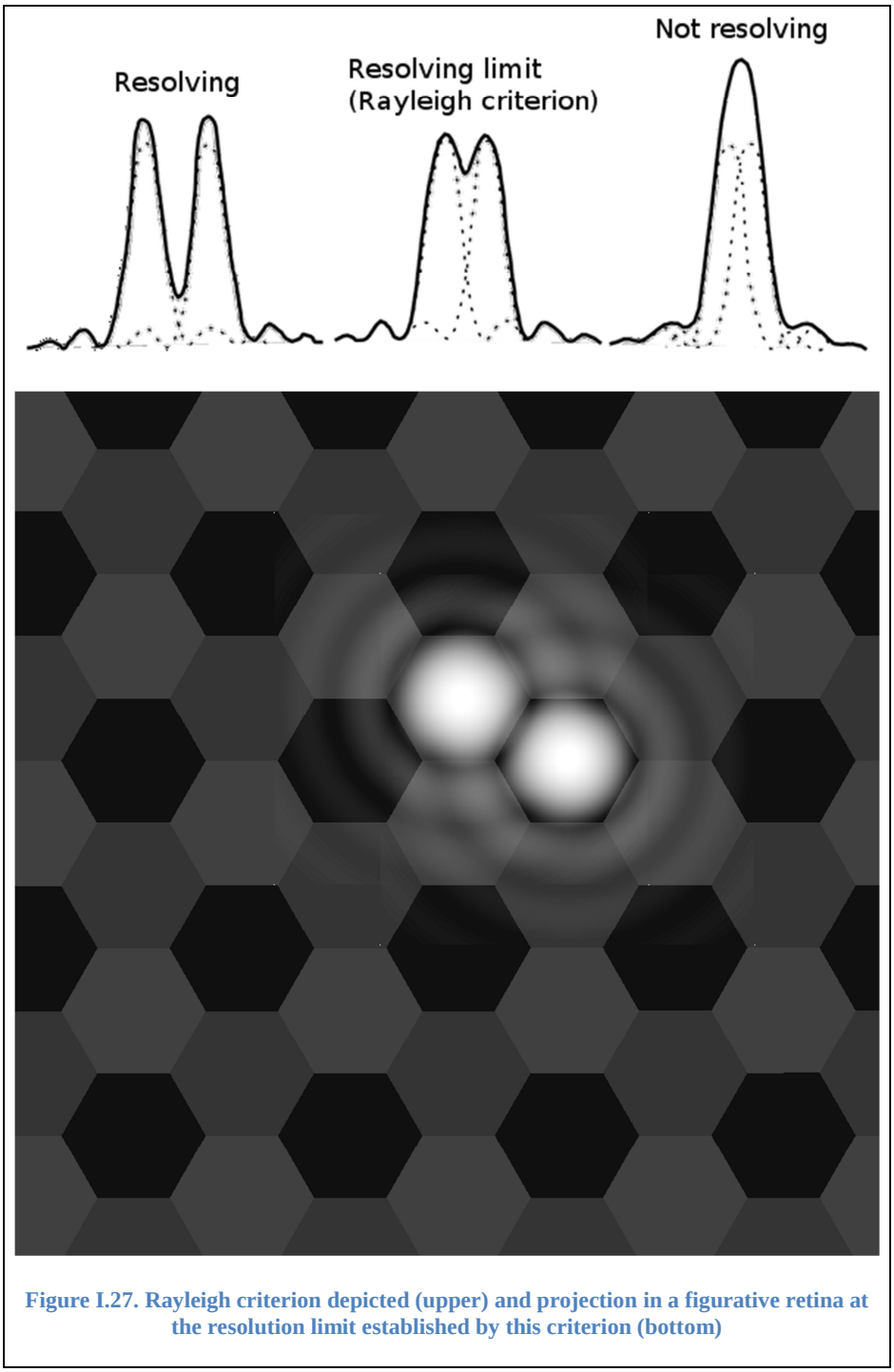

Figure I.27. Rayleigh criterion depicted (upper) and projection in a figurative retina at the resolution limit established by this criterion (bottom)

In connection with the separation of sensors in artificial imaging devices, we will now present some data on the number and density of photodetectors in the human eye. There are different approaches in the literature on the number of cones present in the *fovea centralis*, which covers an area of about 1mm radius. So much so, that a paper (Østerberg 1935) points up on 147.000 detectors/mm^2 whereas another author (Ahnelt, Kolb et al. 1987) estimates a number between 178.000 detectors/mm^2 and 238.000 detectors/mm^2. A later study (Curcio, Sloan et al. 1987) claims a larger interval of 96.900-281.000 detectors/mm^2. It should be remarked that the size of the photoreceptors in the fovea is about 1.5 µm (Kolb), which are spaced from each other

more or less 0.5 μm. They are distributed in a more or less triangular lattice. This size is very similar to the minimum technologically achievable by the pixels of digital cameras. However, in the case of the human eye, each one of the sensors is oriented versus the detection of only a particular colour component of the incident light, reducing by three (let us suppose that the three colour sensors are uniformly distributed over the retina) the resolving capability of coloured images.

The reader may notice on the sub-megapixel resolution of the image projected – thus created – on the fovea. As it may now be understood, while in a regular digital camera the number of pixels is a popular measure for the capability/quality of the device, in the human eye the level of details perceived surpasses the expected by the number of photoreceptors – in an analogy to pixels – present in it.

In connection with the resolving power of the eye, diffraction is in general considered a limit and as already appointed the Rayleigh criterion defines that boundary.

Up to this point, the diffraction of the pupil has not been taken into account. We might assume that the behaviour would be similar to that of diffraction limited systems, but the results in this aspect are rather surprising.

With this in mind, we note the diameter of the eye pupil and see that this diameter varies between 2 mm and 5 mm for a bright day and a cloudy day, respectively. Then, choosing one of the wavelengths of the visible spectrum, for example 550 nm (green tending to yellow), with an opening of 2 mm pupil, would have a Rayleigh criterion limit for resolution of:

$$\theta_r = \arcsin(1.22\lambda / D) \simeq 1.22\lambda / D \simeq 69.202'' = 1'9.202'' \tag{1.1}$$

Diameter (D)	Rayleigh angle $\theta = 1.22 \lambda / D$	Rayleigh distance $d = 1.22 \cdot f \lambda / D$	Minimum resolving angle (2θ)
Pupil as diffracting aperture (λ=550 nm, f=16 mm)			
1 mm	2' 18.4''	10.7 µm	4' 36.8''
2 mm	1' 9.2''	5.35 µm	2' 18.4''
6 mm	23''	1.79 µm	46''
Photodetectors (1.5 µm diameter and 0.5 µm separation)			
5.368 mm	25''	2 µm	50''
Hyperacuity (Reported to "see" 1 sec of arc(Klein, Levi 1985))			
138 mm	1''	0.077 µm	-

Table I.4. Relation between separation of the cones and alleged acuteness achieved when Rayleigh's criterion is observed for λ=550nm. *f* stands for the focal length and D for the pupil aperture

We may next realise about the consequences of applying this criterion in the human eye. As illustrated in Table I.4 the natural distance between two photoreceptors in the fovea is 2 microns (Kolb) but the minimum distance for the existing diffraction – set by this criterion – for a pupil aperture of 2 mm reaches 5 µm.

In Table I.4, the diffraction of the pupil for different apertures is presented, together with the calculations based on the size of the photoreceptors and the hypothetical estimation of the resolution for the minimum visible threshold of 1 second of arc (Klein, Levi 1985). The resolving and seeing capabilities shown, as well as the Rayleigh distances in the retina have been calculated assuming a focal distance of 16 mm in all cases. It may seem at the same time surprising that in order to capture or see details of even 1'' (one second of arc) the size and separation of cones should by far be much smaller than the actual configuration.

It is to be noted that there exists a difference between the capacity of seeing and resolving elements. The resolving power is usually defined as the capacity to distinguish two point sources, which determines the regular visual acuity defined by the MAR (Minimum Angle of Resolution). The capacity of seeing stands rather for the perception of elements without regard of other factors, i.e. just on whether the source point is perceived.

Anyway, from Table I.4, the aperture of the pupil closest to the standard MAR (50'') is 6 mm, whilst the optimal aperture allowing the sharpest acuity is reported to be between 2 and 3 mm diameter (Campbell, Gregory 1960).

Regarding the separation between the maximum of the lobe peak and the first null of diffracted point sources, the Rayleigh criterion establishes an angular resolution of

about 1’09’’ of an arc. Since the standard focal length is 16 mm, the minimum distance between photoreceptors that respects this angle should be of about 5 µm.

So although the diffraction limits set by this rule are not met by the human eye in the fovea the fact is that we can see and perceive details beyond the sampling frequency or concentration of cones.

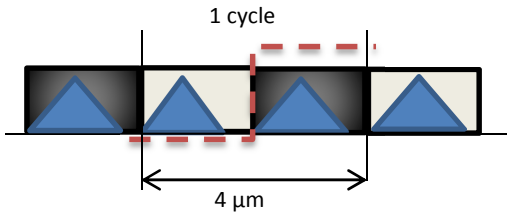

Figure I.28. Spatial sampling frequency

Sampling frequency can be a paradigm of resolving power. The sampling theorem states that at least two samples must be taken per cycle or period of the signal. Thus, the requirement of the minimum distance of 4 µm is observed. In our case, we are dealing with a signal with a realisation in space. Figure I.28 shows a whole cycle covered by two cones. The distance between peaks is half of a period; therefore a period in space will take 4 µm.

We may notice that the two-dimensional spatial sampling frequency can be understood as the density of the cones, which comes to be about 200 k/mm^2 as stated earlier.

3. Different techniques, different capabilities

On another hand, the standard minimum angle of resolution used in optometry – known as the acuteness for a normal vision – is rated in one minute of an arc and it is commonly used at the Snellen chart, a test where the minimum size of an optotype is five minutes of an arc, but with details five times below, also noted by 20/20 or 6/6. 20/20 vision is a term used to express normal visual acuity (the clarity or sharpness of vision) measured at a distance of 20 feet. For a 20/20 vision, the expected acuity (1

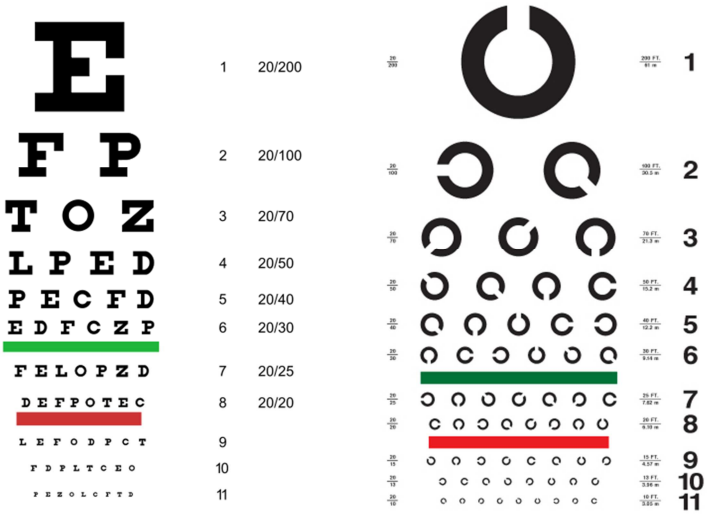

Figure I.29. Snellen chart and Landolt C chart.

minute of arc) is reached at a distance of 20 feet. A 20/100 vision would instead mean that the acuity reached at 20 feet equals that of normal vision at 100 feet.

The most usual procedure used by optometrists nowadays for measuring the visual acuteness is a test called eye-chart, which consist of a series of inscriptions of different sizes to be read at a given distance. Each symbol has some particular dimensions that allow determining an observer's capacity to see. More specifically, the most widely used are the logMAR chart, Snellen chart, Landolt C, E chart, Lea test, and the pre-soviet Golovin–Sivtsev table. All these methods were developed from the idea provided by Heinrich Kuechler (1811-1873). Figure I.29 shows the Snellen chart – which remains as the most popular one – and the Landolt C – nowadays an international standard accepted in many European countries (including Japan) –. In some eastern countries like Russia the Golovin-Sivtsev table is rather used, due to the Cyrillic font characters.

As we say, all these scales indicate the degree of detail the eye can distinguish where the minimum threshold for normal vision at this task is considered to be approximately a minute of an arc, but accuracies of even 30-35 seconds of an arc have also been reported (Westheimer 1976). Table I.5 illustrates typical values arising from these acuity tests

Foot	Metre	Decimal	LogMAR
20/200	6/60	0.10	1.00
20/160	6/48	0.125	0.90
20/125	6/38	0.16	0.80
20/100	6/30	0.20	0.70
20/80	6/24	0.25	0.60
20/63	6/19	0.32	0.50
20/50	6/15	0.40	0.40
20/40	6/12	0.50	0.30
20/32	6/9.5	0.63	0.20
20/25	6/7.5	0.80	0.10
20/20	6/6.0	1.00	0.00
20/16	6/4.8	1.25	−0.10
20/12.5	6/3.8	1.60	−0.20
20/10	6/3.0	2.00	−0.30

Table I.5. Visual acuity scales

Decimal values in the table represent the size of the gap (in arc-minutes) of the smallest Landolt-C orientation reliably identified.

We remind that the community of neuroscience defines with great accuracy the abilities of vision, where tests are performed aiming to measure specific aspects of a phenomenon, and tasks and stimuli are also totally dependent on this. Any scale or test explained up to this point may represent a degree of specific visual acuity but does not itself explain the capacity.

In peripheral vision for example Gabor patches (Figure I.30) and specific tasks are performed often different from those used for central vision. In the picture below, the known as Gabor patches are shown in a task where the alignment of laterals has to be defined by an observer.

Figure I.30. Gabor patch based stimulus

On another level, a nowadays usual way of measuring the acuteness of vision is in fact related to a rather ancient discovery. In 1631, the Franc-Comtois mathematician Pierre Vernier published *La construction, l'usage, et les propriétés du quadrant nouveau de mathématique* explaining the idea of a scale nowadays bearing his name, Vernier. His proposition was to attach permanently an "irregular" scale to a quadrant aiming to measure fractions of an angle with accuracy and ease of use.

The novelty of the invention was the use of a movable scale aligned with a fixed regular one – written in half degrees – with the important difference that this sliding scale was thirty one half degrees long but divided into thirty equal parts. Thanks to his new quadrant – notably the idea of the scale – measuring fractions of degrees became possible.

The Vernier scale has also been used in another context due to the fact that returns exact values of the distance separating two lines. Examples of this are callipers, which would have never existed without an augmentation scale such as Vernier's. They consist of two scales that are read so as to obtain the exact measured value. A large scale provides high order values and a lower subscale the lower order values.

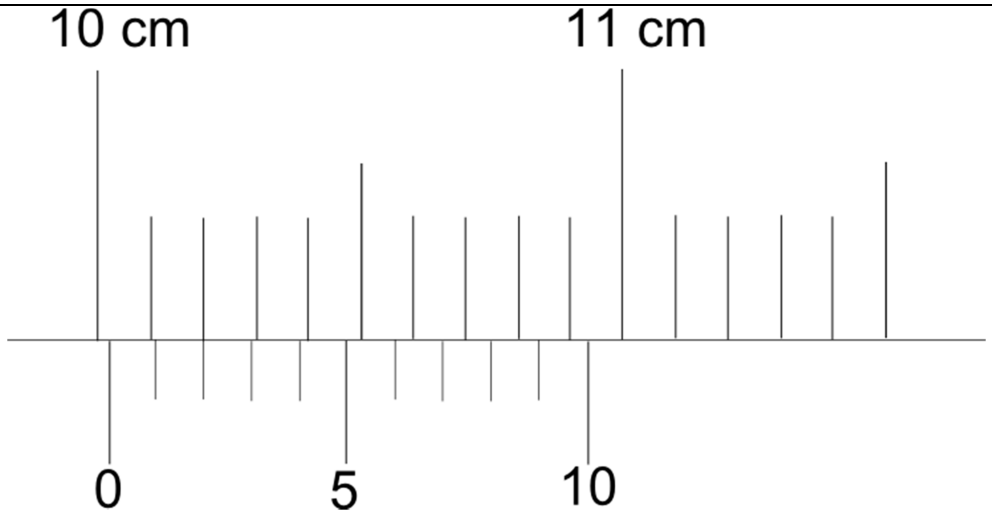

Figure I.31. Vernier scale represented in a caliper

As seen in Figure I.31, the measure given by the position of number zero is 10 cm and 0.2 mm, as the Vernier scale (below) coincides at the second number at the top scale. The scale at the bottom is actually nine millimetres long but divided in ten equal fractions.

Anyway, our interest on the Vernier scale is motivated by the possibility of measuring accurately the separation between two lines.

Figure I.32. Even nowadays, callipers use the vernier scale

Among several visual acuity tests, a well-known one is the Vernier test where a naive observer has to decide how two parallel lines are aligned, in other words, whether the upper or the lower line is on the left. The test lines are put close from each other but randomly on each of the sides (left or right) and every time the subject answers correctly the lines are rearranged closer.

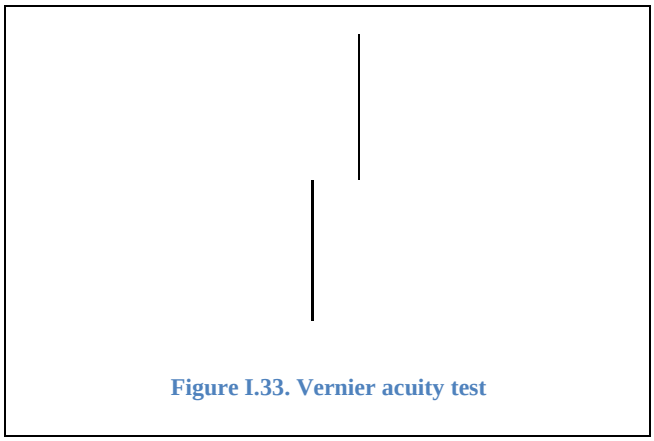

Figure I.33. Vernier acuity test

The separation of these two lines as represented in Figure I.33 and can even be on a sub-millimetre scale. Although an observer cannot in some cases resolve in the sense of distinguishing the width of a line, it can resolve the localisation of two points or lines, i.e. whether it is on the left or on the right. This is

known as the Vernier acuity and several results have been published related to this test, reaching accuracies of seconds of an arc (Westheimer, Mckee 1977), or between 4 and 7 seconds of an arc (Carney, Klein 1997)

In this way, Gerald Westheimer, aware of the eye's capacity to see details below the commonly known limit of visual acuity coined the term hyperacuity. This new word intended to somehow define the eye's capacity to resolve the localisation of points below the regular acuity threshold (defined by the MAR at approximately 1' of arc), reaching capacities of one second of arc and below (Klein, Levi 1985). Anyway, it does not involve superresolution which itself has a different meaning. The term superresolution though is normally understood as related to sub-wavelength resolution. The amazing hyperacuity capacity has been reported to achieve even one second of an arc and even below in the human eye (Klein, Levi 1985).

D. Conclusions

In this chapter we have exposed the physiology of the human eye and how the sensors are used to "see" –actually neurons modified by the natural evolution –and specially trained to be excited when light arrives to them.

There is a controversy on whether the human eye has design flaws, mainly due to the layout of nerves which are arranged "backwards", that is to say, at some extent they obstruct the incoming light. Despite this or other alleged "design mistakes", in terms of angular resolution, the eye outperforms any current imaging device. Moreover, no antenna imaging system achieves the directivity the human eye gets, by means of so few detectors. The layout of the cones is optimised in terms of space, and second, the distance between photoreceptors does not fulfil Rayleigh's criterion to avoid diffraction blur, whereas in digital cameras it is a design constraint.

A surprising fact is the difficulty to find a digital camera capable to beat the resolution of the human eye, although the sensors are less in number and more separated from each other, especially for two consecutive cones of the same colour. In addition, cones are colour specific, and so, sensors capturing object points of same colour are actually farther from each other than at the initial hypothesis.

An important point is that the spatial sampling frequency does not explain by itself the angular resolution obtained by the HVS. In contrast to artificial imaging devices, the Rayleigh criterion shows that the eye *is not designed* to stay below this limit, which means that the main lobe is expanded over a larger area than the one corresponding to a single photoreceptor.

Despite above considerations, the signal captured from these colour specific photoreceptors might in next stages be combined to increase the diversity as we'll see in the next chapter.

Chapter II. Unified Theory of Visual Acuity

A. Introduction

We exposed in the previous chapter that the understood as regular acuity is a magnitude that measures a particular capacity of the human eye which is typically thought to be an arc of a minute and widely tested with standard procedures such as the Snellen chart. This angle of resolution is also often considered being derived from the angle formed by the separation of the cones in the fovea and the aperture – forming an angle of about 50 seconds – as depicted in Figure II.1.

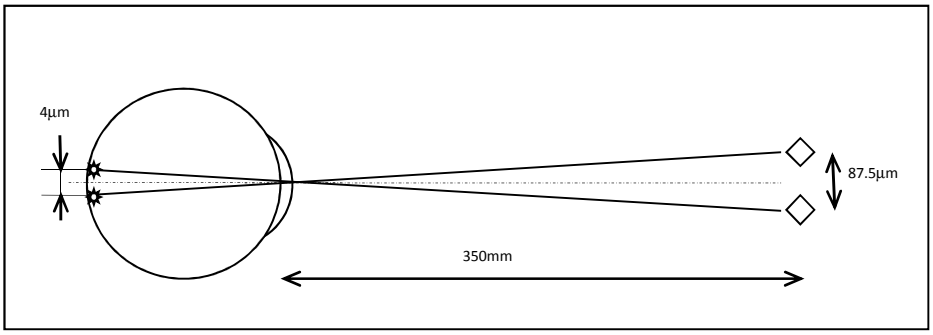

Figure II.1. Angle of resolution of an eye

Nevertheless, as we saw, this angle does not justify itself other visual capacities such as the Vernier acuity – rated in orders of a second of an arc – and hyperacuity – even below a second of an arc -. Either the separation of the cones or their dimensions do not explain their existence or the existence of this phenomenon.

In addition, it is a common belief that the diffraction created by the entrance aperture determines the final bandwidth, the cut-off frequency or the maximum achievable resolution. In other words, the maximum frequency allowed in the projected image over the retina. In fact, there is a limitation related to this frequency, but not the way it is commonly understood, as we will see later on.

As earlier stated, the eye shows extreme capabilities at certain visual tasks for which there have been several explanations in the literature. Among these, we find some popular incorrect beliefs, such as the idea of an integration of different frames of the same image, as well as the idea of having a very large number of cones in the eye (much larger than 1M). These justifications seem unfeasible to us; first due to the impossibility of a buffer of such extent which might record all positions from different frames to be able to combine all of them correctly, and second – as already shown in Chapter 1 – the number of cones in the area of high angular resolution is only about a quarter of a million.

The idea of hyperacuity has already been discussed quite long ago in the literature (Hartridge 1922, Schober 1938). In 1952 Toraldo di Francia stated that the resolving power of 2 points with diffraction may only be limited in practise by noise. There have been publications (Harris 1964, Barnes 1966, Louer, Weigel et al. 1969, Birch 1972) long ago appointing the possibility of going beyond a presumed limit set by diffraction in the way of improving resolution. Westheimer though, has stated diffraction limits resolution of 2 point sources but not localisation of a single point (Westheimer 1976). Some

references (Gerchberg 1974, Papoulis 1975) propose a different concept of achieving super-resolution using extrapolation in band-limited systems.

There are theories which may lead to the idea that the natural pre-blurring in the human eye – understanding this pre-blurring as diffraction – is what enables the so expected hyperacuity. In connection with this, some authors (Kamitani, Sawahata 2010) think that spatial smoothing is totally recoverable under certain conditions and in another paper (Gelius, Asgedom 2011) diffraction is considered potentially helping in seismic imaging to get greater details of a picture.

Within this chapter, we will first discuss some classical theories which intend to justify or describe the capacity either based upon the movements of the eye or diffraction. We do an overview of the most used alternative explanations, which in general – rather than opposing – we find complementary to ours; therefore we use the definition of "unified theory".

Next, we will continue by explaining how blur can be created by diffraction and how this is important for achieving the incredibly high angular resolution of the eye. So, we will focus on diffraction blur and explain how this distortion can be used as an advantage – instead of just being an inconvenience – and works actually as a filter that enhances the sampling process, i.e. it is diffraction enhanced rather than diffraction limited which means it uses diffraction and a post-processing to obtain greater details from an object as well as the capacity known as hyperacuity. We thus describe in detail the steps to achieve such angular resolution and how this could be carried out on three stages by the human neural system.

Additionally, we endow this chapter with an exposition about the trade-off between the amount of diffraction put out by the pupil aperture.

All in all, we intend to explain the extraordinary capacity of the human eye to resolve fine details with a theory that encompasses existing general theories– instead of neither omitting nor contradicting others–.

Eppur si muove – Galileo Galilei.

B. Classical theories for explaining the hyperacuity

1. Some paradigms on neuroscience and psychophysical tests

Along the XXTH century, scientific community has carried out a myriad of tests with several different subjects and scenarios. Vertebrates, as such cats, rats and apes typically, are subject to surgical operations where probes and implants have often installed on them. Human subjects on the other hand are capable to make statements and take decisions on visual tasks but are seldom submitted to clinical intervention to perform any visual test.

Throughout psychophysical experiments and thinking, scientists have discovered and measured new abilities such as different types of eye micromovements, their origin and relation. Regarding visual tasks, there are hundreds– maybe thousands – of papers describing and reporting different skills among which we focus on few specific ones, related to visual acuity.

As soon as the community has noticed on the astonishing angular resolving power of the eye, different explanations have been proposed. Some explanations are indeed wrong, because they do not always have a scientific basis; mistaken statements relating an immense number of photodetectors, justifications arguing cognitive deduction of points, or even a combination of frames stored on the cerebellum.

Regarding cognitive resolution of points, this mechanism indeed exists in the HVS, but the information theory cannot be omitted, i.e. the information is captured or it is not captured, but cannot be figured out from non-existent data. We will see in next sections that micromovements of the eye do exist, and temporal integration does exist in the eye too, and that there are generally accepted theories which might be interesting.

2. Micromovements of the eye

a) Basic review

One of these movements – saccadic movements – is considered to be a strategy of the HVS to prevent saturation of photoreceptors (Martinez-Conde, Macknik et al. 2004). The saturation of photoreceptors makes these sensors stop sending neural signals upon some excitation threshold. The question to answer is on how these movements and/or the blur they create affects visual acuity.

One of the theories connecting the hyperacuity and the micromovements of the eye states that these movements may blur the image projected on the retina, but in turn advocates they might help to fill empty spaces between the cones (Marshall, Talbot 1942, Averill, Weymouth 1925, Hennig, Wogotter 2004). Hennig and Wörgötter though, explained that micromovements of the eyes improve hyperacuity in the peripheral vision, but not in the central vision.

It is clear that involuntary eye movements during attempted fixation (i.e. ocular microtremor, drift and microsaccades) could contribute to increase the blur of the image on the retina. In this regard, microsaccadic movements of the eyes may enhance high spatial detail (Martinez-Conde, Macknik et al. 2004, Rucci, Iovin et al. 2007, Ko, Poletti et

al. 2010). To be more specific, it has been reported that in some cases the integration time of the detection process is larger than the period of these movements (Martinez-Conde, Macknik et al. 2004). In others cases instead these blurring effects can be neglected. Barlow suggests that the information could be gathered as a consequence of temporal interpolation (Barlow 1979), possibly related to the small and quick vibrations of human eye, which would increase resolution by combination of differently similar images.

However, the adaptation of the cones and rods to each particular visual condition, the human eye requires of a certain interval of time, i.e. there is an excitation time even when they are not excited due to the relaxation time needed by the photosensitive cells. This may be characterised by hysteresis behaviour. In other words, a considerable excitation-relaxation time that seems to invalidate the idea of the contribution of small movements to enhancing the acuity of the eye by the combination of images.

Other interpretations based on the randomness of these dynamics argue it can be modelled by a stochastic process (Geisler 1984, Wei 2004, Pitkow, Sompolinsky et al. 2007). From the point of view of the information theory, a relation has been established between the mutual information of a single photoreceptor and one point of scene, with the conclusion that the problem has to be faced globally instead of locally (Zozor, Amblard et al. 2009, Di Francia 1955); in other words, with an ensemble of sensors.

In opposition to the articles claiming the motion enhanced acuity, a rather recent document (Benson, Luke et al. 2009) suggests that the motion pre-blurring method does not improve resolution, but can lead to detection of the direction of movement. The developments reported in this paper concentrate in a composed fly-type eye where the super-resolving capacity of the eye is supposed to be achieved thanks to saccadic movements too.

In connection with these latest findings, a singular illness presumably showing the role of some eye movements is the fibrosis of the extraocular muscles. Individuals who suffer from this disease are affected by not being able to move their eyes, and this, is a serious problem because they lack from all kind of involuntary eye movements, including saccadic movements, which are considered to prevent visual fading. In consequence, they may stop ‘seeing’ after some seconds of fixing their gaze towards some point in space. A special case of a woman diagnosed from this sickness (Martinez-Conde, Macknik et al. 2004) showed allegedly normal visual conditions. This person solved the problem of fading by moving her head in a way that resembled the eye’s saccadic movements. The key point here is that levels of acuity seemed to be normal in this case, which could suggest that there would be other factors beyond eye motion creating blur.

In addition to this assumed case, there are other studies with subjects who were submitted to artificial ocular paralysation (Stevens, Emerson et al. 1976). Within this experiment they were administered low doses of curare. As these authors reported, after some time the subjects experienced visual fading but the results for acuity tests were normal. Nevertheless, in a similar study (Whitham, Fitzgibbon et al. 2011), the details away from the foveal position were perceived below normal levels of acuity. It is

to be noticed the fact that these tests show only normal acuity, not hyperacuity which means there are no definitive evidences on this, but only some traces.

Still, the possibility of enhancing the resolving power in the human eye is totally dependent on neural post-processing. In this sense, these theories argue that the neural systems carrying out acuity tasks by refilling spaces would imply high costs and an expensive maintenance as well, in addition to the complexity of its architecture. In general, all neural networks are costing and require lots of energy to keep them working.

b) Temporal Integration

A look on the temporal behaviour of the HVS can be necessary so as to understand the effect of the eye's movements.

Movies typically use 24 frames per second. During that 1/24 second during which the frame or window shows, a significant adaptation in the eye occurs, and during the subsequent dark moment, when there is no light on the screen and the next frame is moved before the eye lens and readjust and so it does not lose sensitivity at the next frame.

A film that shows only 24 frames gives us a sense of flicker due to the successive adaptation to a bright scene and successive periods of darkness. An ingenious technique prevents flicker during the screening, the film is projected at 24 frames per second, but each frame is shown twice. So we are shown images at 48 frames per second, exceeding the critical fusion frequency where the effect of adaptation becomes imperceptible.

A similar problem occurs on television, where the full sweep is 25 frames per second. To avoid flickering in analogue TVs, image scanning is performed; first the even rows and then the odd rows in pairs. So, the entire screen is refreshed 50 times per second and flicker is thus avoided.

Artistic styles such as op-art or moiré, shown in lower left and right images respectively – named optical art and popular in the 50s – take advantage of these visual processes to create motion blur by repeating lines, squares and dots.

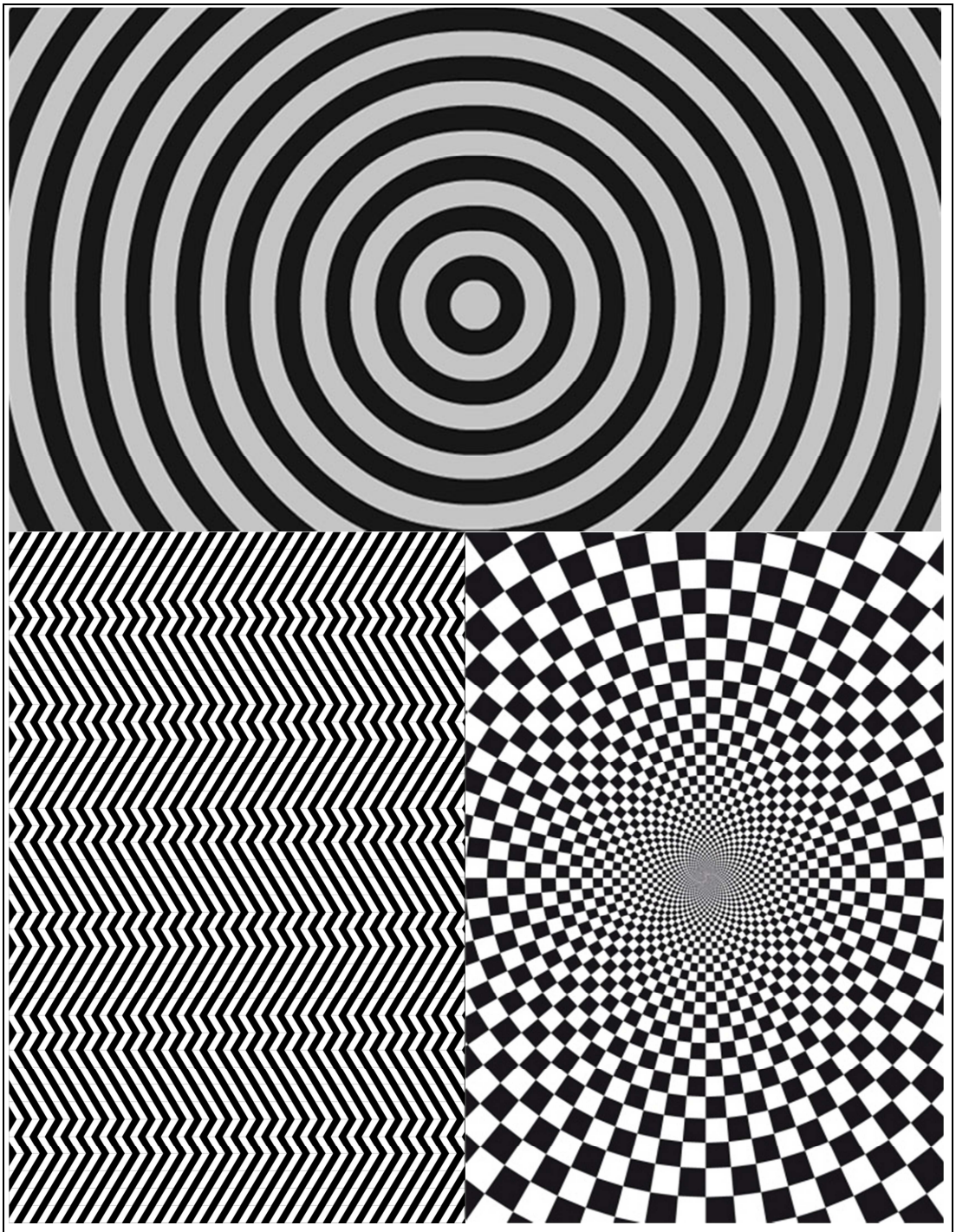

Figure II.2. Op-art creating motion blur. Source: unknown

Moiré patterns also makes use of visual processes to create motion blur by concentric circles. The explanation for these visual patterns lies in the persistence of the image on the retina – which may reach a 1/10 of a second – with the motion of the drawn eyes or blink when we try to focus the attention on a particular point. As there is no specific

point at which to fix the attention, the view goes from one point to another, but it also overlaps with the previous image, due to the persistence of the image on the retina.

At this point, we should remark the temporal integration of the eye movement since signals are presumably integrated by the neurons in a capacitor like behaviour as shown in Figure II.3.

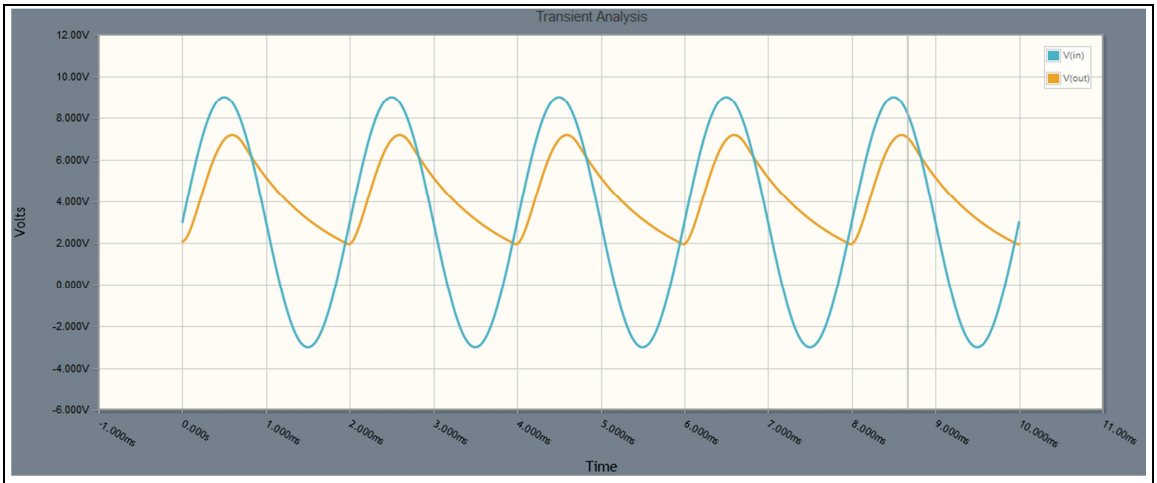

Figure II.3. Simulation of capacitor storing and releasing energy.

Even though the spiking frequency is dependent on the input voltage amplitude, these are transmitted to a next stage and an output signal is formed. This temporal behaviour can also be understood as a capacitor where the energy of the input is stored and the output frequency is reduced.

C. The method proposed

1. The hyperacuity by means of blur

a) Blurred image…Clear vision?

There have been classical theories that attempt to justify the hyperacuity with microsaccades and other effects, and, at the same time the integrating behaviour of sensors has been proven. The combination of both, microsaccades and the integrating effect of sensors, makes the captured image be a blurred image, which in principle is commonly seen as a problem, but nevertheless, is the way of achieving the hyperacuity the human eye. Furthermore, in this chapter, we incorporate yet another – perhaps the greatest of them – blurring factor, the diffraction of the pupil, which has always been present, but was not given appropriate attention.

We'll see how the fact of getting a blurred image at the output of the sensors (connecting with further stages of the HVS) is absolutely crucial to justify the hyperacuity.

b) The importance of being blurred

An immediate conclusion extracted from this fact is that, the distortion or blur created by all the blurring phenomena – including other chemical or physical mechanisms – conflate in a general distortion, and in consequence grant spatial diversity to the image system, apparently dodging the sampling theorem and naturally enhancing the capturing mechanism.

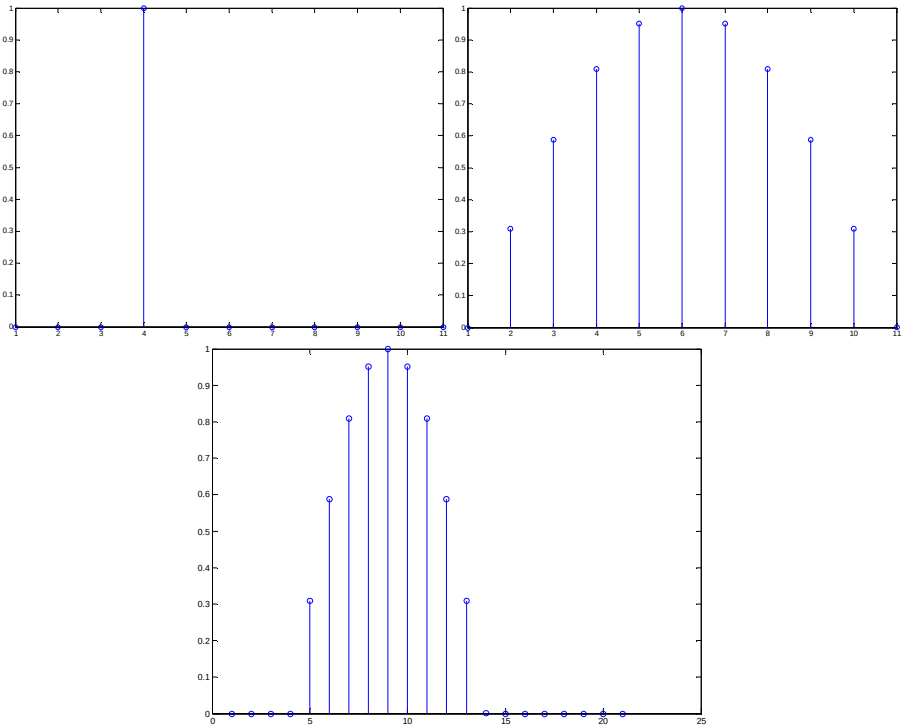

Figure II.4. A discrete delta – spectral line – (upper left) is convolved with a raised cosine like signal (upper right) which result is shown in the picture in the bottom.

A paradigm of this distortion is that a discrete (delta-like) line – or spot depending on the working dimension – is transformed into a squared *sinc* or Airy Disc type pattern, which means that every single point is captured by many sensors or photoreceptors.

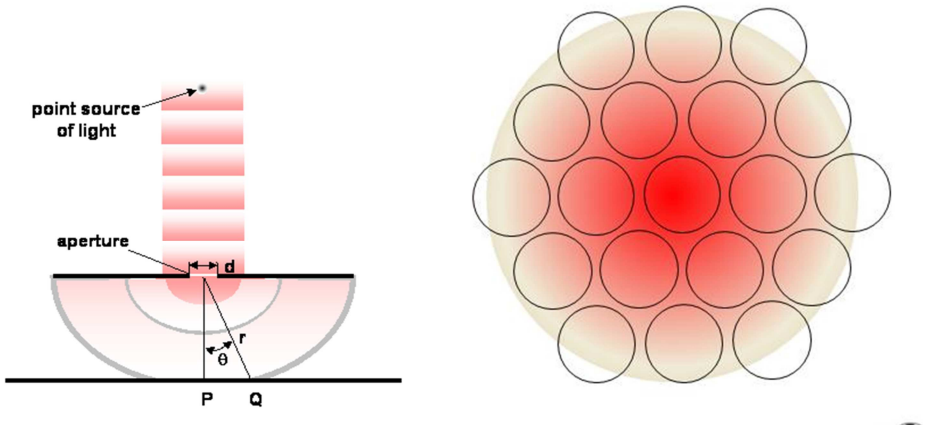

Figure II.5. Plane wave diffracted by an aperture (left).
Figure II.6 photoreceptors capturing the projection of a single point (right)

In other words, the information of one photon is effectively spread over some area, by any or all of the mechanisms explained. In a rough estimation, a pupil diameter of 3 mm could produce a diffraction blob covering 19 photoreceptors, as depicted by Figure II.6.

The important conclusion at this point, is that all sources of distortion can be additive and follow a specific mathematical model.

c) Basis for a known distortion

The starting point is that in natural visual conditions, the image projected onto the retina at the focal plane of the eye lenses (cornea and lens), is a blurry image – rather than a sharp and clear one –. This can also be modelled as a direct low-pass filter.

These stages simulate a real world process where a signal from the continuous domain is sampled by the photoreceptors; actually, the decimation models the sampling process in the retina.

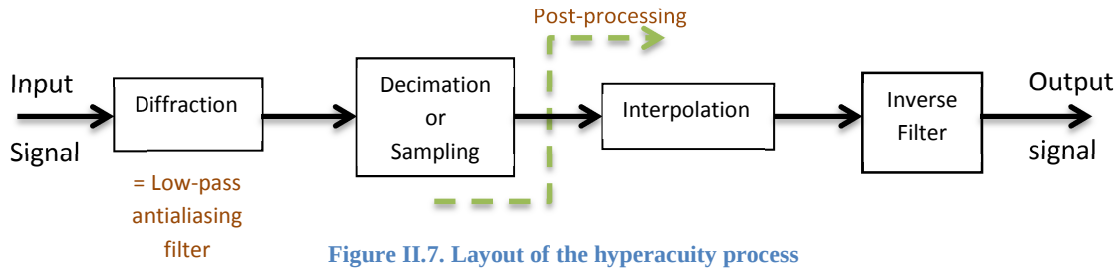

Figure II.7. Layout of the hyperacuity process

Post-processing could simply consist of an interpolation and filtering or deconvolution, perfectly achievable with a neural system.

The step of interpolation is carried out somewhere in the neural system – as will be discussed later – and in our model can be performed by means of different techniques, but basically the idea is to fill the gaps out of subsequent points. There, new samples may be created because it is a slowly varying function.

At the last step, the inverse filtering is the key for obtaining a high-resolution, thereby high visual acuity is achieved.

The question to be solved in next sections is how the widespread information can be gathered or collected in order to display all captured points with increased angular resolution. The answer may come from the steps depicted by Figure II.7, equivalent to the following Figure II.8.

We will see in the next sections that the human eye, thanks to that pre-filtering with the aperture of the optical system, could be performing some kind of post-processing operation to enable hyper-acuity.

2. A deeper look into the phenomenon of diffraction

The diffraction created by the circular aperture in the human eye was first studied by George Biddell Airy, who published an article about this 1835. This was anyway already described by the astronomer John Herschel in 1828.

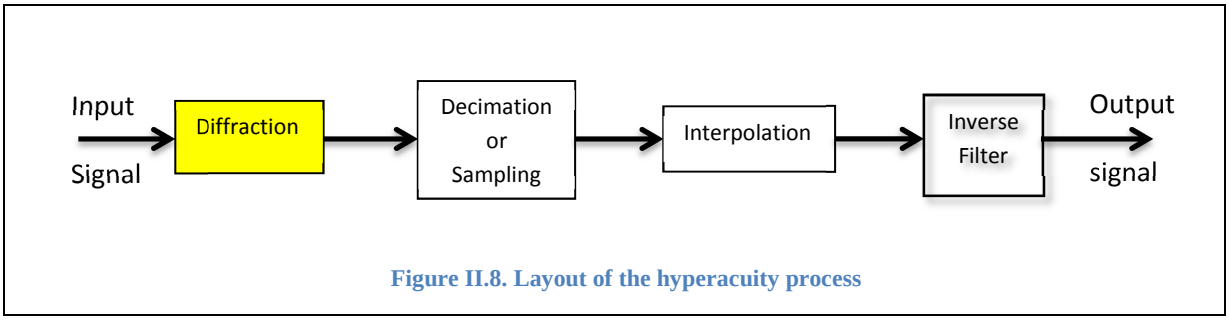

Figure II.8. Layout of the hyperacuity process

The projection of the diffracted image (signal) – has to be said – is not altered in magnitude or angle in our case by the existence of additional optical lens stages – notably the cornea and the lens –.

The incident light entering the system goes actually through multiple obstacles, mainly a circular aperture – pupil, iris, cornea, and lens – which results in a distortion – known as the Fraunhofer Diffraction – described by the Huygens-Fresnel principle. These laws explain how some points of the incident wavefront become sources as they are superimposed when the wave hits an aperture or slit.

In the particular case of a circular aperture, the effects can be modelled by the Airy Disk pattern, which requires a double integration over the surface of the aperture. This problem was first solved by Sir George Airy in 1835 and the solution is obtained in terms of Bessel functions of order unity. This function is given by

$$I(\theta) = I_0 \left(\frac{2J_1(x)}{x} \right)^2 \tag{2.1}$$

The I_0 is the peak irradiance of the pattern which can be measure at the centre of the spot and the $J_1(x)$ refers to the Bessel function of first order defined by

$$J_1(x) = x \sum_{n=1}^{\infty} (-1)^{n+1} \frac{x^{2n-2}}{(n-1)!n!2^{2n-1}} \tag{2.2}$$

where x is defined as

$$x = \frac{2\pi \cdot a}{\lambda} \sin\theta = \frac{\pi \cdot d}{\lambda} \sin\theta \tag{2.3}$$

and it represents the position on the image plane where a represents the radius of the aperture and d the diameter, λ the wavelength, and θ the angle described. Let's note this case is for a uniformly illuminated circular aperture and shows its far-field irradiance distribution.

This diffraction pattern is shown in the figure below, and as can be seen, there are concentrically surrounding rings, which are the result of the side-lobes of the Airy Disk, the PSF (Point Spread Function).

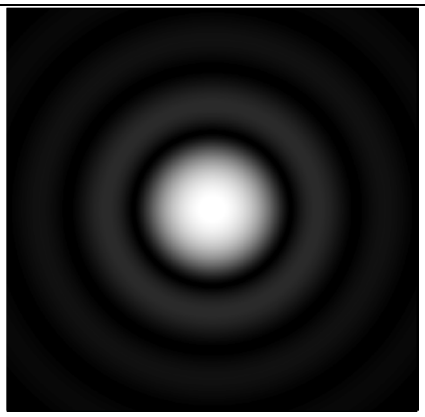

Figure II.9. Computer generated Airy Disk

This pattern has its maximum in the central direction $\theta = 0°$ and the distance from the lobe's peak to the first minima are located at $x=3.832$ (where it matches the first zeroes of Bessel's first order equation). Thus, from eq. (2.3) arises that the separation angle of the first minima are given by

$$\alpha \approx 1.22 \lambda / d \tag{2.4}$$

as it observes dependency on the wavelength (λ) and diameter (d) of the aperture.

A visual conclusion from the previous explanation is that the diffraction makes a single point become spread in several points, as better represented by the Figure II.5 and Figure II.6

In this sense, it is to be denoted that most of the energy of the diffracted point is kept in the main lobe which means that only a few photoreceptors capture the greatest part of the energy of the original signal.

As we may notice, plane cuts of an Airy Disk and a squared *sinc* (Figure II.10) are very similar and observe similar behaviours in the time-space axis. In addition, side-lobes stay in general below the detection threshold, which makes the detected signal resemble even more any of the models exposed.

So, as a model for the diffraction a squared *sinc* function can also be used. This in fact represents the diffraction pattern created by a slit aperture and is a function of spectral power density and observes a similar behaviour for signal processing, but implies less computational costs when generating a test model.

In order to process these signals, as we remark, a squared *sinc* type function can be used. Actually, a simplistic one dimensional signal may be of use for these purposes

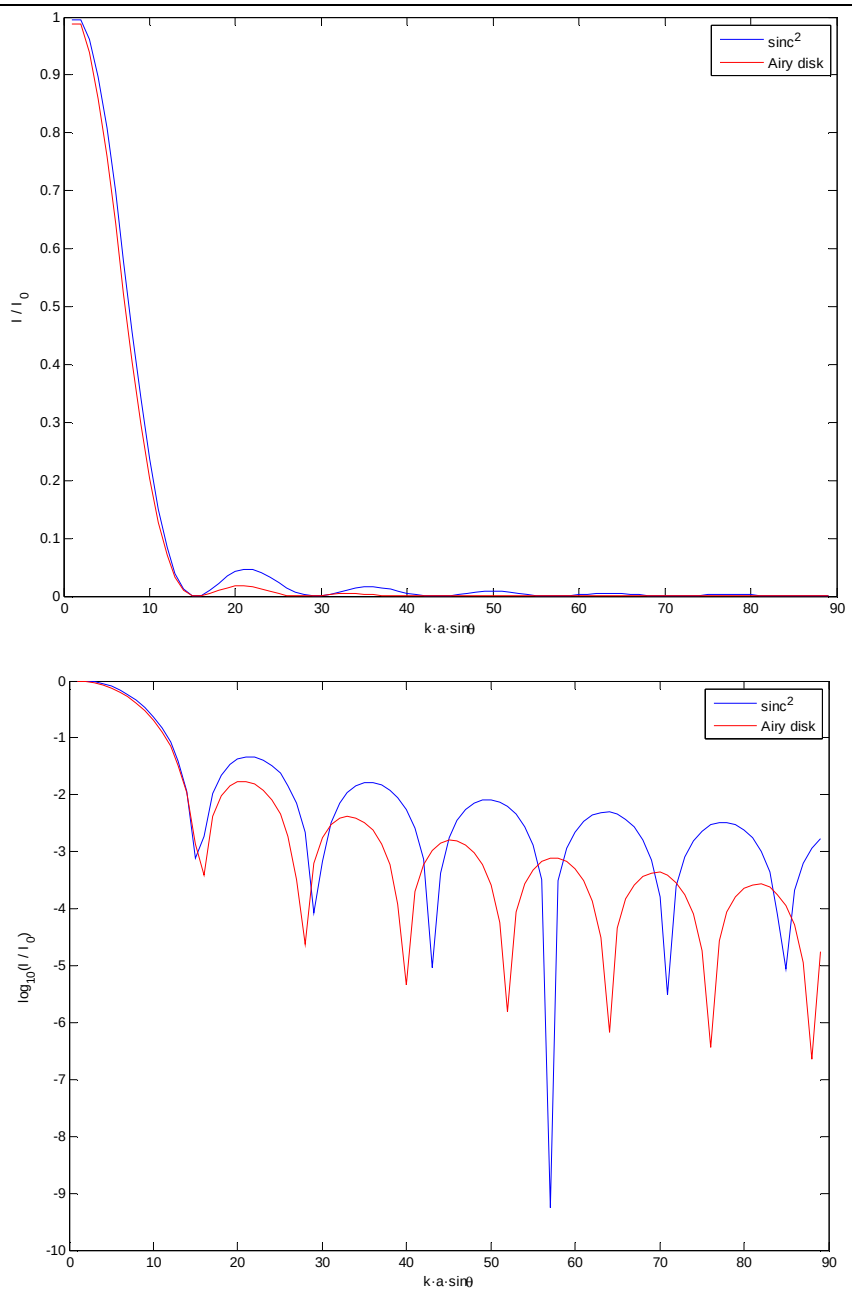

Figure II.10. Superimposed functions; Traced in linear scale at the top and in logarithmic at the bottom. Airy disk (blue) and sinc^2 (red)

Summarising all the effects of the aperture, the human eye pupil and optical system, the overall process can be understood as a low-pass filter, and modelled by a convolution yielding

$$y(m,n) = x(m,n) \otimes h(m,n) \tag{2.5}$$

Where *x(m,n)* stands for the points of the original object, *h(m,n)* expresses the PSF (Point Spread Function) of the aperture and output of the equation *y(m,n)* gives the values of the image projected over the retina. The eye in fact undergoes this process and definitely the result is to capture a blurred signal by the photoreceptors in the retina.

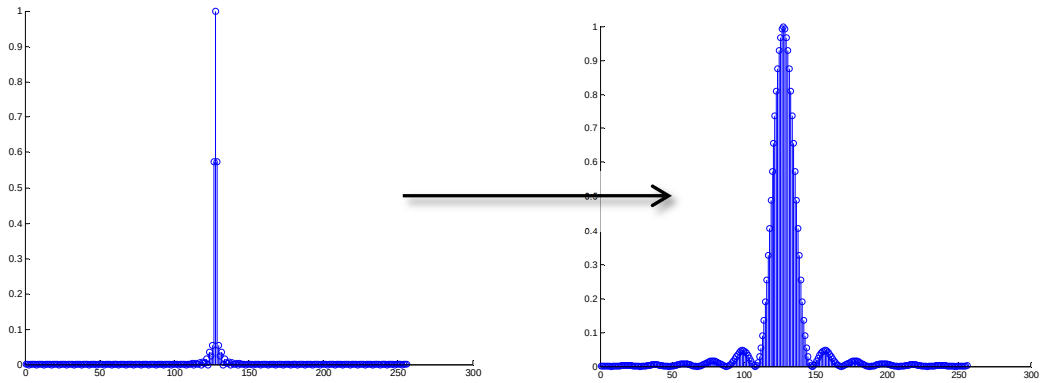

Figure II.11. Undistorted or unfiltered delta-like signal (left) and low-pass filtered version (right).

The so-called filtering process converts each point – this can also be described or understood by the convolution process – in multiple points, as shown in Figure II.11 and also shown in 2D in Figure II.9.

On another hand, the use of low-pass anti-aliasing filters is a standard procedure at any one-dimensional sampling mechanism, e.g. DSPs, samplers, spectrometers, signal analysers…. In fact, the diffraction can also be seen as an anti-aliasing low-pass filter. Nevertheless, the use of any pre-filtering or low-pass anti-aliasing filter in imaging systems is so far uncommon.

3. On the Sampling Process

The sampling theorem –despite widely known as the Shannon-Nyquist theorem – in honour of the truth, was first discovered by Vladimir Kotelnikov in 1933. It describes how a band limited continuous signal should be sampled in order to represent all its information accurate and faithfully in a discrete sequence.

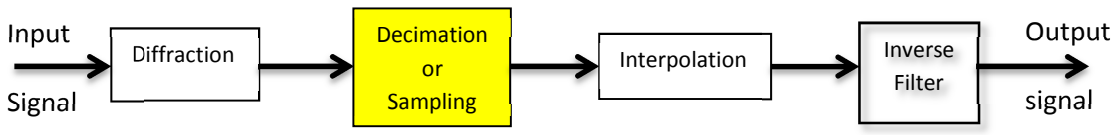

Figure II.12. Layout of the hyperacuity process

A very important regard on the sampling issue is that prior to the diffraction filtering, the sampling of a delta like function such as shown on the left side of Figure II.11 is impossible, since a delta function's frequency, as it is known, covers all frequencies from $-\infty$ to $+\infty$ which makes sampling unfeasible due to the impossibility of sampling at twice the frequency of that signal.

The summarised version of the sampling theorem, often referred to as the Nyquist criterion, sets as a condition the sampling frequency to be used by a signal as

$$f \geq 2 f_0 \tag{2.6}$$

This means that two samples are required per cycle, where these cycles are determined by the fundamental period of the highest frequency of the signal. A more detailed explanation is given in the next chapter, by now we will only focus on the fact that a discrete version containing all the information should be the continuous one sampled following this criterion.

The previous filtering process, is actually diffraction produced by means of the optical aperture, and expands the signal in time (or space, depending the magnitude) thus granting more chances to sample the continuous signal. It is of our interest to be more specific about the relation between the sampling criterion and the filter itself, but as it might be understandable, the ongoing filtering process varies in function of the pupil aperture and the specific distribution at sampling.

Simple sampling or discretisation of a continuous one dimensional signal can be describe by equation (2.7) as

$$x_d[n] = x_c(nT) \tag{2.7}$$

where x_c stands for the continuous signal which is sampled at n integer number discrete locations of T time periods, represented by the discrete sequence x_d. In our case though, we have developed our hyperacuity model based on an initial digital, discrete image. Therefore, we have rather used the similar decimation paradigm,

$$x_b[n] = x_d[nN] \tag{2.8}$$

Here, the already discrete sequence of data x_d (signal, image) is subsampled at an N integer number of samples given by the integer variable n. This entails an expansion of the data in the frequency domain. Anyway, there is an important aspect to notice about, which is the anti-aliasing filter. This filter, represented as $H[k]$ in the illustration below, removes the repetition of the signal patterns related to subsampling.

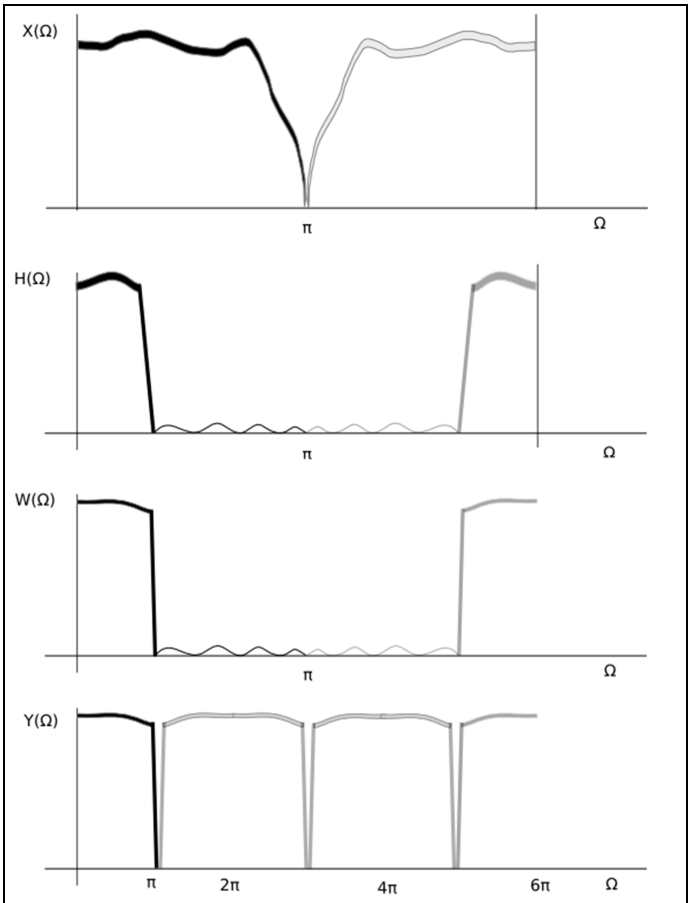

Figure II.13. Decimation process in a one-dimensional signal (existing signal-strong black, filtered signal-grey). Original signal (a). Diffraction-filter (b). Result of filtering the signal (c). Decimated signal (d).

In the example of Figure II.13, the signal $X(\Omega)$ – depicted in the frequency domain with the discrete pulsation $\Omega = \frac{2\pi k}{N}$, being N/k the points per period at the given sample rate –is filtered with the $H(\Omega)$ anti-aliasing filter – which yields $W(\Omega)$ – preventing aliases and this is in turn decimated by a factor of 3 resulting in $Y(\Omega)$.

Although the diffraction acts as an anti-aliasing filter, we should note that the cut-off frequency of this filter is by far below – stricter – a simple anti-aliasing filter. This can be seen on the fact that the diffraction pattern is characterised by more samples than the minimum (2 points/cycle) dictated by the sampling theorem, as shown in Figure II.6.

Even in the case of a signal captured at a sampling frequency below the fundamental frequency of the signal (prior to diffraction-filtering), the sampling criterion could be adapted to the 'new' sampling frequency of the filtered signal (related to the cut-off frequency of the filter). We will see this in greater detail in the next section.

4. About the Interpolation in the Human Eye

Given the sampling layout explained, we can understand that the final image or signal we intend to compose at the output of the system (e.g. visual cortex) will be of greater

detail – it will contain many more samples or points – which means that at some point it is necessary to increase the number of points in order to increase the level of detail or visual acuity in the HVS.

The stage of interpolation can be noticed in Figure II.14 followed by previous stages as diffraction and the signal capturing process.

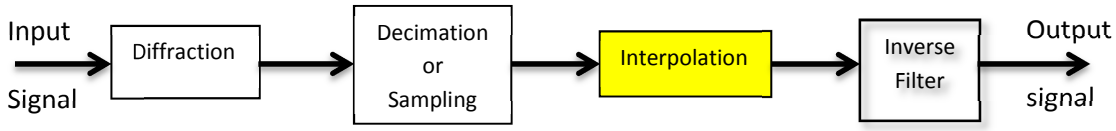

Figure II.14. Layout of the hyperacuity process

Therefore, it is considered that the human neural system performs an interpolation process somewhere in the HVS, possibly at the LGN after some authors.

The figure below shows how the neural interpolation adds points, but this shouldn't fool anyone; any interpolation process, just itself adds or creates no information. No information is suppressed or lost either. But more points are added in an integer factor of 'L', which grants the human visual system with higher resolution (more points) and rather accurate data on new intermediate points. Additionally enables inverse filtering

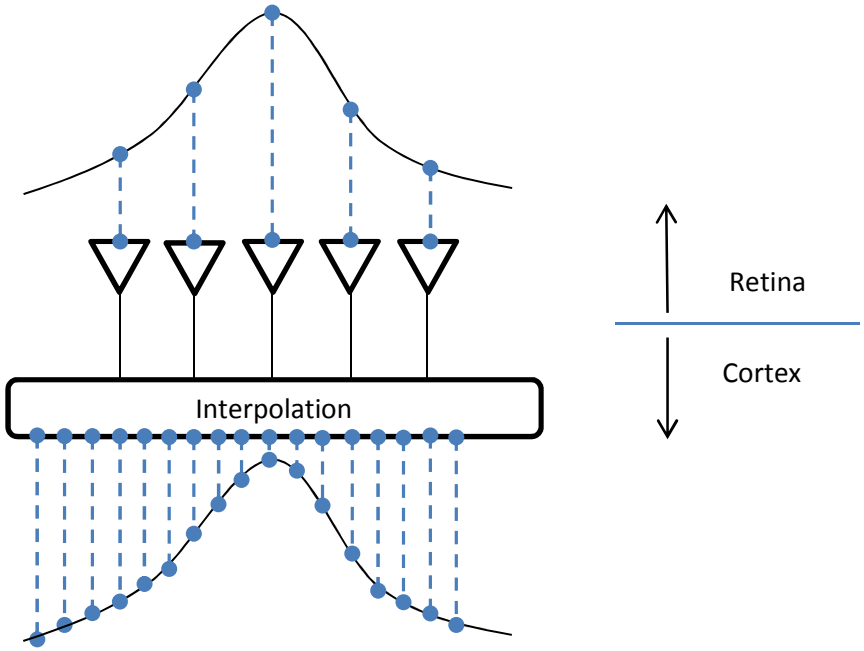

Figure II.15. Illustration of the concept of interpolation.

the interpolated signal in order to achieve a higher acuity.

The process of interpolation is actually a procedure that translates or relocates frequencies, and is generally used in signal processing to change the sampling frequency. This time, it can be seen how the signal is collapsed in the frequency domain, which – again – does not necessarily mean or involve any loss of information, but actually, thanks to this contraction of the spectrum, we handle more easily the recovery of information located at the high frequencies. The interpolation factor sets the magnitude of frequency translation of the signal where the sampling frequency is multiplied by the interpolation factor.

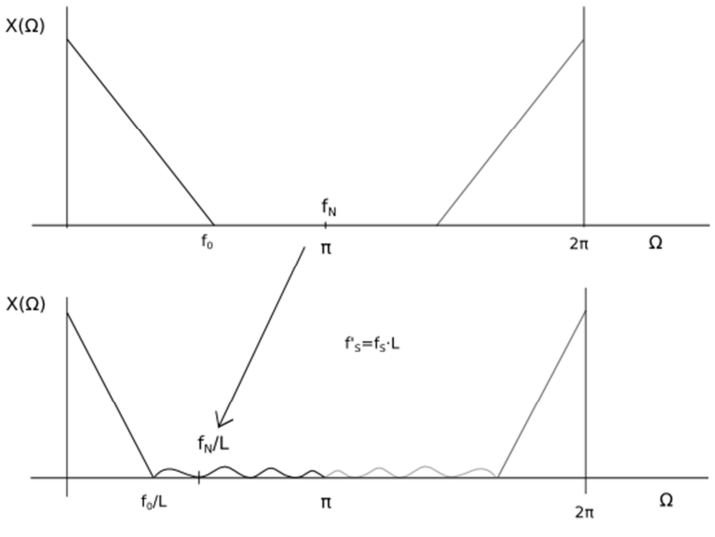

Figure II.16. Frequency translation in the interpolation process in one-dimensional signals.

From Figure II.16 can be understood that the high frequency band can be more easily processed as a result of the sampling frequency translation because they will be located at positions below the more strongly attenuated by the diffraction.

Several interpolation techniques exist which yield different results on each kind of task or estimated function.

5. On the process of inversion-deconvolution

Recovery of "lost" high frequencies is our most immediate goal at this step of inversion, in other words, revert the effects of diffraction which is our inverse problem, that is to say, resolution techniques of inverse problems aim to recover "hidden" or nearly lost data from an input or source of information.

It is worth to mention that any of the previous steps would be useless without an efficient inversion or deconvolution of the signal. But once the previous steps have been completed, the inversion-deconvolution should be computed. Therefore, a variety of methods exist that can be of help in order to compute the inverse of a given model, data or function, but there is neither unique nor general solution for this.

This last stage is crucial for the hyperacuity process, since it will relocate the spread information (blurred) back to its original spatial position. This process involves the use of an inverse filter – or deconvolution – which result, as we say, returns the high resolution image, as depicted by Figure II.17.

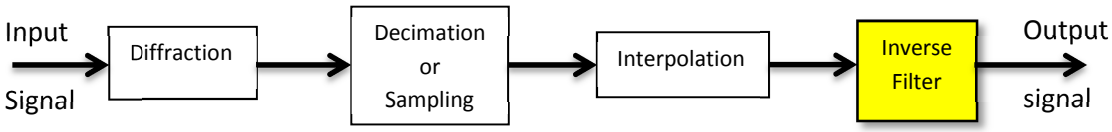

Figure II.17. Layout of the hyperacuity process

At this step, we should bear in mind that there are mathematical constraints like noise and near-zero values which complicate the process. The filtered – or blurred – signal suffers from a great attenuation from the sampling frequency upwards, so there can be noise and attenuation issues to deal with too.

We should not forget that the human visual system solves any of the possible related problems and could be performing some kind of deconvolution by means of its biological neural networks. We will discuss about the feasibility of all steps commented so far including this one in further sections of this chapter.

Above all, it should be remarked that inverse problems as such constitute a whole field of study, which means that there is vast literature written about several approaches to different problems and solutions of inverse problems. Anyway, at this point we do not intend to dig deep into any specific technique. Therefore, we will deal with this subject deeper in the next chapter.

6. Summary of the entire process

We may summarise the four steps of the process and have a whole view of it in the diagram shown below (Figure II.18) in the frequency domain.

At the first stage the image is diffraction-filtered, which comprises a low-pass band and an attenuated high band. These bands are present at the sampling (in our model decimation) stage but there, the number of captured samples transforms the spectra and rescale frequencies fitting the Nyquist's sampling rate. Thereby the frequencies above the sampling threshold are lost.

The interpolation stage expands the signal in frequency including the attenuated band and hence the information of those components is relocated and can be restored at a next step.

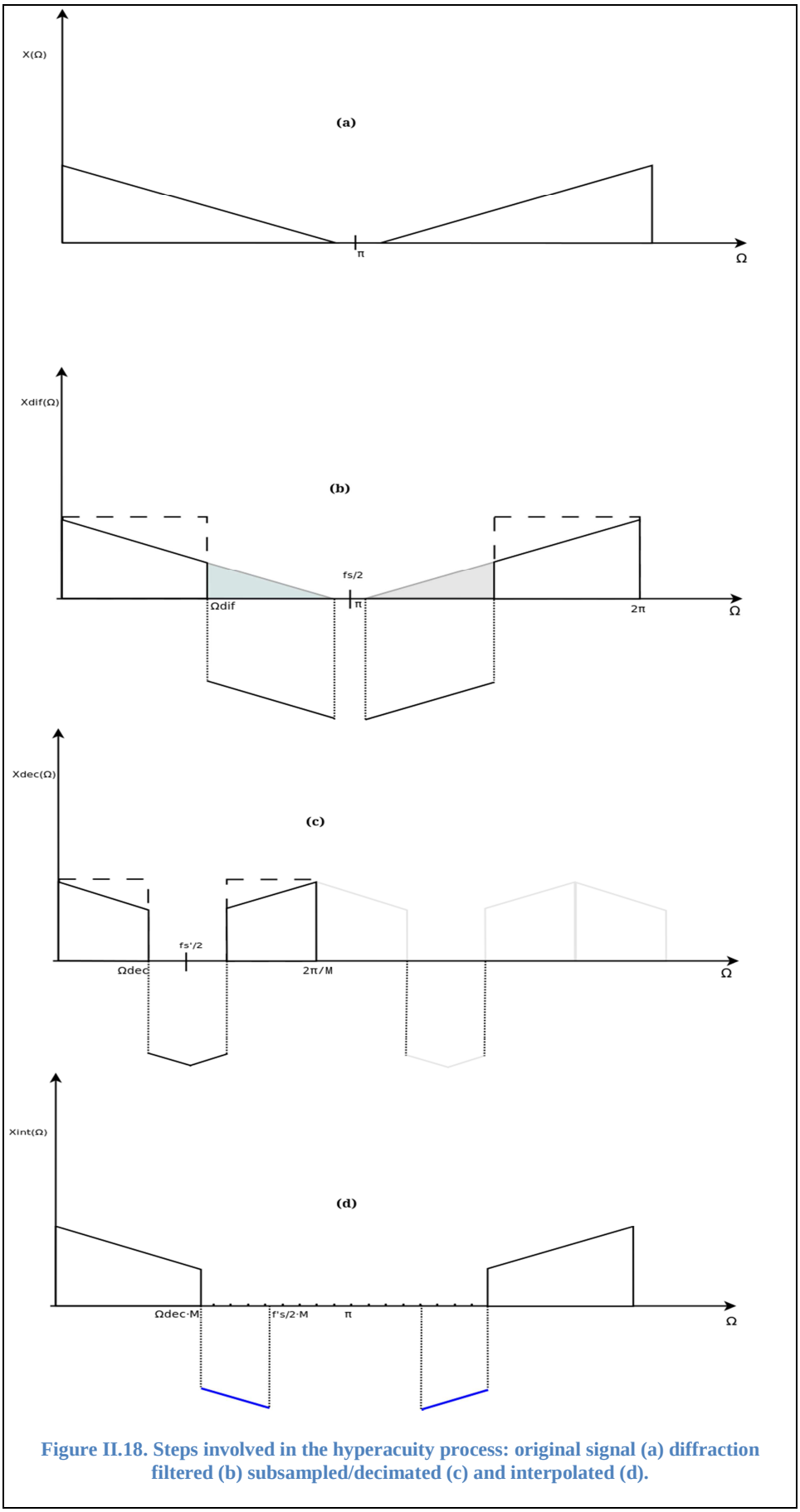

Figure II.18. Steps involved in the hyperacuity process: original signal (a) diffraction filtered (b) subsampled/decimated (c) and interpolated (d).

D. Other considerations: the pupil aperture and visual acuteness

In connection with the diffraction mentioned in the previous section, some authors think that the visual perception hence angular resolution should be higher for large apertures of the iris. This belief is based on the fact that the diffraction blur is lower at big apertures than at small apertures. So, according to some authors the acuity should be theoretically increased when pupil diameter increases due to the narrowing of the Airy disk (Westheimer 2009, James Drever 1972, Bille, Harner et al. 2004). But since in fact this does not happen, they consider that optical aberrations could counteract this enhancement preventing better resolution.

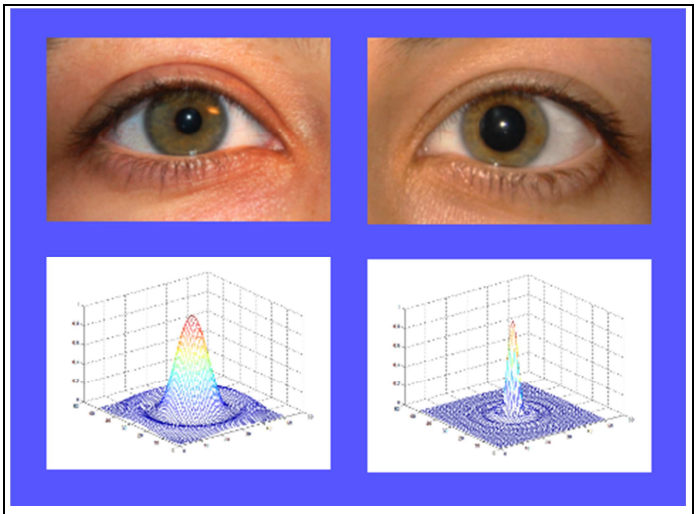

Figure II.19. Myotic pupil (upper left) and corresponding diffraction below. Mydriatic pupil (upper right) and corresponding diffraction below.

A fact that seems to be in conflict with the belief of a possible better acuity for large pupil apertures is that daylight exposure images are perceived as more accurate, with high definition, i.e. which seems to be at odds with the existence of a large pattern of diffraction created as a consequence of the constriction of the iris (Figure II.19). In half-light exposure though, as the aperture is increased, the diffraction pattern is notably reduced as well as the resolution becomes worse.

Interestingly, a pupil diameter increase has the effect of reducing diffraction blobs and therefore spatial diversity. Anyway there may be a trade-off (Donnelly III, Roorda 2003) between the spatial diversity obtained thanks to the diffraction and the hypothetical cut-off frequency (corresponding with the diffraction filter), and the decrease of the captured power by the photo-sensing cells, as the pupil becomes smaller. Although higher diffraction involves greater diversity, probably the idea of an unlimitedly smaller pupil for a higher acuity is wrong. In any case, it is difficult to know whether the acuity at certain pupil diameters is innate or is acquired (Campbell, Gregory 1960).

We remark in this context that the constriction and expansion of the iris is a natural phenomenon in the eye. When an observer is exposed at an intense light, the neural system sends signals to the eye ordering to close the iris (myosis), among other reasons to protect the retina from an over-exposition and prevent any damage. The contrary happens in low-light conditions, where the iris is expanded (mydriasis) in order to capture more light. In this regard, the diffraction pattern – Airy disk – is wide in the

myotic state (small apertures) and it becomes narrow in the mydriatic state (large apertures).

The controversy of the alleged negative impact of diffraction on angular resolution is very popular. Barlow in this sense states that spatial frequencies contained by the retinal image are limited by diffraction at the pupil to about 60 cycles per degree when the pupil is near its smallest (about 2 mm) in bright light and to lower values attributed to additional aberrations when the pupil is larger (Barlow 1979). Another publication attributes worse acuities for a constricted iris because the distortion originated by diffraction is bigger in this specific case (Marcos 2005). And in this sense, another publication (McLellan, Marcos et al. 2002) where the same previous author is included, states that "Wave aberrations cause the visual system to sacrifice resolution at a single wavelength but allow it to gain approximate constancy in spatial sensitivity across the spectrum".

Nevertheless, psychophysical experiments show that there is a mid-point regarding the optical quality and the aperture of the iris; authors in general pinpoint an optimal aperture between 2 and 3 mm (Campbell, Gregory 1960, Campbell, Gubisch 1966) which in our opinion might be due to a trade-off between the power of the signal captured by the photoreceptors and the diversity of the signal obtained thanks to diffraction.

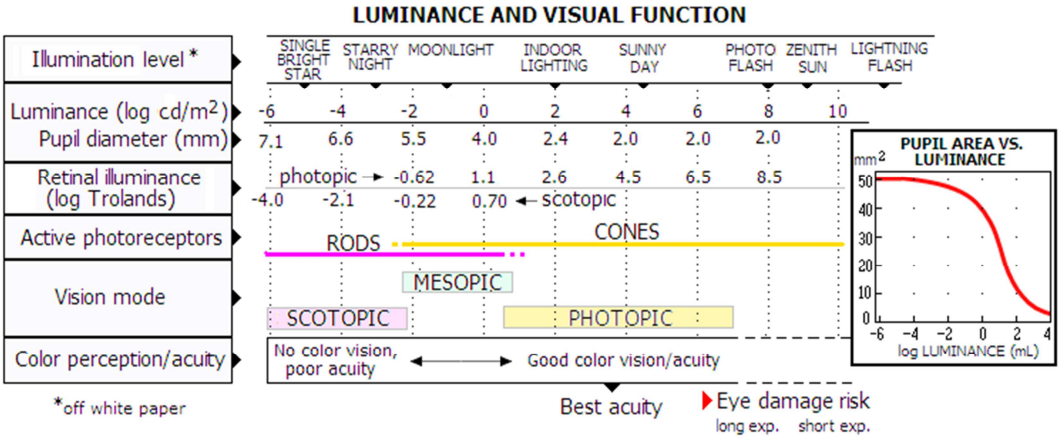

Figure II.20.Dependence of visual functions on illumination (Hecht 1924, Finkelstein, Hood 1984)**. (1 troland=1 cd/m^2 per area of 1mm^2). Credits: Vladimir Sacek**

In Figure II.20 visual functions at different scenarios are shown where the eye is exposed at different intensities of light, and as appointed, the best acuity is reached with photopic vision at an intensity level between 2 and 4 logarithmic luminance units. Cones anyway –unlike rods– are difficult to saturate before the steady and strong presence of light, achieving greater adaptability at both, neural and chemical level.

When the input power of the signal – intensity of light – is too high the HVS adjusts the iris i.e. changes the aperture to a narrower size. As a result of that constriction, the diffraction is increased and the power –at an extent– is kept rather constant. If the intensity of the light decays the aperture is increased and the power detected is in turn raised up to an expected level as shown in Figure II.21.

There seems to be a trade-off between the aperture of the iris – actual mid-point – and the magnitude of the power of the captured signal, which could also be explained by the minimum detection threshold that naturally sets the captured samples to the shape of the distorted signal i.e. a wider main lobe's amplitude is decreased in power and becomes similar to another narrower lobe of higher amplitude. Indeed there exist upper and lower boundaries regarding the optimal acuity; an optimal detection power level exists, whereas the existence of higher diversity (related to the increasing of the diffraction) is conditioned by the minimum power threshold.

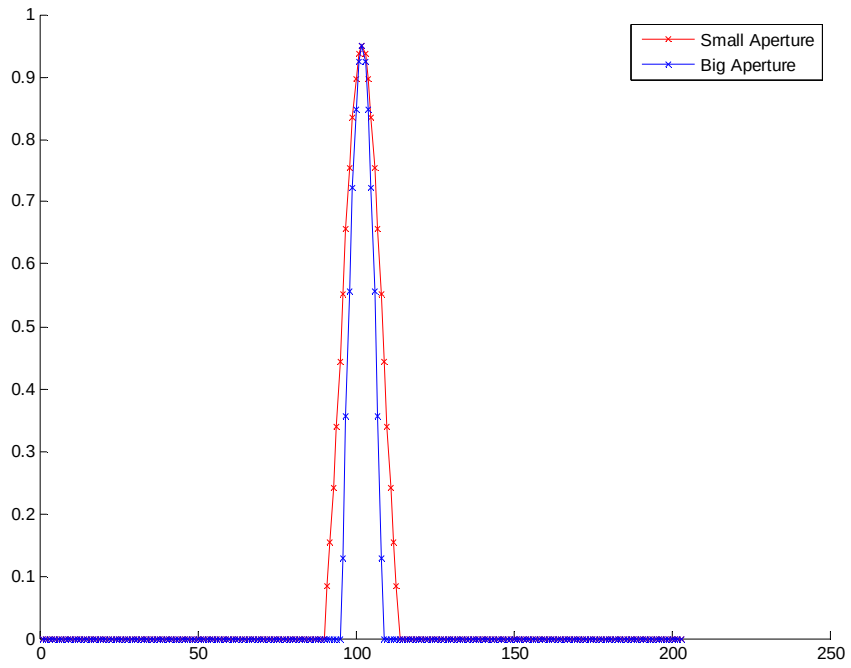

Figure II.21. Model of diffraction pattern in two different situations: the red plot stands for the small aperture of the iris and the blue one for the big one.

E. Biological feasibility of the unified theory for hyperacuity

As it has already been reported, hyperacuity mechanisms in the eye would be requiring some mathematical operations involving steps like spatial interpolation (Hirsch, Hylton 1982) and a subsequent deconvolution. In the human visual system deconvolution could be performed in a single layer of neurons, where the number of neurons equals retinal photoreceptors and every neuron is connected to several retinal cells (excited cells by a single photon), applying a threshold function. However, primary visual cortex (V1) is as well capable to implement these operations in its biological neural network. So by means of a single layer of neurons, the distorted image on the retina could be deblurred, thus increasing the resolution of the perceived image.

There are some advantages of getting an image blurred over the retina to be clarified afterwards, but the most important is that the robustness of the visual system is substantially improved because the information over the retina is redundant. By this method, it could be understandable that different types of cones and rods could be working together to define the fine details of the image in front of the eyes.

Thanks to the inherent coherence of the eye as a detector of photons this could be possible. The effect of a photon over the retina finally excites a set of photoreceptor cells, as it was justified above. The impact point could be identified calculating some kind of deconvolution, by means of its neural networks.

Besides the photosensitive cells, the two additional layers of neurons present in the eye could perform some kind of image processing to build a higher resolution image to be sent to the brain through the optical nerve. In case this was done in only one layer of neurons, there should be as many neurons as detecting cells over the retina such that every neurone was connected to several retinal cells (this number should correspond with the number of excited cells by a single photon) and an activation threshold function would be used as well.

So far, there are no evidences proving any signal processing scheme but only hypotheses. These approaches encompass all kind of alleged phenomena: temporal interpolation, spatial interpolation, information transmitted by chemical reactions…
It is to say our belief in the existence of some neural post-processing that allows humans to see with the acuity described in previous chapter is justified and proven by the fact of resolving beyond the alleged sampling capacity (number of photoreceptors). The big question remains – and at least for some time will – on how this is specifically carried out.

As some authors point up the neural system would be performing a spatial cortical interpolation which would in turn be impossible unless the image captured is sufficiently blurred. This means that in a one dimensional paradigm, information regarding a single point should be dispersed in at least three points (Westheimer 1976, Barlow 1979). One of these authors, states that interpolation can permit to determine the position of the peak of a curve (Barlow 1979). Anyway, we think in general the outstanding acuity in the eye has to be necessarily achieved by means of a blurring scheme (prior to the image capturing process).

Hirsh and Hilton state that spatial information is unpacked presumably at the cortical level by means of neural interpolation. They think of hyperacuity as an efficient strategy of encoding positional information whereas spatial information is sampled at sampling limit in the retina, but for both cases some interpolation stage is considered necessary.

As Hirsch indicated (Hirsch, Hylton 1985), in the central region of the eye or fovea, maybe after some convolution to remove low-frequency components, the signal is transmitted to the visual cortex.

Nevertheless, as dictated by Lex Parsimoniae (also Occam's Razor in actual days), the simplest explanation is often the most feasible. Thus the hyperacuity/super resolving scheme must be based upon some simple neural post-processing. The human neural system includes the ophthalmic system, where there are 2 layers of synapses. Thus the eye could be performing some neural pre-processing before the signals arrive to the LGN – where possibly some interpolation could be performed – and the rest of the signal processing could be performed in the visual cortex.

We can think of some convolution-deconvolution processing as a simple way to blur or sharpen signals i.e. to low-pass filter or high-pass filter signals. This simple processing could consist in an inverse filtering process, which can be undergone within two possible basic schemes in signal processing tasks, in the original domain or in the transform domain.

F. Conclusions

One of the indisputable and most important conclusions to extract from this chapter is that the image signal obtained by the photoreceptors is blurred, by different factors or sources of blur. A known source of distortion might be related to the micro-movements of the eye; as explained the eyes are permanently doing involuntary movements, which could create due to some mentioned features blur motion and another source of distortion as explained is related to the phenomenon of diffraction.

So, the eye uses blur to obtain the necessary spatial diversity which would justify the existence of the hyperacuity.

In this sense, no phenomenon other than spatial diversity can justify the perceived degree of details in an image visualised by the HVS due to the actual low number of photoreceptors. The important consequence of diffraction – and blur in general – is an acuity enhancing factor in the human eye.

There exist a belief that a source of distortion could be related to the coupling of cones and rods, which are connected to horizontal and bipolar cells; these may as well contact retinal ganglion cells on one side and amacrine cells and cones on the other. However, the fact is that this coupling effect does not increase the diversity because there is no additional information introduced in this process. In other words, the signal/image sensed by the photoreceptors might at following stages be altered, but no information is added.

It should be taken into account that so far many authors refer to diffraction as a resolution limiting phenomenon, while others including the author of this research give evidences of being an image resolution enhancer. In this document, results show that diffraction could be the human eye hyperacuity enabler.

Actually, interpolation could be an intermediate step such that the limited number of captured points is transformed into an extended number of points which would permit a post-processing or deblurring neural mechanism to obtain a high resolution and sharp image.

In the context of signal-processing, the pre-blurring and interpolating steps together can also be seen as a process of analytical continuation. First, the pre-blurring mechanism prevents any alias from being captured and superimposed at low-frequencies, and second, the spectrum obtained is collapsed by interpolation, where high frequencies are pulled back below the Nyquist frequency.

Chapter III. From the visual acuity to the Inverse Problem

A. Introduction

As we saw in previous chapters, the Human Visual System gets a blurred image projected on the retina, which after some neural stages is deblurred by some neural computation which enables hyperacuity. This process involves some kind of recompilation or reorganisation of the data (image) which is supposed to be scattered as shown by Figure II.6, i.e. it is an inversion of the direct process. The problem of inversion – the inverse problem – is itself founded as a research field and is widely known, studied and used in many areas and applications because of its great contribution related to the information restored from blurred or partially lost original data.

In 1929 Viktor Ambartsumian published the first known work on inverse problems when he found a relationship in differential Sturm-Liouville equations between eigenvalues and the energy levels of atomic structures. The anecdote is that his pioneering paper, written at the age of twenty, sunk into oblivion because in his words – as an astronomer – he published his mathematical findings – with mathematical contents – in a physics journal.

Inverse problems are some of the most important and well-studied mathematical problems in science and mathematics. Using the observation of the data (d) generated (G) by the model (m), they seek to find the one matching best those data

$$d = G(m) \tag{3.1}$$

They are usually classified into two main groups: linear and non-linear problems. This classification refers to the nature of the inverse problem, instead of the direct one.

In the case of linear problems, the use of linear functional analysis and algebra may provide rather accurate results and efficient algorithms.

Non-linear problems are more difficult, and there are less general results. Anyway, our subject is not related to this kind of problems so we will not go deeper into this field.

Due to the incompleteness – often defined as ill-posed – of the problem and additionally with usual presence of noise, no exact solution exists but any method that brings about any recovery of the original model are highly appreciated. The case of the eye is especially important as it reveals the existence of an exact, stable and robust solution.

Regarding the general inverse problem, there are a myriad of applications or fields where these play a key role. The list of applications using and needing a solution for such a problem is almost endless, but we may cite some, maybe the most popular:

- Sound imaging, submarine sound exploration
- Radar systems, radar imaging
- Communication systems.
- Antenna measurements. Antenna imaging systems.
- MRI and other medical exploration systems
- Geophysics. Seismology. Hydrogeology
- Chemistry

- General Thermodynamics
- Microscopy.
- Astronomy.
- …

All these applications deal at some point with the issue of reversing the effects of distortion created by a system generally with noise.

There are different classifications based upon different factors or features regarding nature of the inverse problem but we will explain them in function of the domain of analysis: time-space or frequency. This does not entail further implications than its applicability for some of the methods explained in subsequent sections.

In this chapter, we will first introduce the direct problem and show the matrix form due to its mathematical appropriateness. In connection with this, the use of linear functional analysis and algebra provides rather accurate results and efficient algorithms. A tool used is the singular value decomposition of the considered operator which we will study in detail as a regularization method, consisting in transforming slightly the problem studied into one that has improved properties.

We will next focus on the inverse problem itself and importance derived from the Human Visual System. Afterwards, we will review existing methods, ordered with the criterion of the working space-time or frequency domain, and how they can be used to find a solution.

In this sense, we intend to show a mainly practical overview of different methods but specially focusing onto those which are found to be most successful. An interesting consideration in this regard is the mathematical resemblance of some of the analysed mathematical procedures and alleged phenomena ongoing in the eye, which results are meaningful and promising.

B. Definition of the direct problem

1. Layout

Our problem itself consists in a filtering process. A signal goes through a system (filter) which is the known part of the process together with the approximated description of the system. In fact, any filter is represented in a regular basis by an *h(t)* as a system with an input and an output.

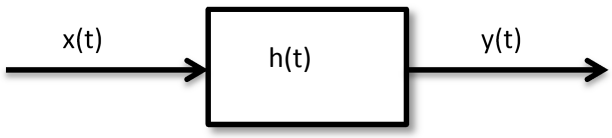

Figure III.1. Filtering process

This process can be defined by a convolution process and is expressed as

$$y = x \otimes h \tag{3.2}$$

2. Convolution

An input signal is convolved by a filter as the following equation defines:

$$y(t) = x(t) * h(t) \overset{\text{def}}{=} \int_{-\infty}^{\infty} x(\tau)\, h(t-\tau) d\tau \tag{3.3}$$

A similar equation expresses the ongoing process for discrete sequences in one dimension:

$$y[n] = x[n] * h[n] \overset{\text{def}}{=} \sum_{m=-\infty}^{\infty} x[m]\, h[n-m] \tag{3.4}$$

The convolution process involves multiplication and summation of sequences. Actually, we may achieve similar or same result, as the convolution theorem states:

$$\mathcal{F}\{x * h\} = k \cdot \mathcal{F}\{x\} \cdot \mathcal{F}\{h\} \tag{3.5}$$

The constant value k may change upon the exact definition of the normalised Fourier transform.

3. Matrix form

It might be interesting to express this convolution process in the matrix form. Therefore, let $\overline{\overline{h}}$, $\overline{y}$ and $\overline{x}$ be the matrix and vector forms of the convolution process. Thus, we may express this convolution with the direct filter as

$$\overline{y} = \overline{\overline{h}} \cdot \overline{x} \tag{3.6}$$

For which we have the one dimensional discrete convolution of a signal *x* with a filter *h* expressed as follows

$$\underline{y} = \overline{\overline{h}} \cdot \underline{x} = \begin{pmatrix} h[0] & 0 & \dots & 0 & 0 \\ h[1] & h[0] & \dots & \vdots & \vdots \\ h[2] & h[1] & \cdots & 0 & 0 \\ \vdots & h[2] & \cdots & h[0] & 0 \\ h[m-2] & \vdots & \cdots & h[1] & h[0] \\ h[m-1] & h[m-2] & \vdots & h[2] & h[1] \\ 0 & h[m-1] & \cdots & h[m-3] & \vdots \\ 0 & 0 & \cdots & h[m-2] & h[m-1] \\ \vdots & \vdots & \vdots & h[m-1] & h[m-2] \\ 0 & 0 & 0 & \cdots & h[m-1] \end{pmatrix} \begin{pmatrix} x[0] \\ x[1] \\ x[2] \\ \vdots \\ x[n-1] \end{pmatrix} \tag{3.7}$$

The dimensions of matrix $\overline{\overline{h}}$ are $(M+N-1)xN$. It is actually a non-square matrix, with more equations than parameters (unknowns) which is not strange since the result of the convolution is longer than the original vector. Among all equations involved in this system, some are linearly independent which form a non-orthogonal base, on the basis of which, can be formed the rest by linear combination, and as there are more rows than columns $M+N-1>N$, the system is overdetermined. The inverse will be a non-square matrix as well, but in this case with fewer equations than unknowns generating a undetermined problem or with infinite different solutions and very unstable.

In addition, in any real world process noise exists which represents a serious add-on constraint to the problem of inversion.

C. Definition of the inverse problem

1. Initial approach: theoretical considerations

In the previous section, we exposed how this signal processing scheme can be carried out in the frequency domain and that the resulting from the inversion of the filter in this domain was a division of matrices arising from eq. (3.6). This operation can be defined as ill-posed, and we will see now why.

A well-known book (Hadamard 1923) published in 1923 explained the new concept of well-posed problems. It noted that a well-posed problem had to observe these conditions:

- Existence of the solution.
- Uniqueness.
- Continuous dependence on data.

Even though a problem can be well-posed, it can be ill-conditioned. In this case, small changes at the input would make a highly changing output.

Inverse problems do not fulfil at least one of the three conditions stated above but that does not necessarily mean they cannot provide important information and results. In our case the direct filter (H) might represent the PSF of the aperture diffraction. The inverse of this represents a fake or imaginary inverse filter recovering the original signal. In this regard, such an optical device represents the direct filter and it is a matter of fact that the inverse filter is somehow carried-out by the HVS, because the information cannot be invented beyond the captured by the photoreceptors.

From another point of view, some rules are required for band limited signals, but strictly speaking, in theory, under certain conditions analytic extension is possible for all signals, which means that subsampled signals in some cases can also be fully represented by a discrete version.

The underlying mathematical fundamentals about the feasibility of an inverse filter which would undo the distortion created by diffraction are described by analyticity. There are two main theorems about that:

- Theorem 1. The two-dimensional Fourier transform of a spatially bounded function is an analytic function in the (u,v) plane.
- Theorem 2. If an analytic function in the (u,v) plane is known exactly in an arbitrarily small (but finite) region of that plane, then the entire function can be found (uniquely) by means of analytic continuation.

We actually capture a part of the information in the retina. This is a diffraction blurred image, and from these theorems it arises that if – in absence of noise – we can reconstruct a part of the spectrum with that captured information, then we can resolve or obtain the rest of the spectrum by analytic continuation. This means that if we get the whole spectrum, we can obtain the whole signal or image.

2. The inverse problem related to linear-filtering

Inverting a process so as to restore the original signal $x[u,v]$, has been a goal since the publication of a document in 1952 informing on this possibility (Elias, Grey et al. 1952). Two years later, the problem of the zero or near-zero values that may appear within this procedure was noted by other authors (Bracewell, Roberts 1954) which may lead as well to mathematical indetermination. Regarding noise amplification issues, Harris published some works describing this and as well as Jones and Misell. In 1971 Arsenault and Genestar proved and verified that despite the existence of zeroes in the transfer function the inverse filtering is actually feasible (Arsenaul.H, Genestar 1971).

Any inverse filter may require amplifying attenuated frequencies to the extent of putting them back to the magnitude they were before they were direct-filtered. As it can logically be understood, it is impossible to recover all frequencies – from zero to infinite – but the challenge is to recover as most frequencies (or information) as possible. In some cases the PSF or blurring mechanism has no inverse or has near-singular values. Furthermore, possible solutions to the inverse are highly sensitive to noise and variations on the original signal (Figure III.2).

$$y[n] = x[n] * h[n] + \eta[n] \tag{3.8}$$

The diffraction phenomenon described in the previous chapter, acts as a low-pass filter. This filter can be depicted in frequency as seen in Figure III.2.

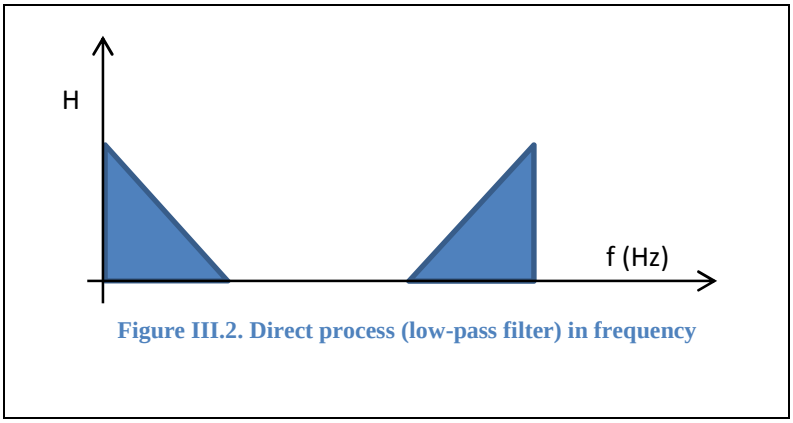

Figure III.2. Direct process (low-pass filter) in frequency

This means that low-pass filtered frequencies – we may see the direct low-pass figurative filter in Figure III.2 – are attenuated and need to be amplified by the opposite (inverse filter) shown in Figure III.3. We remark that Figure III.3 is only descriptive; amplified frequencies in some cases reach very high values due to the over zero division (or near zero) in frequency.

$$\tilde{x} = \overline{\overline{h^{-1}}} \cdot \bar{y} \tag{3.9}$$

The inverse effect of amplifying attenuated frequencies is ideally depicted in this illustration, but we should bear in mind the tricky nature of this problem, and how near-zero values become near-infinite values when a recovery of original (unfiltered) data are expected to be recovered.

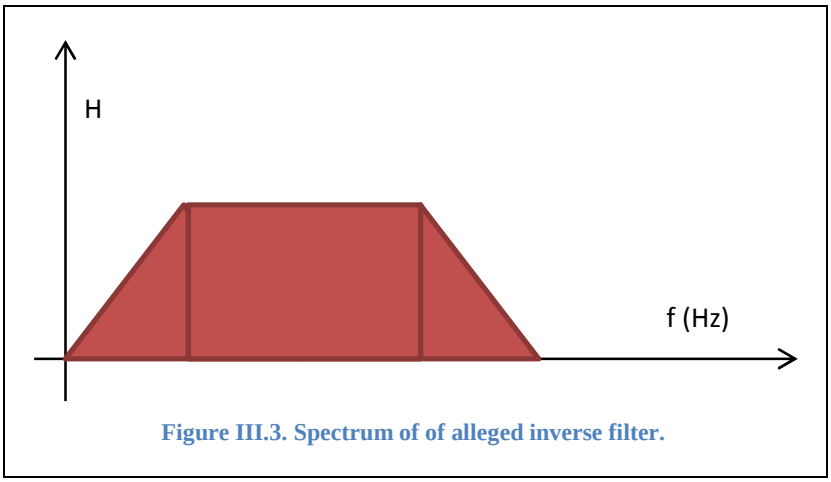

Figure III.3. Spectrum of of alleged inverse filter.

The filter in its Toeplitz matrix form – such as described by (3.7) – can be represented in a three dimensional mesh (Figure III.4), where we can observe the realisation of *sinc* functions. The inverse of this matrix can be computed and as we may graphically conclude from its representation (Figure III.5), the impulse response Toeplitz matrix is unstable and presents peaks that tend to grow and fluctuate unexpectedly.

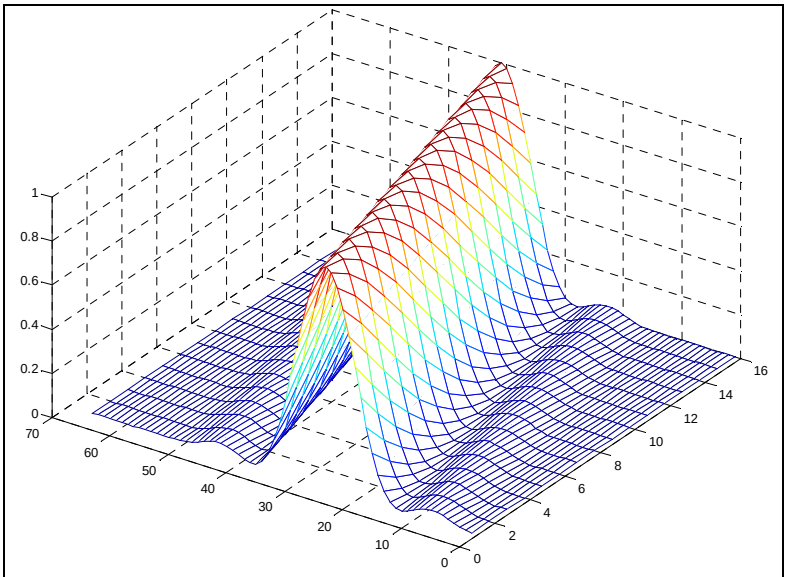

Figure III.4. 3D mesh plot of Toeplitz *h* matrix

An example of the inverse Toeplitz matrix permitting to inspect the values may facilitate comprehension. Let us in advance remind that the $(M+N-1)xN$ matrix becomes an unstable $Nx(M+N-1)$ matrix, which has the particularity of presenting more variables than equations. Let's first represent the $\overline{\overline{h}}$ matrix,

0,000398	0	0	0	…	0
0,003732	0,000398	0	0	…	0
0,010394	0,003732	0,000398	0	…	0
…	…	…	…	…	…
0,979926	0,921626	0,830626	0,71535	…	0,033161
1	0,979926	0,921626	0,830626	…	0,020287
0,979926	1	0,979926	0,921626	…	0,007723
0,921626	0,979926	1	0,979926	…	0,000369
0,830626	0,921626	0,979926	1	…	0,003862
…	…	…	…	…	…
0,020287	0,007723	0,000369	0,003862	…	1
…	…	…	…	…	…
0,000398	0,003732	0,010394	0,019626	…	0,064737
0	0,000398	0,003732	0,010394	…	0,02378
0	0	0,000398	0,003732	…	0,003862
0	0	0	0,000398	…	0,000369
0	0	0	0	…	0,007723
…	…	…	…	…	…
0	0	0	0	…	0,000398

Table III.1. Values of example of h Topelitz matrix

The inverse Toeplitz matrix of the filter should ideally verify the condition

$$\overset{\approx}{h}^{-1} \cdot \overset{=}{h} = I \tag{3.10}$$

As can be deducted from Figure III.5 and Table III.2, the values of the inverse Toeplitz matrix of the filter fluctuate – yellow marked data – and show instability.

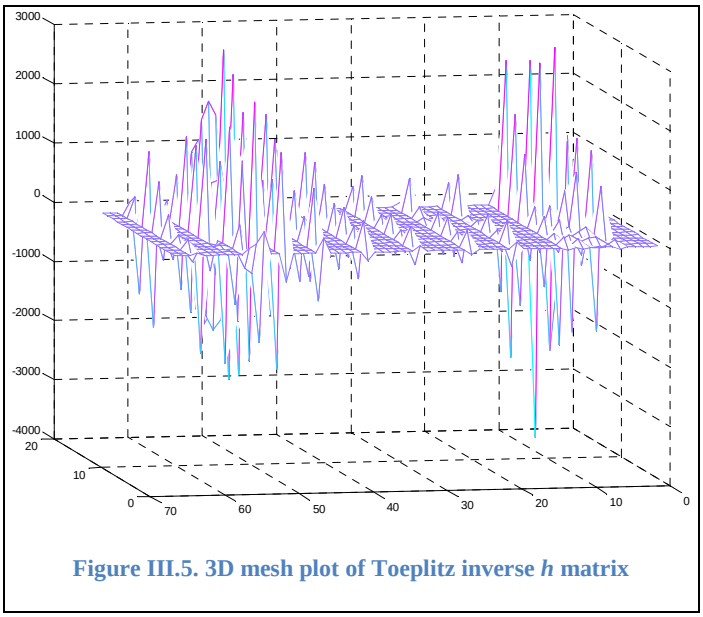

Figure III.5. 3D mesh plot of Toeplitz inverse *h* matrix

Some of the values corresponding to this view are displayed in the following table:

0	0	0	0	0	0	…
…	…	…	…	…	…	
-38,149	71,09286	-35,0305	-132,041	829,0285	-1664,38	…
0	0	0	0	0	0	…
14,35367	-60,6902	75,71547	-59,5617	142,6727	-369,11	…
15,62023	-56,7321	66,40643	-43,4138	76,89457	-137,733	…
0	0	0	0	0	0	…
-29,9043	99,81411	-112,846	69,56216	-109,308	219,2852	…
0	0	0	0	0	0	…
-44,3468	143,8207	-160,234	96,35907	-142,382	282,9606	…
0	0	0	0	0	0	…
…	…	…	…	…	…	
114,752	-343,969	373,2984	-185,859	128,4728	-221,691	…
0	0	0	0	0	0	…
…	…	…	…	…	…	…

Table III.2. List of some values of an example of h^{-1} (inverse) Topelitz matrix

Nevertheless, prior to further analysis, the regularisation of the $\overset{=}{h}$ filter could be an interesting approach we will study in the following section. The concept of regularisation involves changing some values of the matrix, also called conditioning the matrix since it is considered ill-conditioned, due to the lack of independent variables and therefore difficulty to obtain a stable inverse.

D. Regularisation of the inverse problem

1. Conditioning the filter matrix

The idea at this point is to work with vectors (or matrices) and 'fix' the convolution matrix to facilitate the computation of an inverse. As we saw in the definition of the direct problem, the direct filter is an $(M+N-1)xN$ order matrix with more equations than variables. The opposite applies for the inverse one, so we will try some operation in the following lines to arrange a matrix which might yield a more stable solution.

As we saw earlier, the filter $h[n]$ may be expressed in its matrix form. One of the additional constraints linked to the inverse problem is noise, which may be due to several factors and is seen at the output or blurred signal $y[n]$ which may as well be expressed in the matrix or vector form.

$$\bar{y} = \bar{y}_0 + \bar{y}_{error} \tag{3.11}$$

The immediate inversion of the problem can be expressed as

$$\tilde{x} = \bar{\bar{h}}^{-1}\bar{y}_0 + \bar{\bar{h}}^{-1}\bar{y}_{error} = \bar{x} + \bar{\bar{h}}^{-1}\bar{y}_{error} \tag{3.12}$$

We may notice that the term $\bar{\bar{h}}^{-1}\bar{y}_{error}$ is the inverted noise, which tends to be very high, affecting the existing information. Thus, a nice objective can be the regularisation of the convolution matrix $\bar{\bar{h}}$.

One of the well-established methods for regularising the inverse matrix is the Singular Value Decomposition (SVD). We can define the SVD of the $\bar{\bar{h}}$ matrix (resized by zero insertion enabling a square NxN matrix) as

$$\bar{\bar{h}} = U\Sigma V^T \tag{3.13}$$

Where U and V are orthogonal matrices satisfying $U^TU=I_N$ and $V^TV=I_N$ and Σ is a diagonal matrix with $\sigma_1 \geq \sigma_2 \geq \ldots \geq \sigma_N \geq 0$. The fact is that for a blurring function/matrix, this condition is observed and thus, a regularisation condition is to be chosen in order to reject some eigenvectors. The expression for the SVD of the basic approach is

$$\tilde{x} = \bar{\bar{h}}^{-1}\cdot\bar{y} = V\Sigma^{-1}U^T\bar{y} = \sum_{i=1}^{N}\frac{u_i^T\bar{y}}{\sigma_i}v_i \tag{3.14}$$

The system though is considered well-posed if

$$\|\tilde{x}\|^2 = \sum_{i=1}^{N}\frac{u_i^T\bar{y}}{\sigma_i}v_i < \infty \tag{3.15}$$

This condition fails if $\sigma_i \rightarrow 0$ because the continuous dependency between the estimated and observed values cannot be guaranteed. In this case, the problem is defined as ill-posed.

A problem is said ill-conditioned if small changes at the input generate large changes at the output. Therefore an operator H is defined to characterise this feature. In our case it has values that decay gradually to zero and the ratio of top and minimum values is large.

$$cond(H) = \frac{\max\{\sigma_j\}}{\min\{\sigma_j\}} \qquad \sigma_j > 0 \tag{3.16}$$

Eq. (3.16) represents the condition number of the matrix, which in turn will multiply any variation of the system input $y[n]$, therefore if $cond(H)$ reaches high values, the system is very unstable and highly sensitive at any alteration of the input signal. In this relationship can also be seen that high frequency components are highly magnified because of the division by small singular values. These high frequency components dominate the computed solution of the inverse and the result does not at all approximate the original signal intended to estimate. So it is true that high frequency values destabilise the inverse matrix, but they provide as well information about high frequency, giving an idea of the trade-off about the regularisation problem.

The easiest way to regularise an inverse problem is to eliminate most unstable singular values, when the level of noise in the data is increased. For this purpose, there are two widely used methods: Tikhonov's regularisation technique and the Truncated Singular Value Decomposition (TSVD).

We will see next the method named as "truncation of the singular values" (TSVD, Truncated SVD) which consists in arranging the components of the largest singular values, whereas the components corresponding to smallest singular values are deleted.

So we have to decide about the degree of regularisation controlled by a regularisation parameter.

This operation, acts as a filter where a regularization parameter $\propto$ is defined as a threshold for the chosen singular values. In this way, a filter $\omega_{\propto}$ is defined which lets only pass those values greater than $\propto$ as shown by (3.17).

$$\tilde{x} = \sum_{i=1}^{N} \phi_i \frac{u_i^T \bar{y}}{\sigma_i} v_i = \sum_{i=1}^{N} \omega_\alpha(\sigma_i^2) \frac{u_i^T \bar{y}}{\sigma_i} v_i \qquad \sigma_i > 0 \tag{3.17}$$

For the latter, the filter factors (ϕ_i) are defined as weights of value one for large singular values whereas they are set to zero for the rest. This is more specifically controlled with the parameter k, also known as the truncation parameter,

$$\phi_i = \begin{cases} 1 & i = 1,\ldots,k \\ 0 & i = k+1,\ldots,N \end{cases} \tag{3.18}$$

which is similar to $\propto$, named truncation factor, which sets the threshold value for the eigenvalues and acts as a filter as well, letting the dirtiest components pass to the solution of the deconvolution at the extent where this parameter tends to zero. However, as $\propto$ takes values close to 1 (normalised to top eigenvalue), solutions resemble softer functions in the form of sines and cosines.

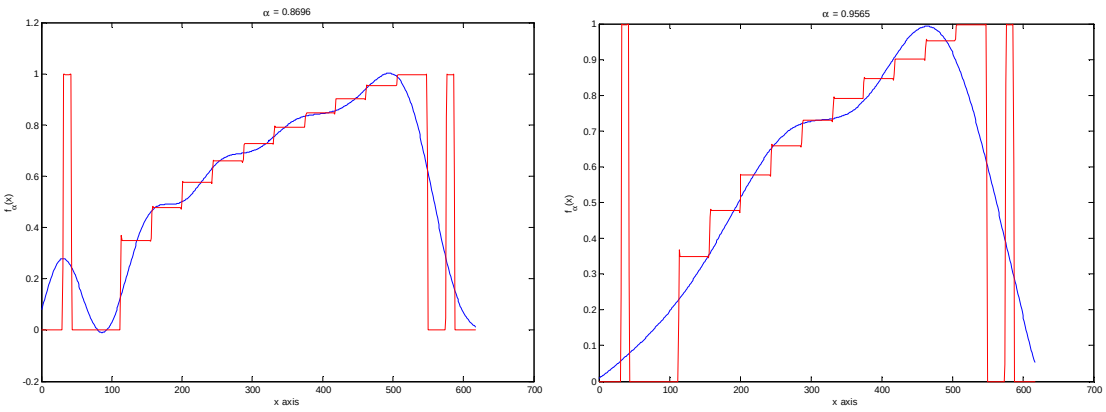

Figure III.6. Resemblance of estimated output to sinusoidal functions due to severely regularised functions (normalised ∝ values). Blue plot: output of regularised estimate. Red plot: original signal.

The system's stability depends largely on the appropriate election of the regularisation (or truncation) parameter, but still and all, there is indeterminacy between noise suppression and loss of useful information, which can lead to not fully satisfactory results.

Under the assumption that the use of a filtering method based on SVD was not computationally feasible, there are other methods of regularisation. One of the best known methods for regularising ill-posed problems is the Tikhonov regularisation. This algorithm was independently developed by Philips and Tikhonov and widely studied in the years 60 and 70 (Hansen 2002).

In the Tikhonov method in turn, the filter factors are defined as

$$\phi_i \equiv \frac{\sigma_i^2}{\sigma_i^2 + \alpha^2} \qquad i = 1, \ldots, N \tag{3.19}$$

And it is related to the minimisation problem:

$$\min_x \left\{ \| \bar{y} - \bar{\bar{h}} \cdot \bar{x} \|_2^2 + \alpha^2 \| D \cdot \bar{x} \|_2^2 \right\} \tag{3.20}$$

It observes that $\propto > 0$ which is the regularisation parameter and D is the regularisation matrix, which is often an approximation to a derivative operator. The term $\| D \cdot \bar{x} \|_2^2$ is called regularisation term and involves a smoothing norm. This norm is the 2-norm of the solution when $D = I_N$. We choose D so that the regularisation term is small when x matches our expectations for good quality solution behaviour. This expression can be

developed based on distance minimisation and verification on base-2 norm. We use anyway the better suited equation form

$$(\overline{\overline{h^T}} \cdot \overline{\overline{h}} + D^2 I) \cdot \bar{x} = \overline{\overline{h^T}} \cdot \bar{y} \tag{3.21}$$

instead of (3.20) for this kind of calculations.

In conclusion, the idea of regularisation is to stay with the equations and values that make sense, in other words, which may be of use, because the inversion of the matrix may return values such as results of divisions by near-zero values. At the same time, the goal is to calculate an approximation as most accurate as possible, or at least one that is not so sensitive to noise. Hence, it might be necessary to modify the process of deconvolution or inverse filtering.

Therefore, the problem can be stabilised by means of regularisation, but high frequencies might as well be lost or erased, which are related to very small eigenvalues. So a good regularisation must not only make the problem stable, but also keep valuable data as untouched as possible.

In the following section we expose some meaningful tests carried out with a *sinc* filter where the commented trade-off between high-frequency resolution and stability can be seen.

2. Some tests and results

TSVD is probably the most commonly used method for regularising inverse problems (most widely used in MRI and medical imaging). For the purpose of testing this method, as in any test, a test signal is used, shown in Figure III.7 which is a 1D cut of an image.

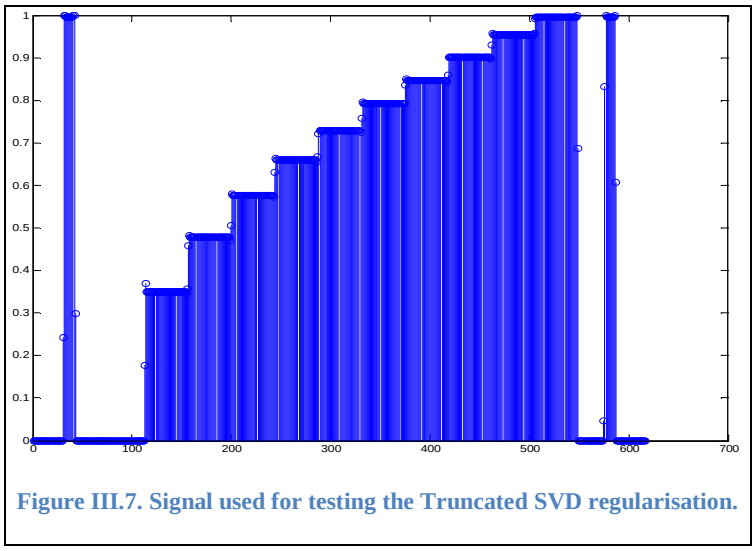

Figure III.7. Signal used for testing the Truncated SVD regularisation.

As a blurring function, a *sinc* type kernel is used to convolve with the input data, which as a consequence gives a blurred signal such as seen in previous sections and chapters. This kernel is implemented in the matrix form (Toeplitz) as indicated in eq.(3.7) and eq.(3.13) and is composed by vectors that can be expressed in a different orthogonal base.

In connection with this matrix expression of convolution, there is a trade-off between the hypothetical existing amount of noise in the convolved (blurred) signal and the degree of regularisation. As the power of noise is increased the number of truncated

parameters must be higher for an optimal result which leads to an image, resembling more the blurred signal than the expected original-like.

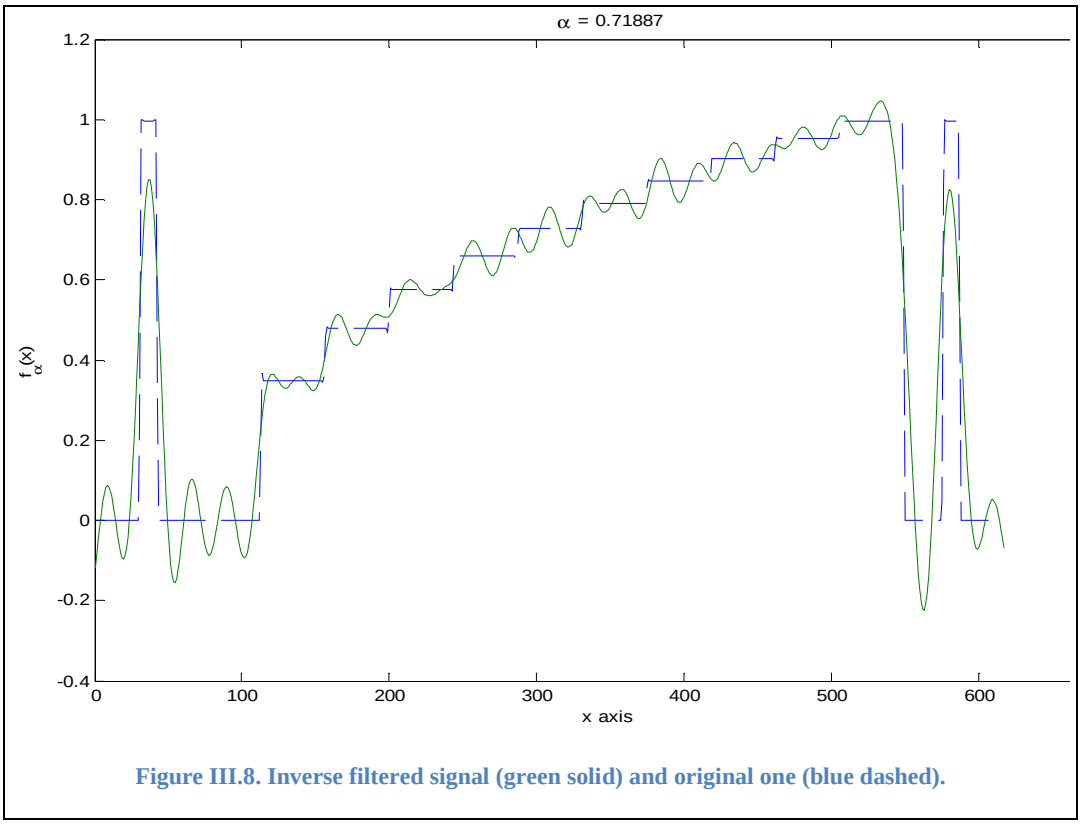

Figure III.8. Inverse filtered signal (green solid) and original one (blue dashed).

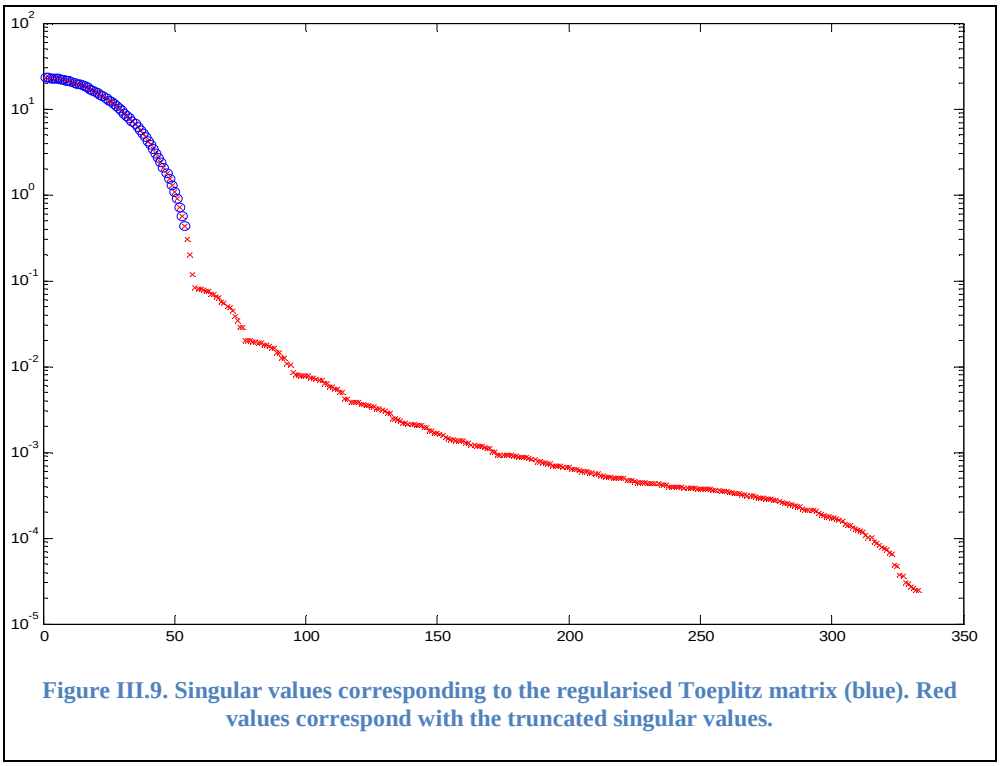

Figure III.9. Singular values corresponding to the regularised Toeplitz matrix (blue). Red values correspond with the truncated singular values.

The optimum truncation factor for recovering the signal from a noisy blurry one – with 2 percent of RMS Gaussian noise in the vector norm of the data – can be observed in Figure III.7. The regularised matrix's vectors which single values below 0.71887 are truncated.

The values shown in Figure III.9 are displayed in the table below:

Singular value #	Value	Singular value #	Value
		35	6,62211065054373
1	23,0008846568782	36	6,10092212787637
2	22,9376570677266	37	5,59936033022258
3	22,8326043522926	38	5,11832768024950
4	22,6862141216395	39	4,65858265639978
5	22,4991644731705	40	4,22074037000390
6	22,2723194772623	41	3,80527416461435
7	22,0067234377819	42	3,41251820356151
8	21,7035939732375	43	3,04267100702645
9	21,3643139748081	44	2,69579989732589
10	20,9904225064721	45	2,37184631170283
11	20,5836047208249	46	2,07063194763396
12	20,1456808718684	47	1,79186572005145
13	19,6785945129965	48	1,53515153982337
14	19,1843999745317	49	1,29999698241334
15	18,6652492204422	50	1,08582303530231
16	18,1233781882228	51	0,891975363024130
17	17,5610927193482	52	0,717738086740637
18	16,9807541901493	53	0,562352434347389
19	16,3847649544293	54	0,425046346269081
20	15,7755537096055	55	0,305093241080514
21	15,1555608976428	56	0,201969684834802
22	14,5272242505503	57	0,116071830957912
23	13,8929645877628	58	0,0813592515815349
24	13,2551719693583	59	0,0813184704972669
25	12,6161923048108	60	0,0789946025065748
26	11,9783145118912	61	0,0789609824394964
27	11,3437583144735	62	0,0755161933621709
28	10,7146627614315	63	0,0751811072660392
29	10,0930755416029	64	0,0700313865741932
30	9,48094316202935	65	0,0697727645086554
31	8,88010204843075	.	.
32	8,29227061823477	.	.
33	7,71904236754361	.	.
34	7,16188000428365	617	2.4351e-005

Table III.3. List of singular values for regularising the data matrix given in this test case.

As can be seen, the values in red do not fulfil the condition for the optimal truncation factor $\propto$=0.71887 and as a result of that, eigenvectors corresponding to those eigenvalues are suppressed.

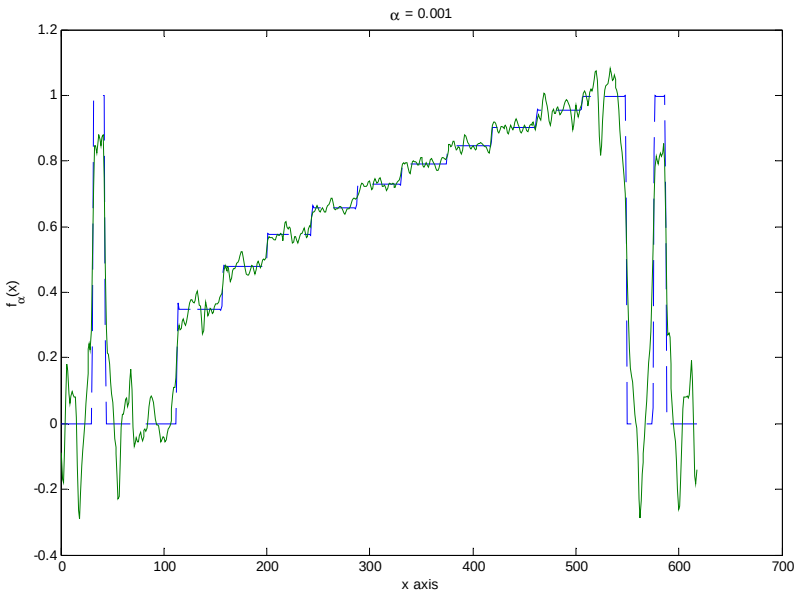

Figure III.10. Computed inverse of the noiseless convolved signal (solid green) and original true signal (dashed blue) using the TSVD regularised filter. Test signal in the original scale plotted in blue

In the case represented in Figure III.10, some noise appears due to the fact that the regularisation parameter is too relaxed; therefore small perturbations produced by noise become harmful in the final inverted result. To be precise, in this case the regularisation parameter was $\alpha=0.001$ resulting that 171 vectors are used to calculate the inverse of the data array (matrix). The rest 446 vectors are not used meaning that most of the information is contained in those first ones.

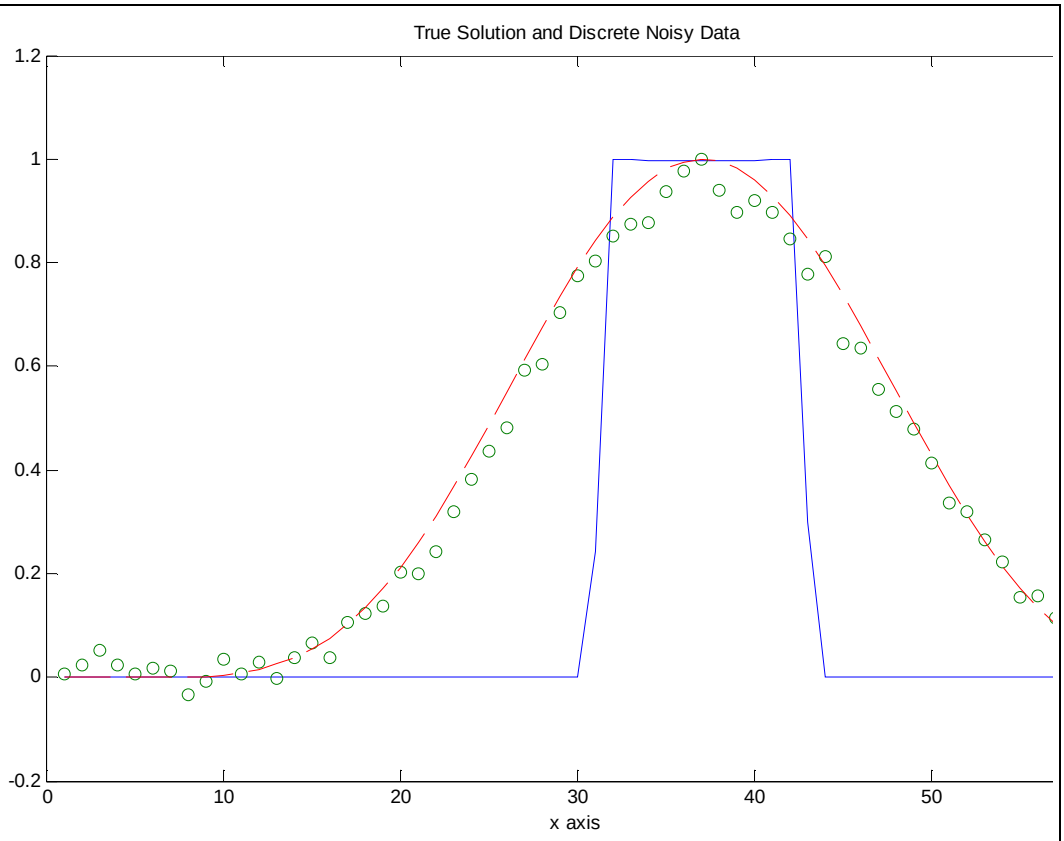

Figure III.11. Convolved and normalised (blurry) signal with noise (dotted) and without noise (dashed). The original signal is plotted in solid blue.

An important conclusion arising from regularisation methods is that if we supress any vector using these regularisation parameters, we would be supressing some high frequency components as well.

Depending on the truncation parameter chosen, the regularisation is more suppressive or more permissive. In addition to the loss of information due to the truncation of vectors, there is a trade-off between the regularisation error and the perturbation error, due to the bias introduced in this process, i.e., the more relaxed the regularisation is the higher the perturbation error will be.

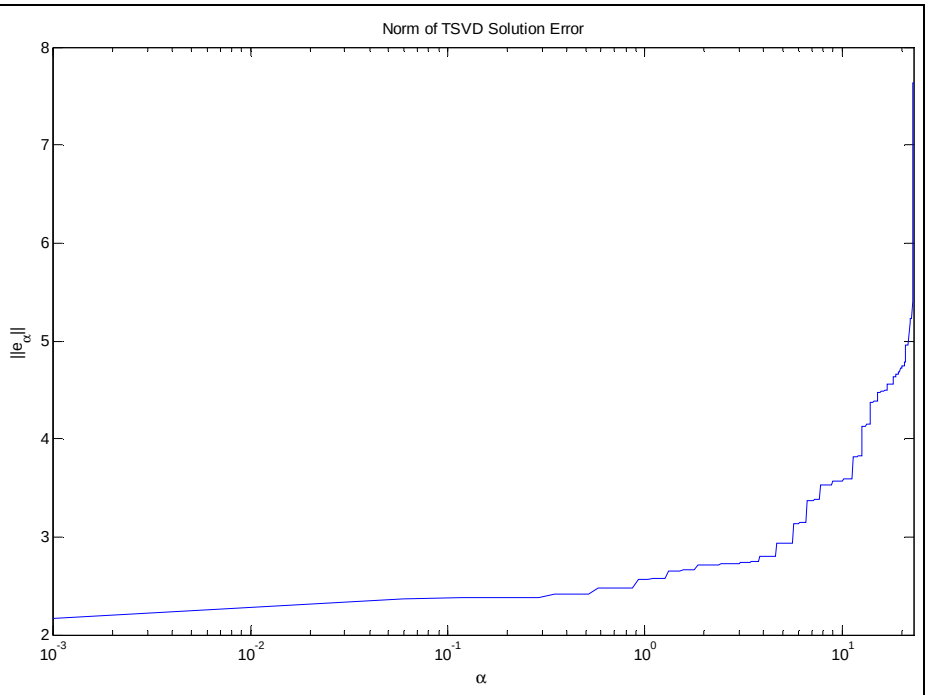

Figure III.12. Norm of the regularization error for TSVD as a function of the truncation parameter ∝ (noiseless input signal).

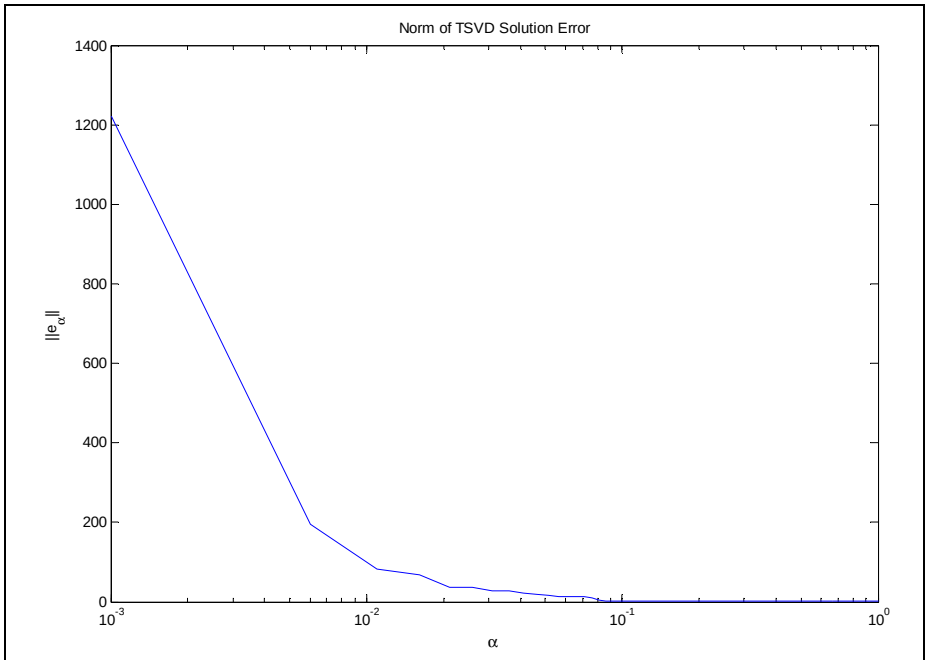

Figure III.13. Norm of the perturbation error for TSVD as a function of the truncation parameter ∝. for a signal with 2% RMS Gaussian noise

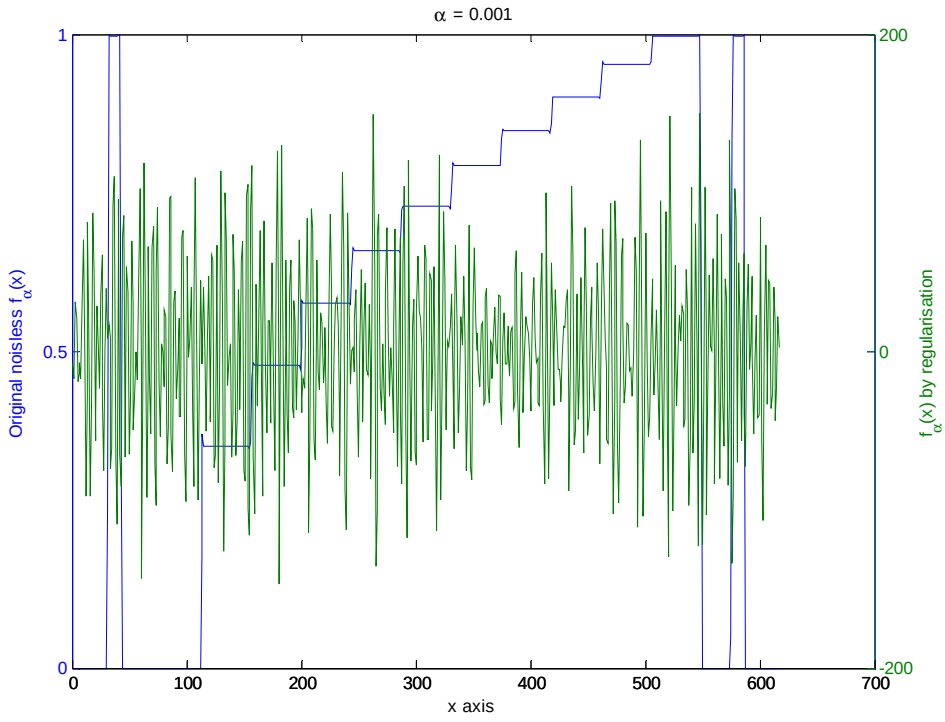

Figure III.14. Computed inverse of filtered signal with TSVD regularisation, using a regularisation parameter ∝=0.001 – with 2 percent of RMS Gaussian noise– (solid) with the original signal plotted in the background (dashed)

But as can be concluded from Figure III.14, when the rejection (truncation) factor is relaxed the result is a noisy useless signal. Let the reader remind that the signal to be inverse filtered has Gaussian noise added at a factor of 2% of the signal's RMS.

We should note that the Singular Value Decomposition, is a method based upon the decomposition of a matrix in orthonormal vectors. A direct consequence of this is the separation of significant different information existing in the original matrix where vectors can be eliminated with a well-established criterion. There is nonetheless extant information possibly enough for several signal-processing applications, but the result is that the deletion of any vector has destructive consequences for our hyperacuity simulation.

In addition, regularisation of a matrix does not itself provide additional information about the problem or data containing the matrix and operating with the data is always subject to the extent or degree of regularisation.

E. Frequency Analysis

1. Discrete Fourier Transform

The nice and welcomed property of the frequency domain enabled by the Fourier Transform is the simple multiplication or division of elements such as

$$Y(\omega) = H(\omega)X(\omega) \tag{3.22}$$

This obviously facilitates and permits any operation just by adjusting the frames or windows where the frequency transform version of the data are calculated. Let's not forget we deal with discrete data, i.e. we work with digital hardware, digital signals, such as images, so we use the Discrete Fourier Transform which observes similar axioms, among others the commutative.

Regarding this transform, from the computational point of view there is a possible method which can be more efficient and with same outcome as the Discrete Fourier Transform, which is the Fast Fourier Transform. It is a computationally efficient implementation of the basic Discrete Fourier Transform (DFT), expressed as

$$DFT\{x[n]\} = X_k \overset{\text{def}}{=} \sum_{n=0}^{N-1} x_n \cdot e^{-i2\pi kn/N} \tag{3.23}$$

which in turn is the discrete version of the continuous Fourier Transform

$$X(\omega) = \int_{-\infty}^{\infty} x(t)e^{-i\omega t}dt = \mathcal{F}\{x(t)\} \tag{3.24}$$

The FFT (Fast Fourier Transform) can be used to process discrete sequences in an efficient manner such that

$$Y[k] = FFT\{y[n]\} \tag{3.25}$$

In order to compute the deblurred signal, the method is simply

$$\hat{X}[k] = Y[k] / H[k] \tag{3.26}$$

and may involve a division by near-zero values, making the outcome reach near-infinite values. These near-zero – or zero – values are the big constraint involving inverse problems, which makes this problem being an ill-posed problem. Here is where the earlier explained conditioning methods add value to the science of resolution of inverse problems.

As reported in (Jansson 2012; 1979), the a priori knowledge about the original signal may be used – even sometimes difficult to obtain – to better approximate the target. Here, the author also affirms that linear methods cannot recover as such, parts of the signal beyond the cut-off frequency. He states that prior information available can facilitate the calculation of the original signal but especially in non-linear methods.

Nevertheless, in the linear approach, the best a priori contribution is mostly the basic value range limit such as the amplitude restriction.

As explained in the previous chapter, for the purpose of modelling the hyperacuity process – for the similar properties of the alleged blurred signals – we may use a one-dimensional function of type

$$h(t) = sinc^2(\omega t) \tag{3.27}$$

– this function actually models the diffraction created by light going through a slit –. Notice that since we are working with one-dimensional signals, we may express these formulae in the spatial coordinate system (x) or in the temporal (t). Its Fourier transform in the continuous domain is given by

$$sinc^2(at) \xrightarrow{FT} \frac{1}{\sqrt{2\pi a}} \bigwedge\left(\frac{\omega}{2\pi a}\right) \tag{3.28}$$

But as we know, we need to work in the discrete domain, where the discrete version of the transform is needed, yielding that

$$sinc^2[\beta \cdot n] \xrightarrow{DFT} \frac{\pi}{\beta} \bigwedge\left[\frac{2\pi k}{2N\beta}\right] \tag{3.29}$$

In both of the former expressions a and β are constants.

The real fact anyway is that we do not sample the squared *sinc* from minus infinity to plus infinity, among other reasons a good one is because it is impossible. This issue involves getting a non-perfect triangular shaped signal in the frequency domain, and some ringing as well.

In consequence, the signal in the frequency domain stays above zero but with many near-zero values corresponding with the suppressed band of the low-pass filter. Mainly because these near-zero values make this signal's inverse unstable, and the possibly existing noise is amplified; those frequencies are supressed or highly attenuated so the signal-to-noise ratio is poor.

There are lots of different linear methods in the literature, but they all have to face similar issues with noise, and in general all of them achieve interesting results for band-limited and noiseless signals. In all, there might not be a single final general method applicable to all types of inverse problems, but maybe only an approach per each requirements filters and noise.

At this point, the Wiener type filter could be a more realistic formulation of the inverse filter since it accounts for the noise too.

$$y(t) = h(t) \otimes x(t) + n(t) \tag{3.30}$$

For the case where $h(t)=\delta(t)$ eq. (3.30) can be cut down to an optimal filter estimation such as

$$H_W(\omega)=\frac{X(\omega)}{X(\omega)+N(\omega)} \tag{3.31}$$

With this filter the effect of noise should be compensated and back in the original domain, the estimated signal could be obtained from the noisy one:

$$\hat{x}(t)=h_W(t)\otimes[x(t)+n(t)] \tag{3.32}$$

The next step would be to incorporate the inverse problem to this filter, so for the general case of any system, $h(t)$, the Wiener filter could be defined as follows,

$$H_W(\omega)=\frac{X(\omega)H^*(\omega)}{X(\omega)\left|H(\omega)\right|^2+N(\omega)} \tag{3.33}$$

$X(\omega)$ and $N(\omega)$ are the Fourier transform of $x(t)$ and of the noise respectively.

$$H_W(\omega)=\frac{1}{H(\omega)}\left[\frac{\left|H(\omega)\right|^2}{\left|H(\omega)\right|^2+\frac{N(\omega)}{X(\omega)}}\right] \tag{3.34}$$

Here we can see how the inverse the filter of the signal approximates $1/H(\omega)$ when noise tends to be zero.

We get the estimation of the original signal by simple convolution

$$\hat{x}(t)=h_w(t)\otimes y(t) \tag{3.35}$$

For an additive and Gaussian noise, this is the optimal filter as long as the noise and the object are known, but these parameters are often difficult to compute.

An important issue of inverse filters is that the information at each point in the transformed domain (e.g. frequency domain) affects all the points in the original/target domain (temporal or spatial domain). This can also be a reason for using Wiener's inverse filter because it takes into account the effects created by noise provided that the noise is Gaussian and additive and has the constraint of needing to know the original signal to estimate the filter properly.

2. Cepstral approach

Homomorphic filters consist in a non-linear mapping of a domain onto a target domain, where linear filtering is applied and eventually return with inverse mapping back to the original domain. This concept was first developed by Stockham, Oppenheim and Schafer in 1960.

Following to this, the definition of cesptrum was first made public in a paper by Bogert et al. in 1963. This novel form – or transform – permitted to show the compressed spectrum (logarithmic) of a signal in the frequency domain transformed back into the original (e.g. time) domain.

$$y'_B(t) = \left| \mathcal{F}^{-1}\left\{ \log(\left| \mathcal{F}\{y(t)\} \right|^2) \right\} \right|^2 \tag{3.36}$$

From this expression, it follows an important property which permits addition and subtraction of frequency components

$$y_1 * y_2 \rightarrow y'_1 + y'_2 \tag{3.37}$$

As it arises from (3.37) we can subtract the convolving filter from the blurred signal and obtain the cepstra of the estimated original,

$$\hat{x}' = y' - h' \tag{3.38}$$

Thus, the original estimated signal can be computed by getting back to the original domain, but in this method a big issue comes about with the phase, as the logarithmic operator hinders the recovery of phase. In other words, for

$$\log\left|X'(\omega)\right| = \log\left|Y'(\omega)\right| - \log\left|H'(\omega)\right| \tag{3.39}$$

But it is not possible to reconstruct the original phase from the transformed signals.

$$\angle\left|X'(\omega)\right| \stackrel{?}{=} \angle\left|Y'(\omega)\right| - \angle\left|H'(\omega)\right| \tag{3.40}$$

Since additivity does not in general hold arbitrary 2π multiples can be added to the main values. One way to solve this issue is to ensure the continuity of the result. We have therefore implemented Opphenheim's definition

$$\begin{aligned} Y[k] &= \mathcal{F}\{y[n]\} = \left|Y[k]\right| \cdot e^{j \cdot \arg\{Y[k]\}} \\ Y'[k] &= \log\left|Y[k]\right| + j \cdot C \cdot \arg\{Y[k]\} \\ y'[n] &= \mathcal{F}^{-1}\{Y'[k]\} = \mathcal{F}^{-1}\left\{ \log(\left| \mathcal{F}\{y[n]\} \right|) + j2\pi m \right\} \end{aligned} \tag{3.41}$$

where *m* is the value required to properly unwrap the angle or imaginary part of the complex log function. The spectrum of a discrete signal is periodic, continuous and must be so between periods.

If the complex cepstrum *h'[n]* resides in an interval less than one pitch period *N*, then the two components can be separated by cepstral deconvolution.

The inverse transforming procedure will at last be

$$y[n] = \mathcal{F}^{-1}\left\{ e^{(\left|\mathcal{F}\{y'[n]\}\right|) \cdot j2\pi m} \right\} \tag{3.42}$$

But in our case the $h[n]$ filter as is, it is not a minimum phase filter, plus it is unstable and ill-posed which makes us face similar problems as explained in other methods.

F. Time-Space domain analysis

1. Process of Deconvolution

It is in general known as deconvolution the process to revert a convolution, such that the original 'unconvolved' signal – like $x(t)$ in eq.(3.3) – is recovered.

So far, there have been many different developments and approaches to methods in order to achieve the goal of recovering the original signal or object.

a) Direct approach

The most basic technique of deconvolution is the known as Direct Approach. The simple idea of deconvolving a signal can be represented by undoing the effects of a filter, such as

$$h * h_{inv} = \delta \tag{3.43}$$

But as stated earlier, there can be problems with stability and ill-posedness.

Reminding that eq. (3.2) represents the convolution; we note that its discrete version can be calculated as:

$$y_m = \sum_k h_{m-k} x_k \tag{3.44}$$

For pure convenience, we may use the commutative property of convolution and rewrite this expression. Let L be the starting and finishing samples of the resulting response,

$$y_m = \sum_{l=-L}^{L} h_l x_{m-l} \tag{3.45}$$

We may follow the following example where $L=1$. Thus, the values of the estimated original signal can be calculated with some steps,

$$y_0 = x_1 h_{-1} \tag{3.46}$$

$$\hat{x}_1 = y_0 / h_{-1} \tag{3.47}$$

$$y_1 = x_1 h_0 + x_2 h_{-1} \tag{3.48}$$

$$\hat{x}_2 = (y_1 - \hat{x}_1 h_0) / h_{-1} \tag{3.49}$$

…

The general case would be observed by the following expression:

$$\hat{x}_{k+1} = (y_{k-L+1} - \sum_{l=-L+1}^{L} h_l \hat{x}_{k-L+1-l}) / h_{-L} \tag{3.50}$$

As we may notice on the first two steps the fact of dividing each calculated element by h_i enlarges the value of the target element, in some cases might happen even an over zero operation. An additional effect could be the noise and the imperfections coming from the real world. We should not omit or forget that the input value (y_i) is actually mixed up with noise, inaccuracies and possible miscalculations giving rise to huge errors at the estimated signal $\hat{x}_k$

Moreover, it is typical to find small values at the spread function h_i. When operating with such values, we may realise that any imperfection at y_i would lead to catastrophic results.

b) Van Cittert deconvolution

Another basic approach is the Van Cittert's algorithm for deconvolution. It was published in 1931 and the idea was to use the convolved captured signal *y(n)* as a first approximation of the estimated original signal. The difference between a new estimation and the previous one is used to compute the original signal, either in the convolved/blurred signal or in the target original one. As an example of this, the first step is shown below:

$$\hat{x}_{(1)}[n] - \hat{x}_{(0)}[n] = y[n] - h[n] \otimes \hat{x}_0[n] \tag{3.51}$$

And the algorithm general equation in consequence,

$$\begin{aligned} \hat{x}_{(k+1)}[n] - \hat{x}_{(k)}[n] &= y[n] - h[n] \otimes \hat{x}_k[n] \\ \hat{x}_{(k+1)}[n] &= \hat{x}_{(k)}[n] + \left\{ y[n] - h[n] \otimes \hat{x}_k[n] \right\} \end{aligned} \tag{3.52}$$

Thus, the previous equation (3.52) computes the deconvolution by means of the differences on the output values and the estimated original ones.

We would like to comment, that as a mathematical formulation of the convolution, it can be rewritten into a matrix format, such that

In this expression, we note that *[h]* represents the Toeplitz matrix of the filter. As we say, this method consists in an iteration of the values where the index k defines the iteration number.

We could draw an example of an iteration to facilitate comprehension

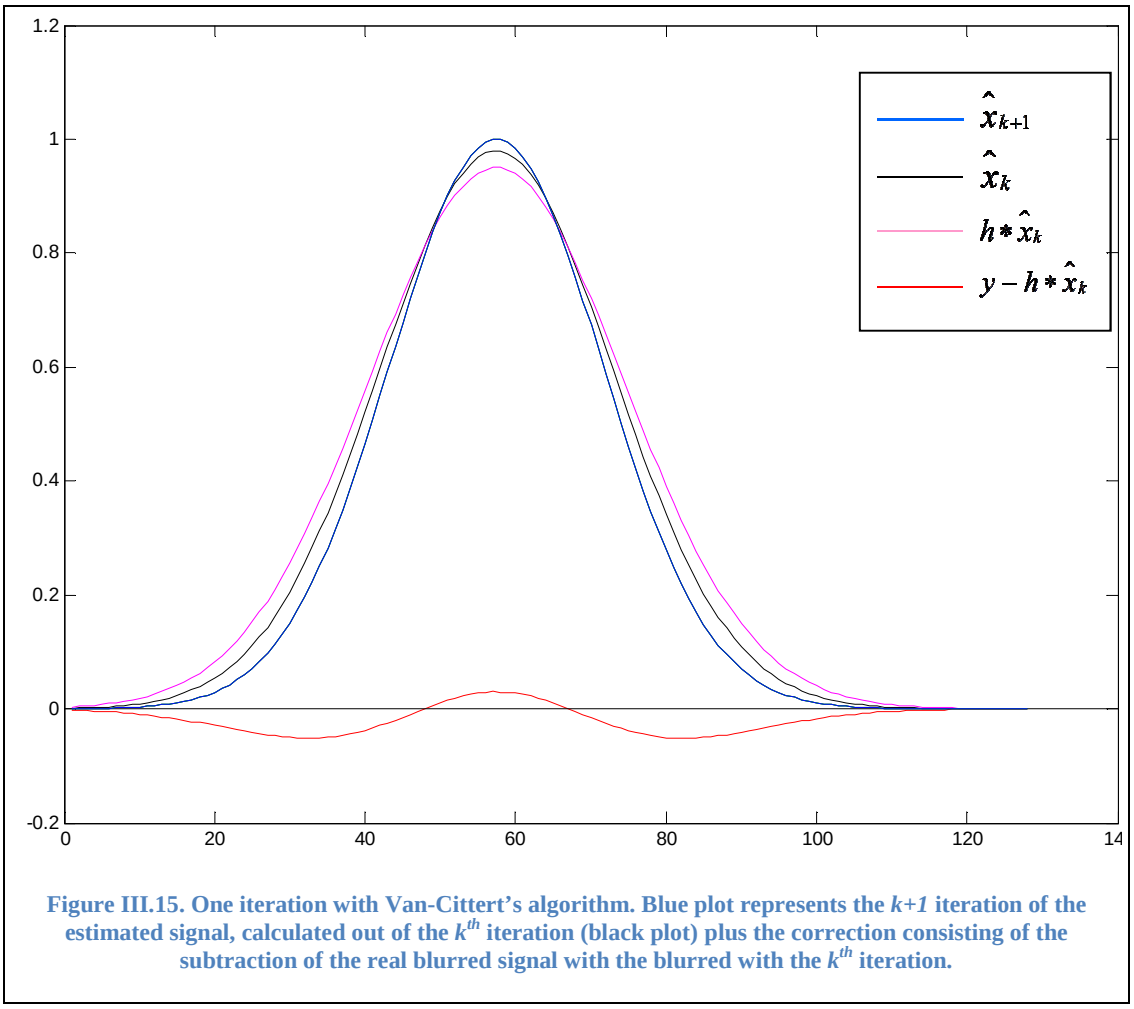

Figure III.15. One iteration with Van-Cittert's algorithm. Blue plot represents the *k+1* iteration of the estimated signal, calculated out of the k^{th} iteration (black plot) plus the correction consisting of the subtraction of the real blurred signal with the blurred with the k^{th} iteration.

As shown by Figure III.15 the signal is deconvolved following an error correction at each iteration, based on the error appeared at the output, which is the result of the estimated original signal.

c) Lucy-Richardson deconvolution

This algorithm was unveiled in the field of astronomy and medical imaging. The success of this method comes from the implementation of a solution of maximum likelihood and its apparent ability to rebuild a high-quality image in presence of high noise levels. It was initially derived from the Bayesian theorem. Being related to conditional probability, this algorithm takes into account statistical fluctuations of the signal and therefore has the ability to reconstruct images with noise.

The iterative algorithm in terms of convolution is as follows

$$x_{k+1} = \left\{ \left[\frac{y[n]}{x_k[n] * h[n]} \right] * h[-n] \right\} x_k[n] \tag{3.53}$$

Where *h(n)* represents the PSF, *x(n)* the estimated signal and *y(n)* the blurred or degraded one. It is necessary to set an initial condition as x_0 to make the algorithm start and iterate until values converge.

Non-negativity constraint is one advantage of this method if $x_0(n) \geq 0$. Furthermore, energy is conserved along the iterative process.

With this method we can improve and sharpen an image after some iterations, which is empirically proven to converge to the maximum likelihood solution for x_i but on the other hand, the error committed in the estimation of the original signal (deconvolved signal) is not tolerable.

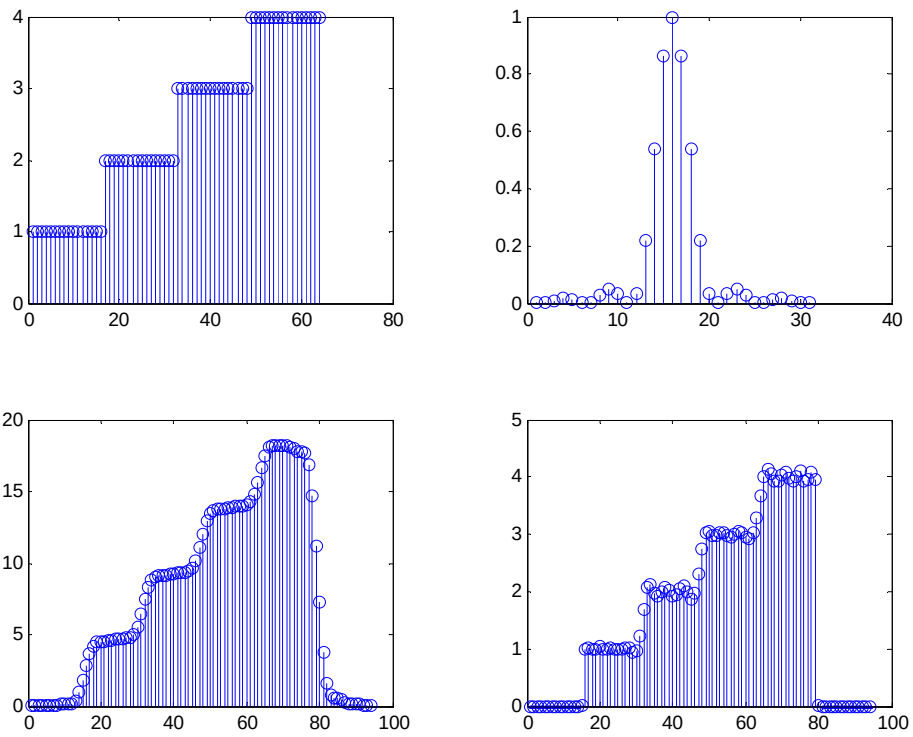

Figure III.16. An original one-dimensional signal (upper left) is convolved with a squared sinc function (upper right) and its result (bottom left) is deconvolved with the Lucy-Richardson algorithm (bottom right).

As seen in the result, the error in the deconvolved signal persists even after convergence has been reached up to an unacceptable extent.

d) Blind deconvolution

Blind deconvolution is one of the best-known methods and it's a non-iterative deconvolution where both the original image and blurring function or PSF are unknown. At first glance, it appears to be an equation in two unknowns with no unique solution. If the image and the PSF have a finite or compact support (have null values from a finite region onwards), theoretically, there is a unique solution if the signal has more than one dimension, always subject to trivial ambiguities.

The method tries to find the intensity of the original object (image) and the function PSF which are more likely to have created the measured data. Blind deconvolution is

commonly used for restoration of atmospheric images, where the exact PSF or dispersion pattern produced by microscopes and the atmosphere is difficult to know.

All deconvolution techniques seen so far perform some kind of high pass filtering which enhances high frequencies but amplifies noise and error as well, which are cumulative.

In our case the filter function is known which makes seems not suiting or making the most out of this particularity. Anyway, it is still an unsolved problem, which is a motivation to check other paradigms that could lead to a more complete recovery avoiding and minimising the inherent problems described.

We will see in the next section an implementation of a spatial processing artificial neural network where the main lobe of a blurring filter ($sinc^2$, Airy disk,…) is intended to recover or transform back in the delta or impulse generated at the prior to the filtering stage.

2. Artificial Neural Networks (ANN)

Another way to implement deconvolution or any filtering scheme is by artificial neural networks, which were created intending to copy the computing power of biological – presumably human – neural systems. The simplicity of these configurations makes it robust and flexible, but at the same time the underlying mathematical model depends precisely on the signal – in case of – processing model emulated.

Any approach with ANNs towards a solution to the inverse problem is motivated by the implementation with a different architecture permitting the use of a smaller number of coefficients at the operation of deblurring.

We search a solution with a finite number of coefficients, giving credibility to the possible deployment by the nervous system in the human eye. Though, all systems explained so far look for the solution of a system of equations, i.e. fix all equations at once, making all assertions certain and clearing solution. The solution in the frequency domain also requires the globality of the coefficients to find the final solution.

In this sense, any convolution can be implemented by means of ANNs, but the opposite condition cannot be satisfied because ANNs can model recurrent (IIR) and even non-linear processing schemes.

Due to the signal processing performed by the HVS by neural networks, any attempt for artificial emulation sounds reasonable. Hereafter, the deconvolution process is formulated as a machine learning problem and the inverse operator is interpreted as a connectionist model consisting of linear units.

In this sense the model of a neuron – named processing unit – used in ANN is built inspired in the biological model as depicted in the following figure

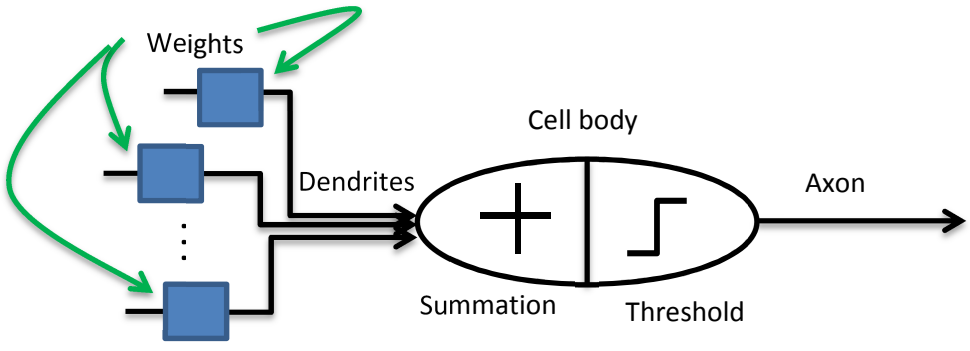

Figure III.17. Layout of an artificial neuron

The fact anyway is that artificial neural networks are widely used in many applications and can outperform other processing methods, as they compute values of signals in parallel.

Artificial Neural Networks (ANN) are composed by processing units (PU) which perform add and multiplication task in parallel, i.e. they do not perform subtasks. In Figure III.18, the first column of circles represents the processing inputs, the central column of circles a layer (in this case we can assume it is the hidden layer), and the right column of circles the output processing units.

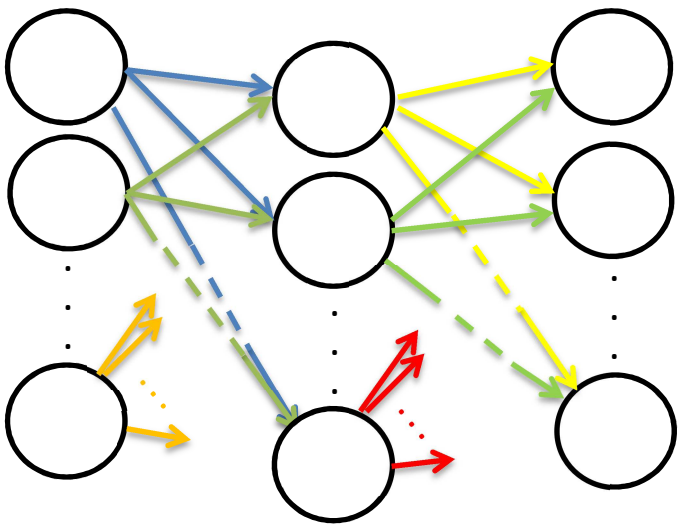

Figure III.18. Example of artificial neural networks

One of the most popular classifications of these networks is based on the way the neural networks adjust the weights of the neurons. Three paradigms of learning exist: supervised learning, non-supervised learning and reinforcements learning.

The first one consists in supervising the output values by an external agent, which corrects the weights so as to obtain the desired values. In the non-supervised learning paradigm, the network adjusts itself the weights by minimising the cost function. Reinforcement learning at last, the supervisor's task comes down to reinforcing the signalling depending on whether the output obtained in the network matches the desired (success = +1, or failure = -1), and accordingly adjust the weights based on a mechanism of probabilities. From the point of view of their active or decoding phase, artificial neural networks can be classified into feedforward (static) and feedback (dynamic, recurrent) systems.

Maybe, the biological paradigm of artificial neural networks would lead us to the unsupervised learning paradigm, statistical classification methods and self-organising maps. But beyond these considerations, we have carried out an efficient model intending to solve the inverse problem using a feedforward neural network with the Levenberg-Marquardt learning algorithm. This learning method combines the speed of convergence and stability of the Gauss-Newton and the steepest descent method respectively. These two methods have been used depending on the approximation.

We have formulated the problem using a one-dimensional cone shaped pattern intending to resemble the distribution of a blurred signal through a space of nine cones. The neural network emulates the response of the deblurring process and intends to return the right value at the output.

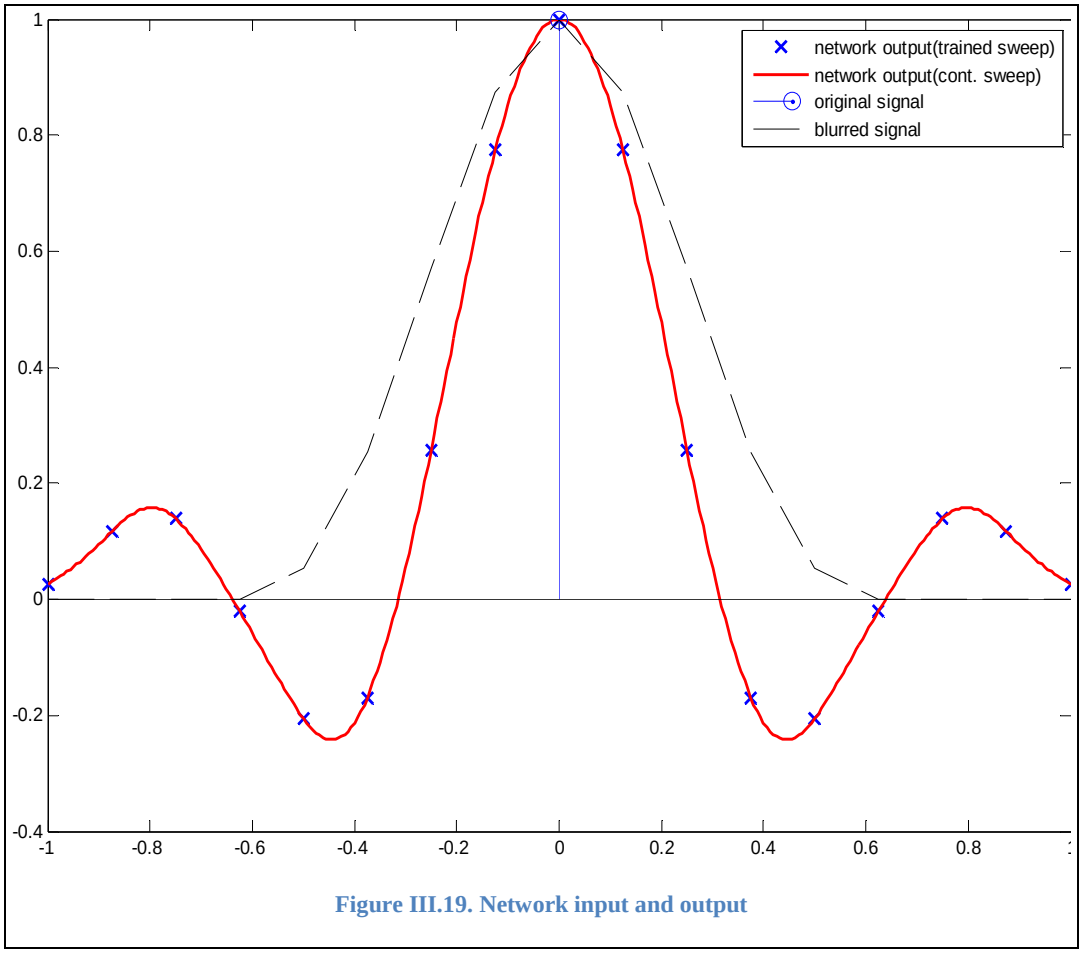

Figure III.19. Network input and output

The most optimal solution reached by means of the tested configurations of neural networks resemble highly other methods of deconvolution, where issues like ringing and sensitivity to noise are present. The reason for this might be related to the need of using all coefficients, which makes all these methods very sensitive to possible noise in the sensors that capture the image.

In addition, the output signal is likely to create side peaks when a threshold is applied to the blurring function and all the problems and constraints appearing in previous signal processing paradigms are present again as shown in Figure III.20.

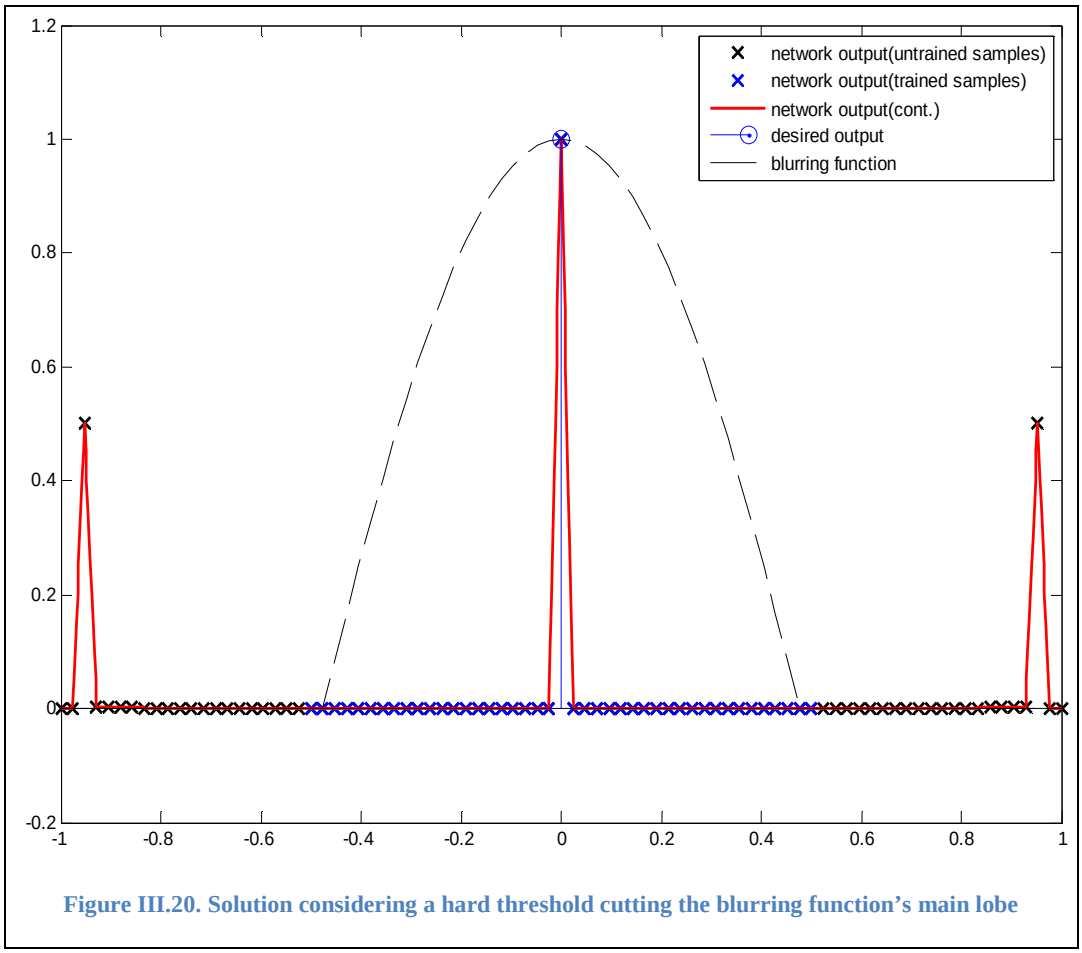

Figure III.20. Solution considering a hard threshold cutting the blurring function's main lobe

Although we have seen the architecture employed could not solve the problem, we have been able to conclude that for the stated problem has a complete and stable solution should tend to a fully meshed network and end accounting, or allowing the entire system of equations (Koudelka, del Rio Bocio et al. 2013).

3. Systems described by difference equations

a) Finite Impulse Response or Infinite Impulse Response

In principle, the impulse response of a system can be characterized by a sum of discrete terms, as the following expression defines

$$y_n = \sum_{k=0}^{N-1} h_k x_{n-k} \tag{3.54}$$

This expression is commonly known as the discrete convolution of two functions, which in our case is the signal x convolved by the filter h.

Any two systems or functions which can be convolved can also be processed by difference equations, but this can only be observed for a Finite Impulse Response system, which means that the system is non-recurrent i.e. y_n does not depend on previous samples (y_{n-1},y_{n-2},…,y_{n-k}). That is to say, a linear filter h, can be expressed or implemented by difference equations but when the system happens to be recursive, i.e.

of IIR (Infinite Impulse Response) type the model of eq. (3.54) cannot verify this requirement, as it can only take a value of y.

An IIR type system does depend on previous output samples which means that the convolution between the input signal and the system is not possible because the system is said to be recurrent. So, the expression showing this behaviour stands that

$$\sum_{m=0}^{M-1} a_m y[n-m] = \sum_{k=0}^{N-1} b_k x[n-k] \tag{3.55}$$

Where b_k and a_k represent the filter's coefficients. The developed former expression yields

$$a_0 y[n] + a_1 y[n-1] + \ldots + a_{M-1} y[n-M+1] = b_0 x[n] + b_1 x[n-1] + \ldots + b_{N-1} x[n-N+1]$$

$$\text{in case that } a_0 = 1$$

$$y[n] = b_0 x[n] + b_1 x[n-1] + \ldots + b_{N-1} x[n-N+1] - a_1 y[n-1] - \ldots - a_{M-1} y[n-M+1] \tag{3.56}$$

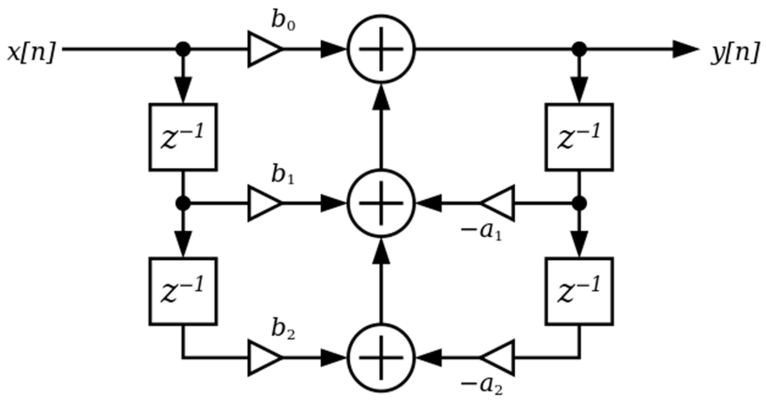

Figure III.21. Direct Form I (DF-I)

The diagram above shows the behaviour of a recurrent system where previous samples of y_n are introduced back into the system, weight compensated and subtracted from the resulting output once and again for each new sample.

A similar case but different implementation is the Direct Form II (DF-II) represented in Figure III.22 shown below

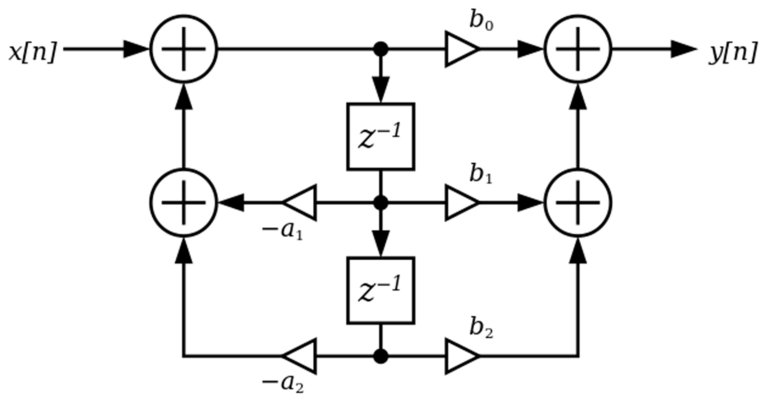

Figure III.22. Direct Form II

The outcome in both cases is the same but the implementation is different.

b) Some calculations in the Z transform domain

A useful tool for working with difference equations is the Z transform, which permits a better comprehension and analysis of FIR and IIR systems. It is defined as

$$H(z) = \mathcal{Z}\{h[n]\} = \sum_{n=-\infty}^{\infty} h[n] z^{-n} \tag{3.57}$$

Due to the properties of the Z transform, an IIR in the Z domain turns out that

$$H(z) = \frac{Y(z)}{X(z)} = \frac{B(z)}{A(z)} = \frac{b_0 + b_1 z^{-1} + \ldots + b_N z^{-N}}{a_0 + a_1 z^{-1} + \ldots + a_M z^{-M}} \tag{3.58}$$

Reversing the process would mean that $H(Z)$ should be inverted, i.e. the denominator and the numerator swapped,

This is the expression for a recursive – direct – filter, but if we are modelling the inverse filter, we may swap all a_i coefficients with b_i coefficients and obtain the inverse filter in the transform domain yielding.

$$H_{INV}(z) = \frac{X(z)}{Y(z)} = \frac{A(z)}{B(z)} = \frac{a_0 + a_1 z^{-1} + \ldots + a_M z^{-M}}{b_0 + b_1 z^{-1} + \ldots + b_N z^{-N}} \tag{3.59}$$

The impulse response of the inverse filter would, in a general basis, be expressed as $h^{-1}[n]$ but at this time cannot be expressed as such due to the recurrent coefficients. So the inverse Z transform – difference equation – of this filter would give as a result

$$\begin{aligned} \hat{x}[n] = y'[n] = \frac{a_0}{b_0} x'[n] + \frac{a_1}{b_0} x'[n-1] + \ldots + \frac{a_{M-1}}{b_0} x'[n-M+1] - \\ - \frac{b_1}{b_0} y'[n-1] - \ldots - \frac{b_{N-1}}{b_0} y'[n-N+1] \end{aligned} \tag{3.60}$$

Which we mark as prime elements that stand as the new inputs and outputs, i.e. the new input will be the blurred signal and the new output the estimated signal.

The reader may notice that the first coefficient in the denominator of (3.59) must be a non-zero value – so that the re-weighting of all coefficients can be possible – because the b_0 must get '1' value in order to fulfil the difference equation.

$$\sum_{m=0}^{N-1} b_m y'[n-m] = \sum_{k=0}^{M-1} a_k x'[n-k] \tag{3.61}$$

Hence, a FIR system can easily be reversed into an IIR system by swapping a_k and b_k coefficients.

In short, the concept of this technique basically consists in inverse filtering a blurred signal. In addition, it is very flexible because it allows eliminating selectively coefficients or manipulating them in order to make the inverse filter stable, as we will see next in the section of stability.

Every filter or system in order to be feasible has to comply with the rules of causality and stability. Regarding the former, the system is said to be causal if it does not depend on samples prior to *'0'*, i.e.

$$h[n] = 0,\ n < 0 \tag{3.62}$$

The limitation at this point though relies on causality, since the inverse filter $H_i(z)$ – also seen in expressions (3.60) and (3.61) – shows dependency on samples prior to *'0'*, especially of the recurrent section since the numerator coefficients of $H_i(z)$ will generally be reduced to the instantaneous input $x'[n]$. Thus, for the causality of the system to be fulfilled, the filter can be padded with zeroes until causality is fulfilled.

In addition, the value of initial coefficients of the filter has to be chosen or controlled so as to avoid amplifying effects and make the inversion unstable. In addition, the stability of the inverse filter can be sensitive to any phase mismatch, but as we will see, these effects can be diminished.

Now we have seen the Z transform tool we can also analyse the stability of the inverse filter in this domain as we expose in the following section.

c) A view on stability

A discrete-time LTI (Linear Time Invariant) system is said to be stable if

$$\int_{-\infty}^{\infty} |(h(t)|\, dt < \infty \tag{3.63}$$

But this is the sufficient condition.

Again, as we know, based on the equation (3.58) or (3.59), the transfer function can be expressed as

$$H(z)=\frac{Y(z)}{X(z)}=\frac{B(z)}{A(z)}=\frac{b_0+b_1z^{-1}+\ldots+b_Nz^{-N}}{a_0+a_1z^{-1}+\ldots+a_Mz^{-M}} \tag{3.64}$$

Thanks to the fundamental theorem of algebra, we know that the numerator has N roots (called zeros) and the denominator has M roots (called poles). Factoring this transfer function we get

$$H(z)=\frac{(1-q_1z^{-1})(1-q_2z^{-1})\ldots(1-q_Nz^{-1})}{(1-p_1z^{-1})(1-p_2z^{-1})\ldots(1-p_Mz^{-1})} \tag{3.65}$$

where q_k is the k-th zero and p_k is the k-th pole. The zeros and poles are generally complex, and may therefore be drawn in the complex plane. Ultimately, the zeroes are the solutions of the equation obtained by equating the numerator to zero, while the poles are obtained by equating the denominator to zero.

For a causal system to be stable, the poles of the function should always meet that $p_kz^{-1} <1$, ie $p_k <z$, and being complex numbers poles, the overall stability is given when all poles on the full z plane, $|p_k| <1$, meaning that drawing all poles of the transfer function in the z diagram should be inside the unit circle.

Hence, for discrete systems, the stability condition is defined by the ROC (region of convergence) of the z-transform, and it is fulfilled if it includes the unit circle. In a causal system, the ROC is the open region outside a circle whose radius is the magnitude of the pole with largest magnitude. In conclusion, in order to achieve stability on a system, all poles must be inside the unit circle in the z-plane, but it must include that unit circle.

A useful mathematical tool is the zeros-poles diagram, where we may visually analyse at which extent the system/filter is stable. In turn, we can deduce if its inverse is or might be stable. Moreover, we can not only analyse the filter but also modify it in order to reach stability. So in order to manipulate zeroes-poles at the given filter, we use the Z transform domain where we can graphically understand the level of stability of our system.

If we compute the z transform of a FIR filter where all coefficients are located in the numerator of *H(z)*,

$$H(z)=\frac{Y(z)}{X(z)}=\frac{B(z)}{A(z)}=b_0+b_1z^{-1}+\ldots+b_Nz^{-N} \tag{3.66}$$

In Figure III.23 we may see a zero-pole plot of a squared *sinc* type function *(*example with *N=256)*. This function, as previously mentioned may well describe a diffraction blurring mechanism. We could see that some of the zeroes are inside the unit circle, but some other zeroes corresponding with this function are in the outside, which means that the inverse will not be stable.

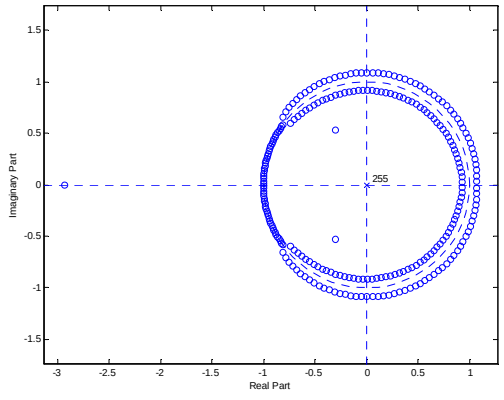

Figure III.23. Pole-zero plot of a sinc^2 function

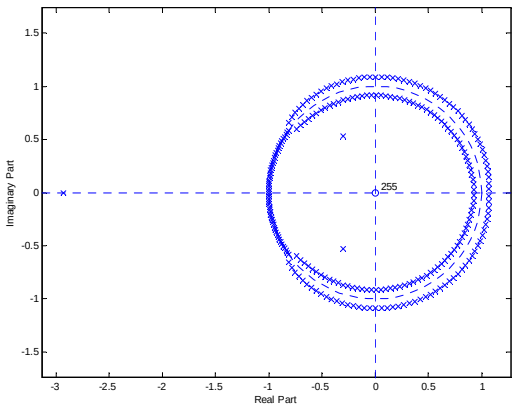

Figure III.24. Zero-pole plot of an inverse filter of a sinc^2 type function

Stability is not a compulsory condition to be observed but a stable function/filter/system has a "summable" response. In the following picture (Figure III.24) a snapshot of the inverse of the previous one is shown.

We may as well see how this inversion makes the former expression (3.66) become an all poles IIR filter,

$$H_{INV}(z)=\frac{X(z)}{Y(z)}=\frac{A(z)}{B(z)}=\frac{1}{b_0+b_1z^{-1}+\ldots+b_Nz^{-N}} \tag{3.67}$$

As we may notice, all points except those at the origin of the coordinate system are poles. Nevertheless, we can avoid zeroes choosing the right sampling rate i.e. matching the zeroes between sampled points. As we say, another way to reach stability is to pull the zeroes inside the unit circle.

Next, an illustrative example of stabilisation is shown in the following figures. More specifically, in order to test and improve instability of this type of filters we give an example in the following where we use the filter shown in Figure III.25 and red plotted in Figure III.26.

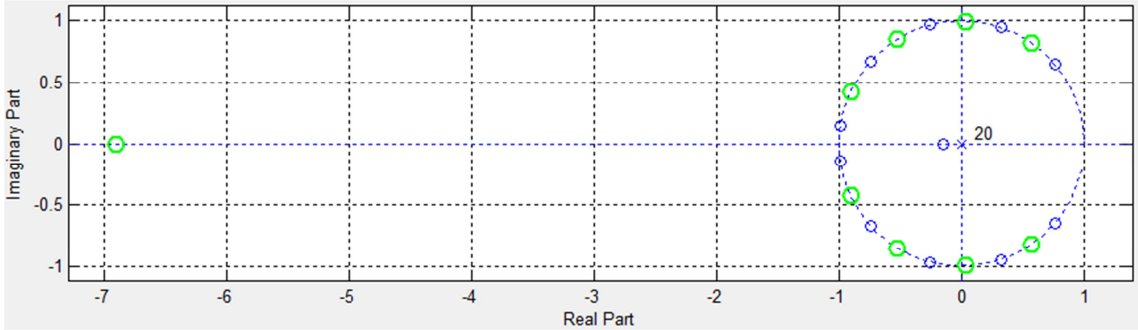

Figure III.25. Direct filter h[n] with zeroes (blue) outside the unit circle

Thereby, stabilisation can be "forced" by pulling the zeroes inside the unit circle of the z plane as shown in Figure III.27. Notice that along this section we have been dealing with one-dimensional filters. Image processing though requires two-dimensional filters, therefore two-dimensional processing as we will hereby expose.

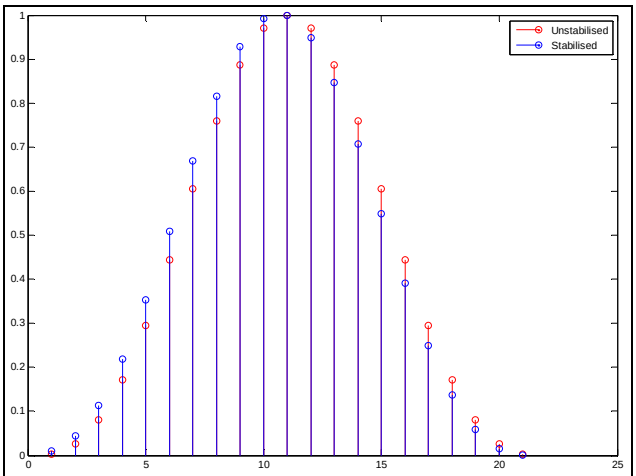

Figure III.26. sinc^2 filter composed by 21 samples

Once the filter has been stabilised as shown in Figure III.27, the output is stable and can be calculated without reaching infinite values.

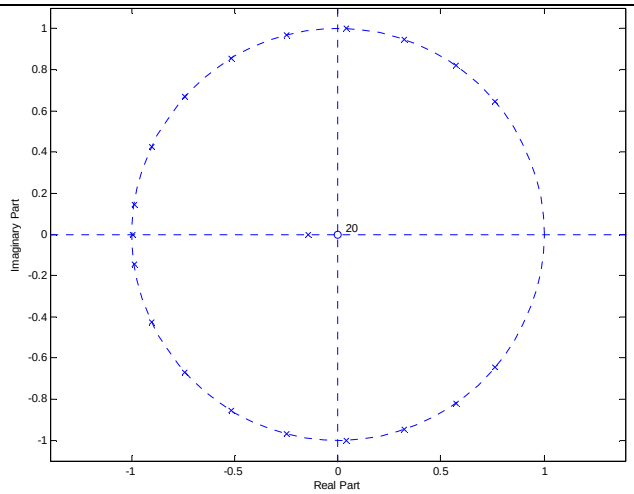

Figure III.27. Zero-pole plot of stabilised h[n] filter. All poles are located inside the unit circle.

d) Two Dimensional IIR Inverse Filtering

The two-dimensional processing can be performed by following the elements in two dimensions. The general expression for the two-dimensional IIR difference equations can be written as

$$y_s = \sum_r b_r x_{s-r} + \sum_{r>(0,0)} a_r y_{s-r} \qquad \text{where } r, s \in \mathbb{Z}^2 \tag{3.68}$$

Thus, r and s will be the two-dimensional filter's order which can be represented in the Cartesian coordinate system by M and N. The filter does not necessarily have to be of equal dimensions on each of the coefficient arrays. On the other hand, r and s (M and N) represent the previous samples to be processed by the difference equation and the particular condition of $r>(0,0)$ arises from the fact that y_S is precisely the term to be solved and the value of $r=(0,0)$ actually corresponds with the initial value of y_S which lies on the left side of the equation where a_0 is given as a value *'1'*.

i-M,j-N								
	…							
		i-2,j-2						
			i-1,j-1					
				i,j				
					i+1,j+1			
						i+2,j+2		
							…	
								i+M,j+N

Figure III.28. Equation Differences in Two Dimensions.

Notice we are dealing with the general 2D IIR filtering scheme, which means that at this point we have not changed or swapped the $a_{m,n}$ and $b_{m,n}$ elements, but as in one-dimensional IIR filtering explained in the previous section, the inverse can be achieved by swapping the coefficients.

A major concern arising from the general difference equation is the possible unstable nature of this filtering method, which rises from the location of the poles, but again, this is an issue related to stabilisation rather than to this particular method.

Since our two-dimensional IIR filter is recursive, each $h_{i,j}$ element depends on previous samples, up to M,N. The red coloured box (Figure III.28) indicates the current element to be processed, which needs not only the values present in the input data array but also the output values of the output data array. The need of these previous samples is in fact related to the condition of causality of every feasible filter.

The difference equation for a two-dimensional filter for the alleged case of equal size coefficient matrices can be written element by element as

$$y_{ij} = \frac{b_{i,j}}{a_{i,j}} x_{i,j} + \frac{b_{i-1,j}}{a_{i,j}} x_{i-1,j} + \frac{b_{i,j-1}}{a_{i,j}} x_{i,j-1} + \ldots + \frac{b_{i-M,j-N}}{a_{i,j}} x_{i-M,j-N} + \\ + \frac{a_{i-1,j}}{a_{i,j}} y_{i-1,j} + \frac{a_{i,j-1}}{a_{i,j}} y_{i,j-1} + \ldots + \frac{a_{i-M,j-N}}{a_{i,j}} y_{i-M,j-N} \tag{3.69}$$

and we should again take care of the first element of the filter $a_{m,n}$ coefficient matrix. It can be noticed that the last of either elements – $a_{i\text{-}M,j\text{-}N}$ or $b_{i\text{-}M,j\text{-}N}$ – might not be as large as MxN, as they are not necessarily supposed to be of same size, but as defined by eq. (3.68) they only reach values within their domain of definition which means that those values out of their range will be set to zero.

Eq. (3.69) can be re-arranged to form the inverse two-dimensional filter such as

$$y_{ij} = \frac{a_{i,j}}{b_{i,j}} x_{i,j} + \frac{a_{i-1,j}}{b_{i,j}} x_{i-1,j} + \frac{a_{i,j-1}}{b_{i,j}} x_{i,j-1} + \ldots + \frac{a_{i-M,j-N}}{b_{i,j}} x_{i-M,j-N} + \\ + \frac{b_{i-1,j}}{b_{i,j}} y_{i-1,j} + \frac{b_{i,j-1}}{b_{i,j}} y_{i,j-1} + \ldots + \frac{b_{i-M,j-N}}{b_{i,j}} y_{i-M,j-N} \tag{3.70}$$

Here, the potentially disturbing element is b_{ij} so it must be verified that it does not greatly amplify the values of the equation.

In turn, as arises from eq. (3.68) it should be noticed that the previous elements to that of $h_{i,j}$ are defined just as such, as elements preceding the one being processed. In other words, the data represented in Figure III.28 are displayed as elements of an array in the Cartesian coordinate system, but this is not really a necessary condition, as we will expose in the following section.

One of the most important remarks with this technique is the fact that only the filter coefficients and the same number of few data elements are needed to compute the deconvolution, keeping the problem localised, in the sense that noise, rounding and other errors remain localised and are not expanded or spread throughout the outcome of the filtering process.

G. Conclusions

One of the key points about the inverse problem in the human eye is the undeniable existence of the neural post-processing that removes the distortion from the projected image on the retina. In other words, the neural system solves somehow the inverse problem by means of still unknown mathematical operations.

Inverse problems are in general tricky and present the additional problem of varying extensively with small changes at the input, produced generally by noise. Yet, the inverse problem is a major challenge still unsolved, since there is no definitive method or solution known for such.

A possible approach to solve this instability is precisely to make it stable or quasi-stable. One way of doing this is calculating the equivalent minimum-phase filter, or moving zeroes or poles in the Z transform domain, facilitating to compute the inverse or by making the inverse filter stable, hence, avoiding the transfer function tend to infinite. Another way of stabilising the problem is by regularising the sparse convolution matrix by either regularisation method. This can be a successful way to obtain a mathematically computable inverse operation, but If some of the dependent or quasi-independent equations from the whole system of equations is supressed, it might happen that a part of the information intended to recover is eliminated as well, and these erased data are generally located at high frequencies, i.e. they provide the high resolution details. In summary, the high-frequency components which are essential in the hyperacuity model of the eye are lost.

Data processing in the frequency domain has been an important milestone in the history of telecommunications which happened thanks to the great discovery of the Fourier transform. When data are transformed into the Fourier domain all frequencies can be visibly interpreted and what is more, data or signal matrix can be processed or filtered by simple multiplication. In addition, these operations have progressively been implemented in computationally efficient algorithms, some nowadays mostly implemented in the Fast Fourier Transform.

In addition to space-time and frequency analysis, there are other new methods currently being studied notably for MRI and seismic data processing.

Basically, these new techniques intend to solve the inverse problem based on Krylov subspaces (Ipsen, Meyer 1998, Mojabi, LoVetri 2009) using CGLS (Rubaek, Meaney et al. 2007) (Conjugate Gradient Least Squares) and variants, such as GN-C (Ashtari, Noghanian et al. 2010, Zhang, Liu 2004) (Gauss-Newton CGLS), GN-T (Gauss-Newton Tikhonov) and also NNRGA (Neural Networks Real Genetic Algorithm).

These methods in general concentrate their efforts in sharpening edges partially or totally flattened by any blurring mechanism which is an important duty for some applications where any slight recovery can be crucial (tumour detection, earthquake prediction…). But these methods are in generally used to get rid of light blur or separate areas of interest, thus, they are not so useful to put our unification theory in a practical

context, in part due to their complexity, and in part because they do not respect constraints related to the resolution enhancement process we here describe.

Chapter IV. Testing Hyperacuity

A. Introduction

In order to check the feasibility of the diffraction theory, we have carried out a series of experiments of the human vision that consist in using diffraction type low-pass filtering at the entrance of the system.

Let us remind that the signal processing scheme we implemented, consists of four basic stages:

- Diffraction
- Decimation/sampling
- Interpolation
- Inverse filtering or deconvolution

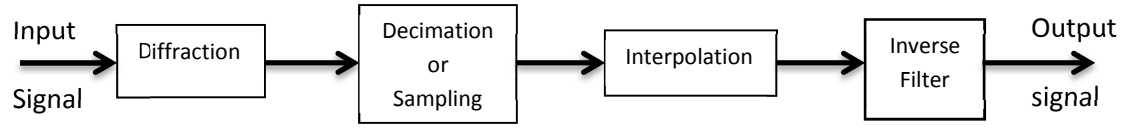

Figure IV.1. Lay-out of the entire process.

Although these tests can be done with signals of one dimension, with the goal of being more illustrative, we have carried out these tests with a two dimensional signal, that is, an image and thus visually observe and inspect the results at each stage.

We will first start explaining the way we blur the test pattern – or original image – followed by the decimation process, where data are sampled and thus lost. Next we provide details on the interpolation stage, how it adds new points by inference or continuation of the spectrum and at last, we present the results of the inverse filtering mechanism applied.

Then we will show the same test image when captured by a diffraction limited imaging system so as to visually compare the results obtained with our novel paradigm.

Additionally, we complete this chapter with an exposition about the way processed images are measured and provide more results with a spectral approach on the two-dimensional IIR inverse filtering technique.

B. Step one: Blurring the test image.

We have analysed our hyperacuity model using a test pattern used in a common basis on TV. This test pattern is very suitable because it may help to visually measure the level of details, colours, distances and basic shapes processed throughout the process. Thus, the test image shown in Figure IV.2 has been used to emulate the object observed by a viewer. We may notice the shapes sweeping frequencies from the lowest to the highest, i.e. vertical small bars stuck together with increasing separation from right to left, as well as a black small triangle shape showing a frequency sweeping in the vertical axis.

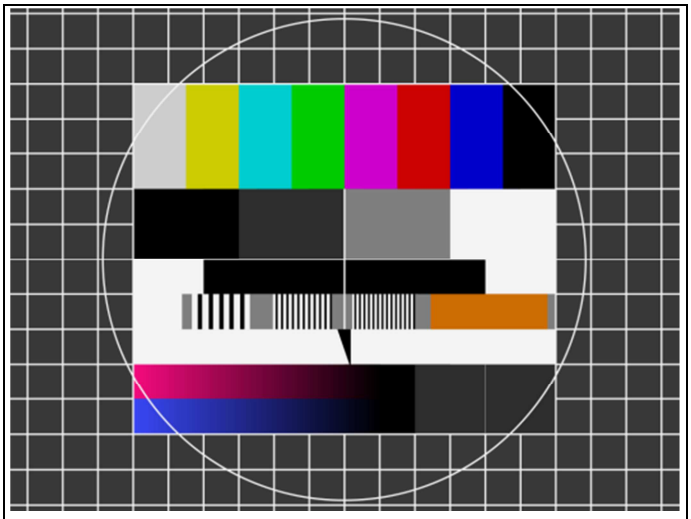

Figure IV.2. 2000x1500 pixel resolution image emulating the high resolution test image

As we know, any (full) colour image is composed by three colour components. The test used along this simulation is an RGB image so the three components need to be processed separately and then assembled in order to display a full colour image such as shown in Figure IV.2.

This test sample is an RGB image formed by 2000x1500 pixels and three colours, in a three dimensional array, that is, a size of M_X x M_Y x 3. It is to mention that within our series of experiments, we have used double precision numbers, or in other words, 64 bit floating point numbers.

Regarding the diffraction, the specific blur distortion used in this experiment is given by the following expression

$$h = \mathrm{sinc}^2(5n\frac{5\pi}{1000}) \tag{4.1}$$

This one dimensional filter can also be extrapolated to a two dimensional model, but above all we should notice that the impulse response that it represents expands a single point – delta – onto many points at the sampling (decimation) process. In this specific case, we could say that each point is spread over 27 points only in the main lobe. There are also side lobes but most of the energy is concentrated into the main one. Depending on the specific distortion (e.g. diffraction) the expansion of the information (points) is different, but this is a factor that we control in our simulated model, which can also be controlled in a real one (aperture). The maximum amplitude has been normalised to one.

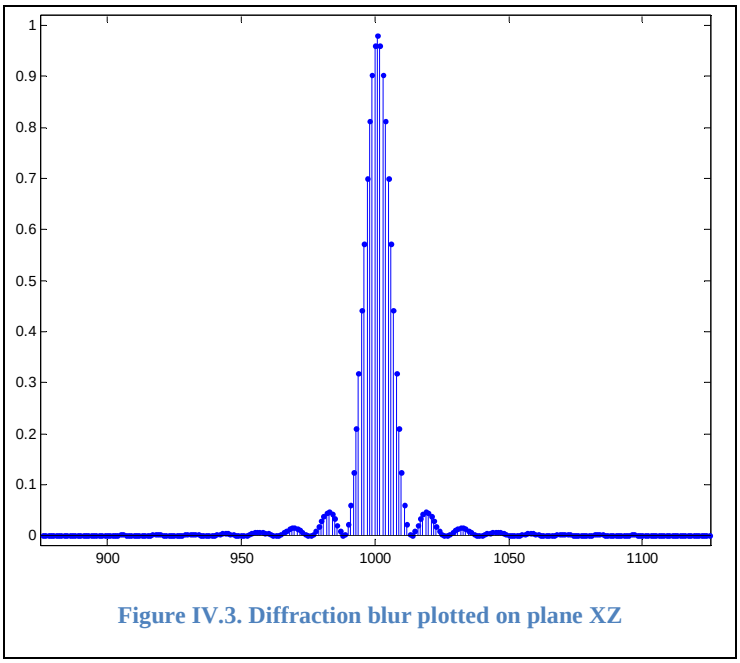

Figure IV.3. Diffraction blur plotted on plane XZ

By extending this one dimensional spread function over the other axis, we can get a picture of the resulting blur distortion, i.e. the spread function on the XY plane.

Let us remind that we intend solely to approximate a presumed blur distortion, which we have modelled as a squared *sinc* function. We do not seek to match an accurate model of the total distortion existing on the projection of the image over the retina.

The process of blurring is carried out by means of a simple convolution, which means that a multiplication and summation process is performed for each pixel at each position of the sample test image, as shown by Figure IV.4. A direct consequence of this (of any convolution)

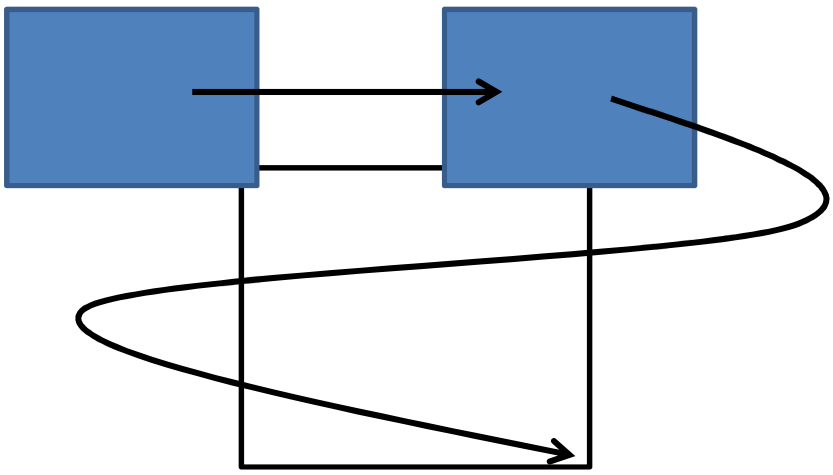

Figure IV.4. Process of convolution in a two-dimensional signal (image)

is that the size of the resulting image – signal – grows to the size of (L_X+M_X - 1, L_Y+M_Y - 1) points.

Being aware of this larger size of the convolved image, we should mention that the boundaries are surrounded by a black frame corresponding with the black or dark points of the convolver, but this black frame has been removed for space economy and because it does not provide any further information. There is indeed information about the boundaries of the original unblurred signal within this surrounding black frame prior to its inverse filtering, but not after (this border frame has been removed in Figure IV.6).

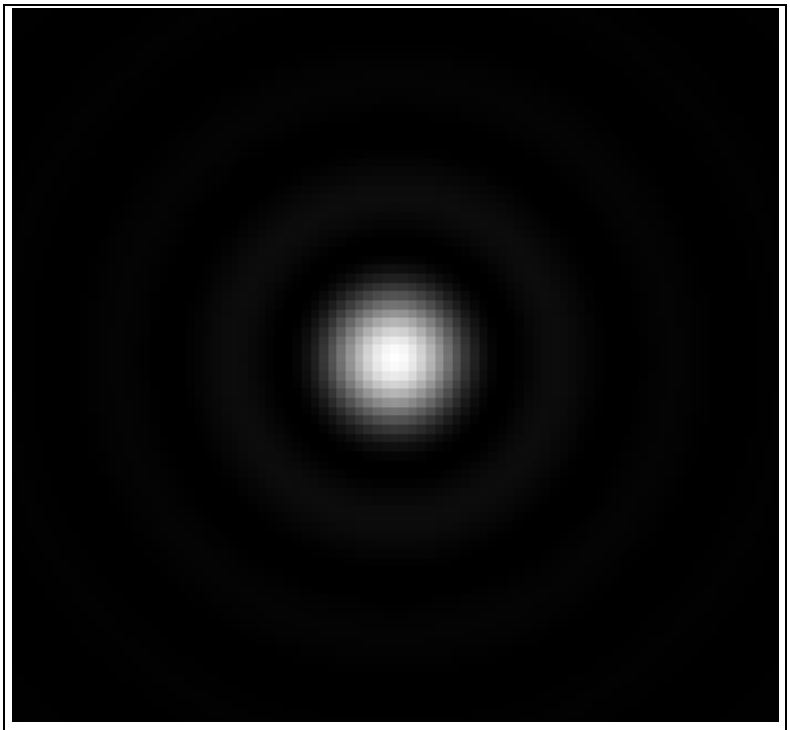

Figure IV.5. Two-dimensional representation of the spread function

The pixelation on the image (Figure IV.5) may be noticed, on one hand, because of the zoom magnification of the image, and on the other hand because this distortion (spot) is formed by approximately 27x27=729 points. Even though we have used this whole diffraction pattern, secondary lobes can be neglected due to their relatively low amplitude in comparison to the main one.

Subsequently, the test signal or pattern shown in Figure IV.2 is convolved by the signal (image) shown in Figure IV.5. The result of that can be seen below in Figure IV.6.

We remark that hereafter every single point which before the blurring effect was applied was clear and sharp will now be distorted, blurry.

We remember that this phenomenon is normally avoided and prevented at any imaging application; diffraction blur is an important constraint in any artificial imaging device, from home regular digital cameras, telescopes and any scientific optics.

So now, we get this blurry image which information is spread over many points, and at least at some extent, indeed mixed. It is also true that although by means of this convolution we are getting a blurry image, a great deal of detail is still present.

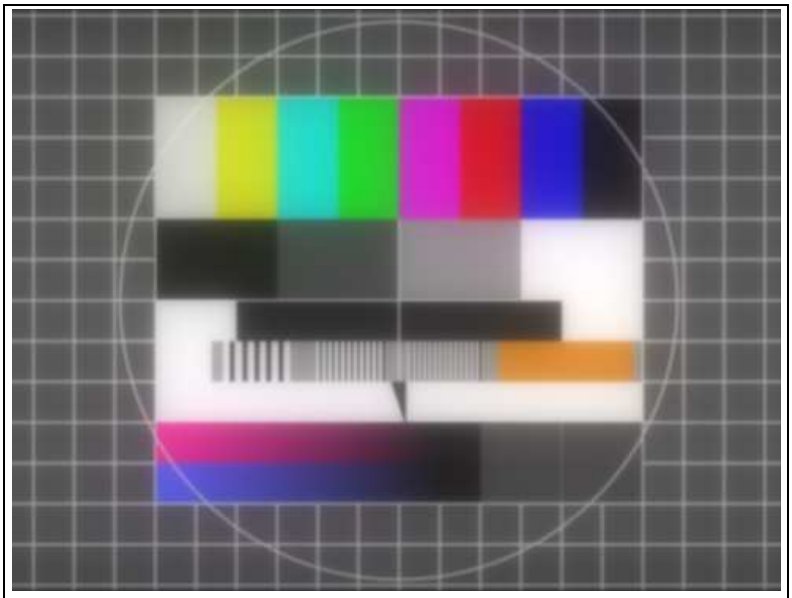

Figure IV.6. Original test image blurred with the sinc function as indicated.

The function (kernel) used for the convolution at this step is a low-pass filter, and we should not forget that any low-pass filter involves a cut-off frequency. For us, this cut-off frequency is not an unsolvable problem, but it is important to take into account that if too strict, the information at high frequencies are filtered, extremely attenuated and any hypothetical recovery by means of inverse filtering or deconvolution technique becomes unfeasible.

C. Step two: Decimation (Subsampling)

Prior to any deconvolution or inverse filtering, it is a requirement to capture or sample the signal to be processed. Thus, seeking to model the sampling or capturing stage, decimation of the original data is performed – let us remember we seek to reconstruct the original signal or object as best as possible at the final stage of our hyperacuity scheme –. In this sense, it is a question of major importance to sample correctly the blurred signal, since we aim to collect all the necessary information that corresponds with the original signal.

Decimation comprises the removal of samples and a decimation factor (M) is therefore defined. This factor indicates the number of samples among M to be retained from the original signal. Samples are consequently equally spaced at an interval (M-1) of the initial sequence.

For decimation – also known as subsampling or downsampling – some considerations should be taken into account.

Subsampling Frequency: the decimation from the initial sequence involves the reduction of the sampling frequency by a factor M, i.e., the resulting subsampling frequency is M times smaller than the original sampling frequency

$$f_{subsampling} = f_{sampling} / M \tag{4.2}$$

So as to be able to reconstruct the original signal it must fulfil the Nyquist sampling condition:

$$f_{subsampling} \geq 2 \cdot f_0 \tag{4.3}$$

This requirement is compulsory because if not observed, the signal reconstruction is deficient. But we should remark that the subsampling frequency matches the actual sampling frequency in the process described in the previous chapter.

Figure IV.7. Blurred test image (sub)sampled giving as a result an image of resolution 200x150 points

At this stage, we should be aware that in order to model the hyperacuity layout we subsample the blurred – as explained at the previous section – discrete signal or image. This frequency ($f_{subsampling}$) should be such that at least two points are captured per each cycle of the fundamental frequency; this fundamental frequency would be the highest desired frequency of the signal to be sampled i.e. the highest frequency determines the highest acuity but it also depends on the cut-off frequency of the low-pass (blurring) filter.

As already explained, there is a trade-off between spatial diversity and cut-off frequency of the direct (low-pass) blurring filter, which on one hand enables hyperacuity but on the other hand attenuates high frequencies. In connection with the sampling frequency, the logical minimum sampling frequency is determined by the cut-off frequency of the direct filter, which may be

seen in the time-space domain as a minimum of two samples per period which have to be captured to completely characterise the spectrum.

D. Step three: interpolation

The basic idea is to interpolate the image shown in Figure IV.7 i.e. to add intermediate points so as to extend the signal throughout all those new points.

It is thus important to estimate as most accurately as possible the new intermediate points. When at choosing an interpolation method, precision in the frequency domain – as in our case – is considered as important as for the temporal or spatial domain, FFT, Sinc or Upsampling Interpolation should be used. Anyway, it should not be forgotten that the Upsampling technique implies the use of a low-pass filter, which in fact introduces some distortion in frequency and phase.

We have therefore used the FFT interpolation technique, which might yield optimal results depending on the signal to estimate. One of the reasons for that optimality is the minimisation of the interpolation noise or error. This technique does not probably match the computation performed by the HVS but at least fits our needs at emulating an artificial hyperacuity system.

This technique consists in the addition of '0's to the Fourier Transform of the signal to be interpolated and thus, no information – including frequency and phase – is altered or erased. Given the equation

$$DFT^N\{x[n]\} = X_k \overset{\text{def}}{=} \sum_{n=0}^{N-1} x_n \cdot e^{-i2\pi kn/N} \tag{4.4}$$

as presented in the previous chapter – which returns the discrete transform of $x[n]$ – we can pad the transformed sequence with zeroes:

$$V[k] = \begin{cases} X[k] & k = 0,\ldots,\lceil N/2 \rceil - 1 \\ 0 & k = \lceil N/2 \rceil,\ldots,\lceil N/2 \rceil + M - 1 \\ X[k-N] & k = M + \lceil N/2 \rceil,\ldots,N+M-1 \end{cases} \tag{4.5}$$

$V[k]$ is composed in this form in order to keep periodicity in the transform domain.

Once $V[k]$ has been calculated the inverse Discrete Fourier Transform should be computed with the total number of points that form $V[k]$, that is to say, in all would be $N+M$ points. Notice that the number of zeroes is M. The interpolation factor would be $L=1+(M/N)$.

$$v[n] = IDFT^{N+M}\{V[k]\} \tag{4.6}$$

As a result of the interpolating process, an error is committed which can be quantified. A typical method to measure this error is the MSE and/or the PSNR which are equivalent (but not same) magnitudes.

Other methods, based on polynomial expressions present significant oscillations at high frequencies, but in terms of power and bandwidth are not greatly affected. FFT interpolation shows best performance regarding frequency, but differences are minimal at any operation compared to other techniques such as Sinc and Upsampling.

Beyond any numerical result concerning the interpolation error, the most important property is the phase of the signal's transform, which must be kept untouched or as least modified as possible, because any phase shift will produce catastrophic results at the next inverse filtering stage.

It is for this reason that at this stage the numerical result of the interpolation error is not so important as long as the chosen method guarantees the integrity of the phase.

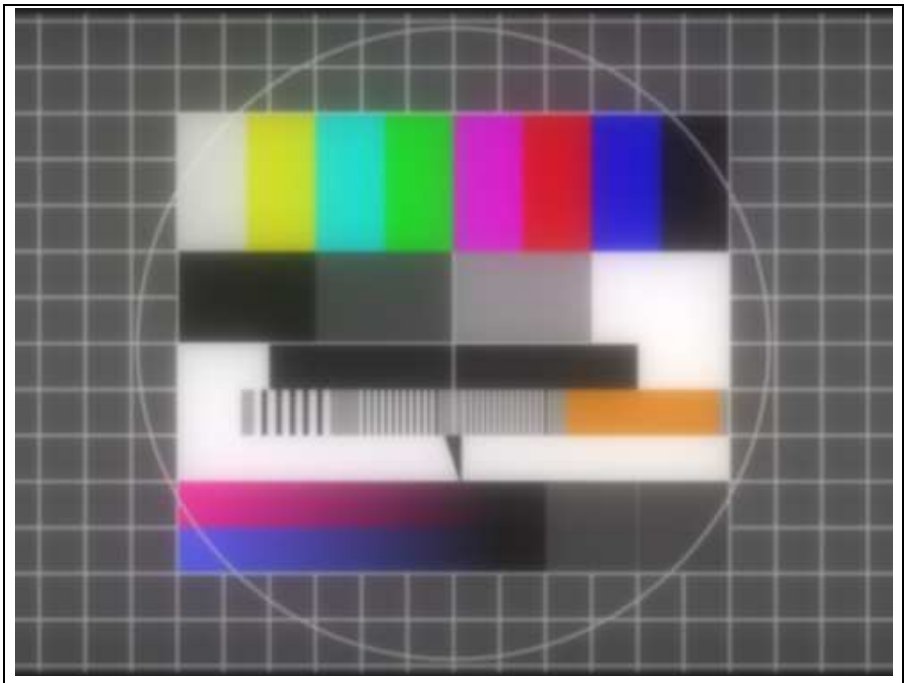

Figure IV.8. Interpolated blurred sampled image with a resolution of 2000x1500 points

As observed in Figure IV.6 the diffraction blur is present on the image. Furthermore, there is slight difference between this figure and the diffracted one.

One of the important goals at this interpolation step is to recover the original aspect ratio of the image, in this example a size of 2000x1500 pixels. The way the information is scattered is a major issue that cannot be solved with any one technique, that is to say, any variation of the final size would shift frequency and phase, making even more difficult an optimal restoration of the image.

E. Step four: inverse filtering

No optimal solution exists so far for a particular real world image restoration problem consisting in a deconvolution, but as seen in the previous chapter several techniques exist for dealing with the inverse problem, even when noise is present. So at this chapter, we will not go deeper on this aspect, but only expose the methods we have basically used.

The following test was carried out by means of the Fourier transform, where the inverse has been computed by simple division, that is,

$$\widehat{X}[k] = Y[k] / H[k] \tag{4.7}$$

All these tests were computed in absence of additional noise. We should mention again that attempting to solve the inverse problem in frequency has the drawback of needing an accurate match of the inversion as otherwise any imperfection in frequency is scattered in the spatial domain over all the final image.

Terms like “recover” or “restore” are used within this section because at this step the goal is to set an image back to its original undistorted state, but the reader may notice at this point on the more complex nature of the whole hyperacuity modelling process being performed, rather than a more common operation of image sharpening.

During this research a lot of different experiments and trials have been computed. One of the significant tests is shown along this chapter and the final result can be seen in Figure IV.9.

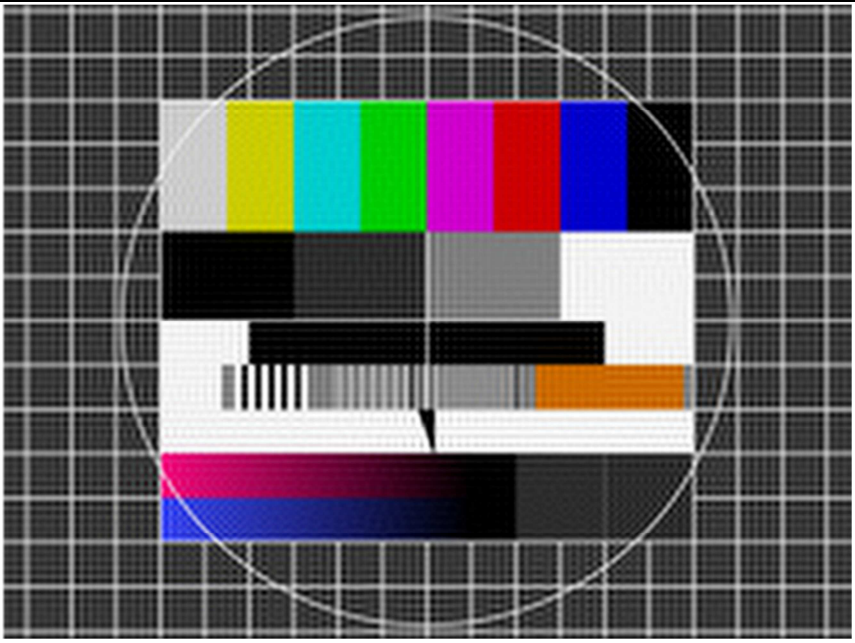

Figure IV.9. Interpolated and inverse filtered image emulating the hyperacuity, as perceived by the human visual system.

F. Comparison with diffraction limited imaging systems AKA current photographic digital imaging

An interesting comparison with the artificial imaging paradigm can be done by sampling the test image from Figure IV.2 at the same rate as with the hyperacuity paradigm, that is, a factor of 10.

We should remind that in artificial cameras, such as regular digital photo cameras, video cameras etc. diffraction is prevented as well as any other kind of optical distortion. Definitely, the information is neither spread throughout the image nor in multiple points avoiding spatial diversity.

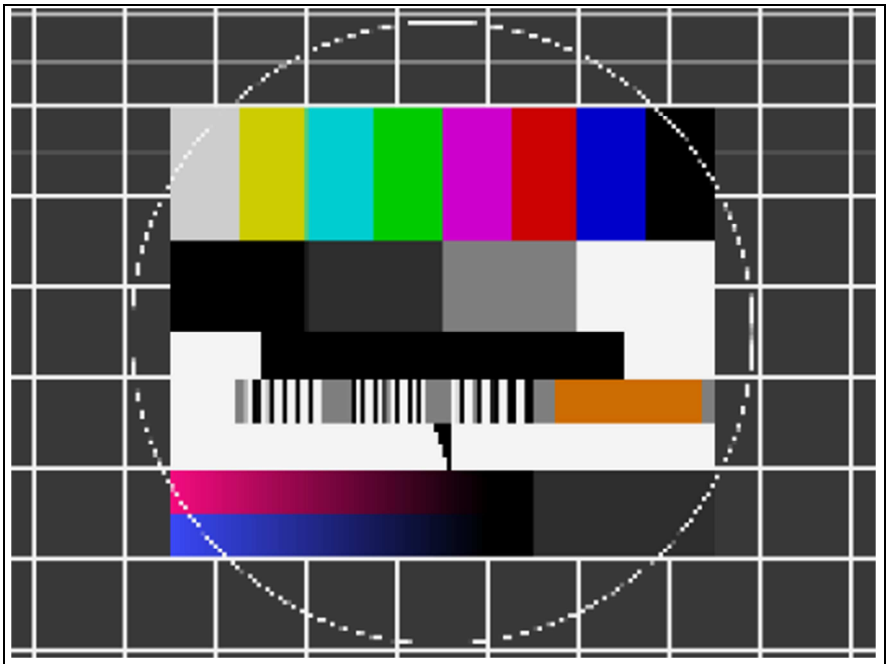

Figure IV.10. Image captured by sensors of a regular CCD device of 200x150 sensors, but augmented by sample-repetition (with the purpose of an optimal visualisation) to 2000x1500.

This means that the information not sampled – not captured – at the sampling process will just not exist. In comparison to the hyperacuity model, some information is lost because the sampling rate was not high enough to capture missing points.

The loss of details on an image captured at a certain sampling rate – in this case subsampled or decimated at a factor of 10 – is shown in Figure IV.10.

The discontinuities of the white surrounding circle can be clearly seen and the randomness of the vertical black lines on the fourth row denotes the loss of information due to the sampling process. The black triangle below shows the harsh – square – transition between pixels.

The lack of details on an image in photographic cameras is an issue that the industry of photography has tried to solve in general terms by increasing the number of photoreceptors – *megapixels* in popular terms – but due to the condition of the

minimum separation between sensors related to the Rayleigh criterion the frame of the photoreceptors' area has also been increased.

The hyperacuity image may be attributed as a defect the moiré style checked noise pattern which could be due to the ringing of the windowed processing scheme used.

We should recall that we are sub-sampling by a factor of 10 the test image from Figure IV.2.Thus, the image on the left shows the acuity obtained with a typical digital imaging device at that same rate.

In this way, the results show clearly how the high-frequency areas of the image get the viewer wrong by shapes which did not originally exist, such as the square white boxes and the vertical black bars. In addition, the lack of white grids and lines is visible.

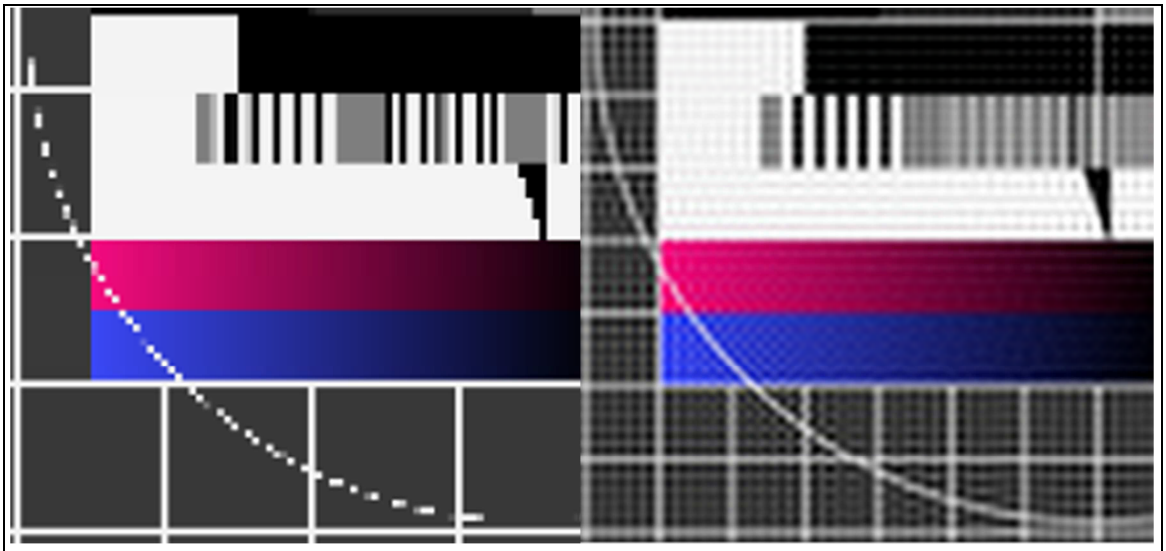

Figure IV.11. Comparison of the typical photo-camera technique (left) with the hyperacuity paradigm (right)

G. Measuring the results

1. Often used and often misused

An important question when obtaining or publishing one self's results, is the magnitude how these are explicitly measured. It arises that the right magnitude – km/h, mph, degrees-per-second… - used for measuring the speed of cars, vessels, movement of the earth, are all related but different scales.

One of the typical methods used to quantify the degree of error found when comparing two images, is the Mean Squared Error (MSE). This parameter is based on the Euclidean distance between two points, giving an idea of how different they are. The errors are summed up to and averaged by the number of points. To be more specific,

$$MSE\left(\bar{X}\right) = E\left(\left(\bar{X} - \mu\right)^2\right) = \left(\frac{\sigma}{\sqrt{n}}\right)^2 = \frac{\sigma^2}{n} \tag{4.8}$$

The $\bar{X}$ accounts for the sample means, μ for the mean of the population, σ for the deviation and n for the samples. In the case of two-dimensional signals/variables i.e. images, though,

$$MSE = \frac{1}{m \cdot n}\sum_{i=0}^{m-1}\sum_{j=0}^{n-1}[I\left(i,j\right) - K\left(i,j\right)]^2 \tag{4.9}$$

Here $I(i,j)$ and $K(i,j)$ represent the estimated and expected value vectors – images – respectively and m,n the dimensions of the image. As such, the resulting number can be very large and we know that for some measurements a logarithmic scale could be more significant or representative. Therefore, another mathematical tool is widely used called PSNR, which is roughly the same MSE but in a logarithmic scale,

$$PSNR = 10 \cdot log_{10}\left(\frac{MAX_I^2}{MSE}\right) \tag{4.10}$$

As we know, depending on the variable type used to represent an image, the scales are different (16 bit unsigned integer, 32 bit integer,…). As a consequence of that, compensation is seen convenient or even necessary, which is implemented as the variable MAX_I, which stands for the maximum possible value of the image.

In the following Table IV.1 the measured PSNR values are listed for the hyperacuity model image and the diffraction limited digital photographic model with the experiment shown earlier in this chapter.

Image Processing Paradigm	PSNR
Diffraction Hyperacuity	17.14 dB
Diffraction Limited Digital Imaging	14.36 dB

Table IV.1. Measured PSNR values of the experiment with the FFT inverse filtering

Nevertheless, as stated at the beginning of this section, the actual fact is that two images might be similar in terms of PSNR but after a visual examination, the subjective opinion might be that the sharpness of the image changes in great extent.

Thus, it is in general considered necessary the visual – subjective – analysis of results of processed images for the reasons formerly explained, as well as because the details present in an image are of different nature.

Notwithstanding, in order to support objective conclusions out of any image test or processing, there have been some efforts to produce a series of tests which may conduct to a numerical result.

As reported by some authors (Zhou Wang, Bovik et al. 2002) there have been several efforts in the last four decades to develop new image quality assessment methods which include perceptual quality measurement paradigms aiming to meet the expected by the HVS. As it may seem pretty surprising, there are not many successful approaches in this field and it has been appointed that none of these complicated metrics found in the literature has shown significant advances over the widely used MSE and PSNR methods (Martens, Meesters 1998, Eskicioglu, Fisher 1995)(Martens, Meesters 1998, ITU 2004, ITU 2004, Campbell, Green 1965)(Martens, Meesters 1998, ITU 2004, ITU 2004, Campbell, Green 1965)(Martens, Meesters 1998, ITU 2004, ITU 2004, Campbell, Green 1965).

There are many propositions as well on the assessment of video/image quality and the International Telecommunication Union has been working on the elaboration of a standard which would allow an objective and harmonized method for this purpose (ITU 2004).

2. The spectral approach

An interesting and objective way to inspect the acuity on a signal processing task could be the frequency of the signal present in the image, thus, a verification of the existence of the originally existing frequencies. As such, we have used the following test image to check the applicability of the two-dimensional IIR inverse filtering scheme: As can be seen in Figure IV.12, the checked pattern provides high frequencies along the X and Y coordinates of the image. We may compute the blurred image convolved by the diffraction filter by either means;

2D convolution or 2D FIR filtering, because it yields same results. But prior to that, we may compute the Fourier transform to check the frequencies.

Peaks can be noticed all over the mesh represented. Central peaks correspond with the lowest frequencies whereas the green bluish peaks on the quadrants – higher distance from the centre means higher frequency – represent high frequencies.

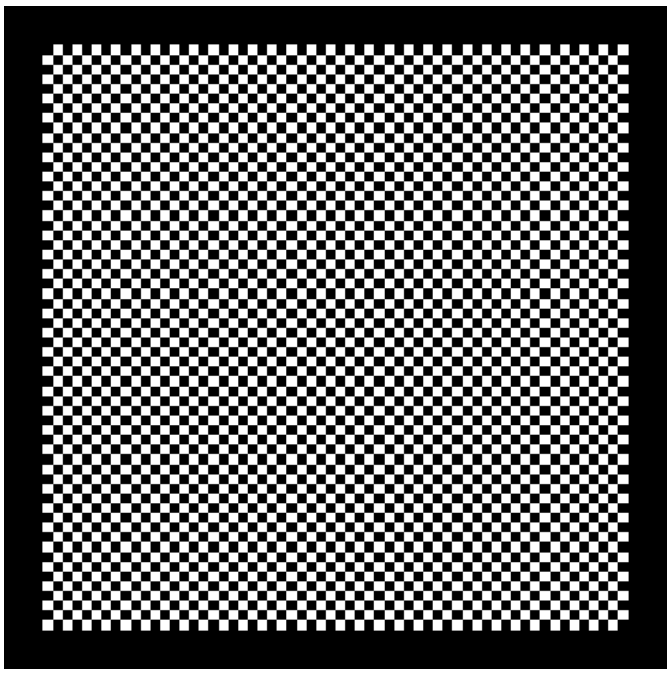

Figure IV.12. Original image for the 2D-IIR inverse filtering test

The filtered image then will be a blurry image, as diffraction is introduced as a distortion. This image can be obtained by many filtering paradigms, among others FFT and spatial convolution. But this time we will show the effects of the two-dimensional infinite impulse response inverse filtering.

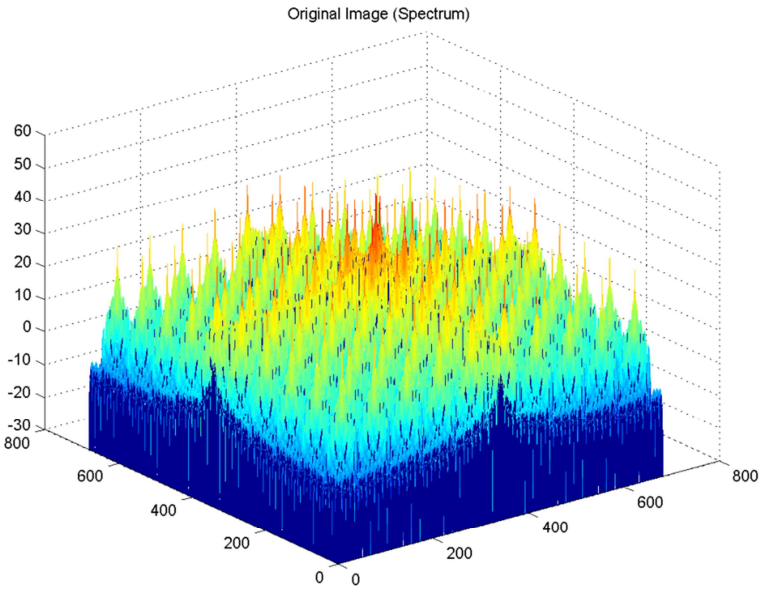

Figure IV.13. Log-magnitude 3D plot of the test image in the frequency domain

The diffraction as may be noticed blurs the test image and in consequence black-white or white-black transitions in the check board pattern are softer, less clear or less sharp. This is quite indicative of the lack of high-frequency information. The spatial shifting can also be seen with respect of the top-left corner of the image. This is due to the causality condition set in the two-dimensional difference equation processing, explained in the previous chapter.

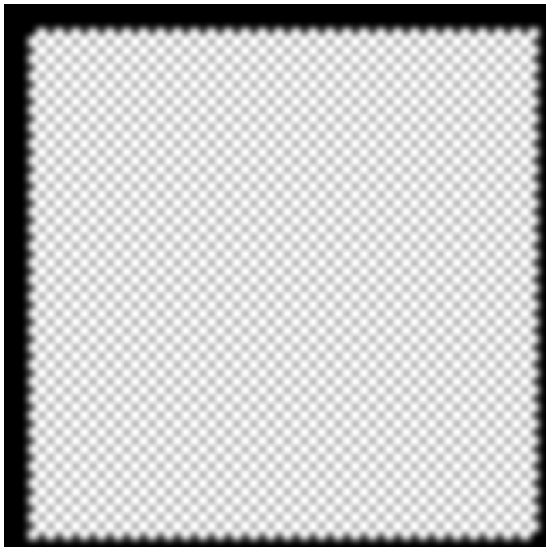

Figure IV.14. Diffraction blurred or filtered (low-pass) test image

In the following figure (Figure IV.15) we may see this phenomenon in the frequency domain

The outer corners of the quadrants correspond with the highest frequencies. In this case (Figure IV.15) they seem to have been removed or extremely attenuated.

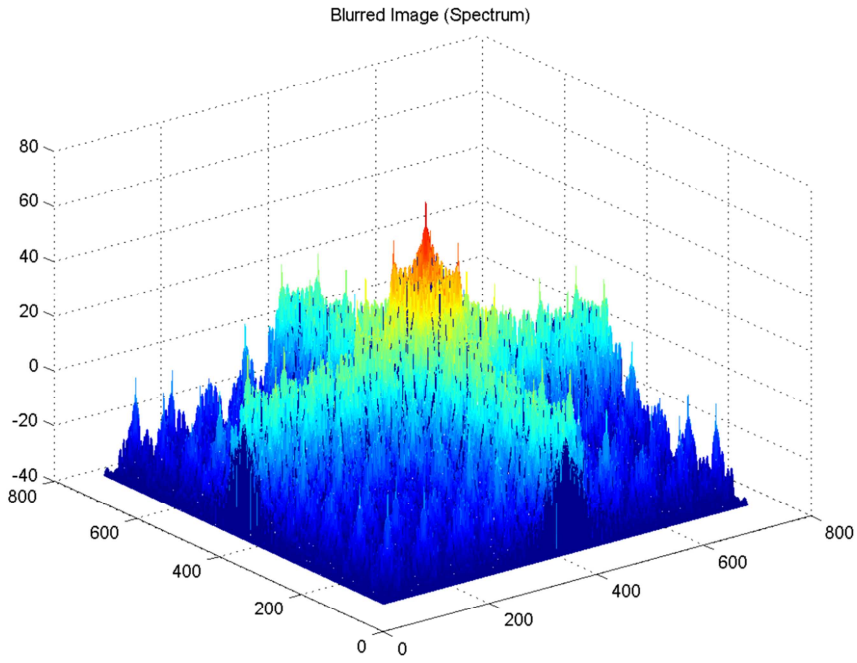

Figure IV.15. Blurred original image in the frequency domain represented in log-magnitude scale.

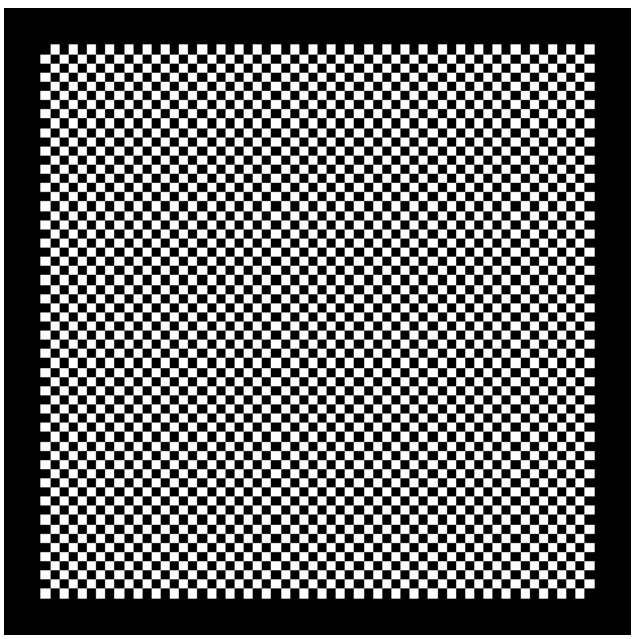

Figure IV.16. Image recovered from the blurred image

Finally, the blurred image is recovered thanks to the 2D-IIR inverse filter,

It may be concluded from Figure IV.16 that the 2D-IIR inverse filter is exact and allows total recovery from a prior low-pass filtering scheme such as the diffraction low-pass filter.

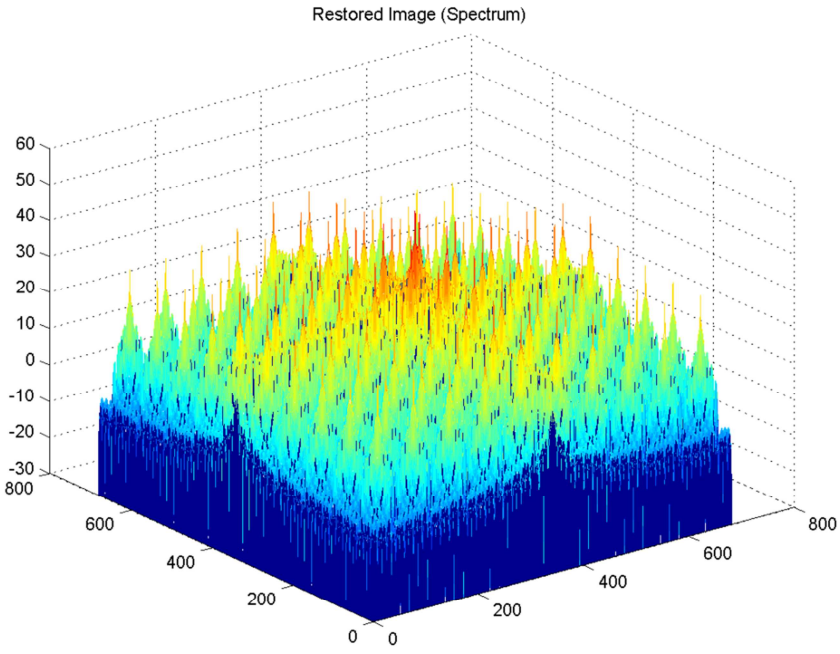

Figure IV.17. Log-magnitude 3D plot of the recovered test image in the frequency domain

3. Brief comparison of the error committed with interpolation techniques with two-dimensional signals

There are several different methods for interpolating signals, but in this research, we do not aim to go into a deep analysis on interpolation techniques. Nevertheless, we have performed a short comparison of some commonly used interpolation techniques which we found suitable for the hyperacuity model simulation. Beyond this, more results on tests with one dimensional signals are presented in the annex chapter.

In order to carry on this test, the blurred (diffracted) image presented in Figure IV.18 was decimated by a factor of 4 prior to interpolation, and then interpolated by a factor of 4. The results have been compared and shown in the table below.

The error introduced at the interpolation step can accurately be measured with MSE and PSNR error scales because the error measured depends directly on the algorithm that approximates new points, and the "new" information relies on the previous information, unlike at image restoration or inverse problems.

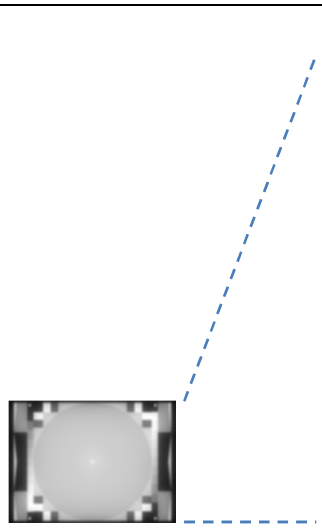

Figure IV.18. Subsampled MxN image.

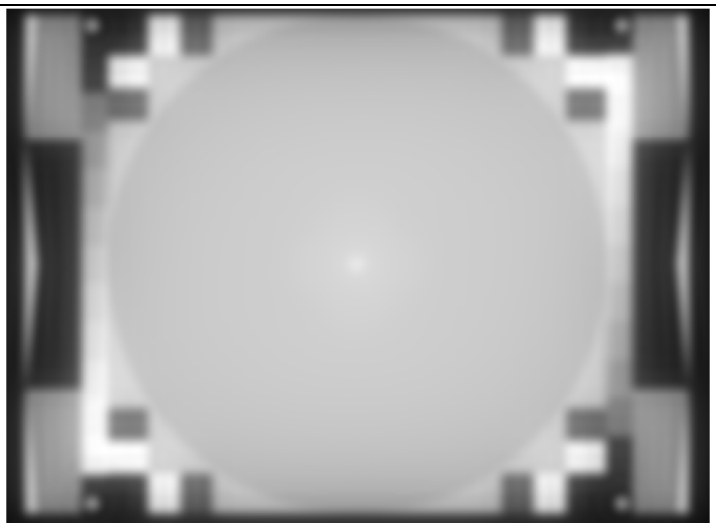

Figure IV.19. Interpolated image with a resulting resolution of (4M)x(4N)

Interpolation technique	**Decimation factor M = 4**		
Test signal : x_1	**M.S.E.**	**Variance**	**PSNR (dB)**
Linear	0.0322672	8.832278e-9	29.82 dB
Spline	6.07194e-5	1.02903e-16	84.33 dB
Hermite	0.031984	8.837285e-9	29.9 dB
FFT	8.46091e-7	1.66025e-24	121.45 dB
Sinc	0.03051363	7.550756e-9	30.31 dB

Table IV.2. Comparison of interpolation techniques for a two-dimensional signal

Beyond this circumstance or factor there are optimal dimensions for piecewise interpolation techniques, but the frequency-phase distortion prevents from an efficient inverse filtering scheme with them. In addition, as it is shown in the table, the FFT interpolation technique is by far the most efficient regarding the absolute error (and variance), which in turn is based upon the Euclidean distance.

H. Conclusions

In this chapter, we give a practical outlook of what can be achieved with the hyperacuity paradigm we implement and test.

Given that the sampling/interpolation factor is 10 the results look quite promising, and as can be visually deducted from the resulting picture a great deal of high frequency information is recovered: white grid, vertical black lines…

A very important aspect about the hyperacuity paradigm is that the information shown is the information that has been captured; there are no "lies" in between. At most, some noise can be perceived, maybe due to rounding and/or inaccuracies related to interpolation, but in the resulting image, a great part of the original information can be found.

There is a nice remark to be done on the decimation process. As it is widely known, any decimation or sampling requires a low-pass filter to remove the alias or high frequency components that can overlap desired low-frequency components. In this scheme, we believe it is naturally performed by the diffraction filter, which is equally a low-pass filter. Nevertheless, this filter should be understood as a mechanism which scatters the signal over many sensing points.

Additionally, we should be aware of the lack of information at the CCD imaging paradigm. When the image is displayed we cannot know the degree of similarity with the original object. The most typical phenomenon in this regard is pixelation which implicitly warns the viewer on this issue. So we should remark that due to loss of data, the captured image in this CCD paradigm can be delusive which can be deducted from many details but also specifically from the lay-out of the vertical black bars in Figure IV.2 and Figure IV.10.

The interpolation step is more important than it might seem to be, because many of accurate interpolation methods estimate new points without respect of the position of the new inferred data, which can be critical. This can be a major issue when the inverse is computed in the frequency domain and as a consequence of this point shifting, the phase might be changed which may represent a serious problem for computing the inverse in the frequency domain.

The images shown in this chapter have initially been inverse filtered by means of the FFT transform, due to lack of noise and easiness of computation and programming. But the important thing about this is the possibility to carry out all these operations in a fast and efficient manner, and actually, many of our optimal results have been done with this tool. Nevertheless, there are good reasons to choose other paradigms or methods on the way to find a solution for our inverse problem, and one of them is the scattering of the information when this transform is computed, i.e. the error contained by each of the values of the array to be transformed is scattered in the target domain. In addition, these transform tools do not by themselves solve the inverse problem, nor seem to facilitate it, i.e. zeroes and/or NZV might exist regardless of the transform. We may find a slight exception on the cepstral method; this is an interesting yet simple approach

permitting in some cases the inversion of the problem due to its logarithmic nature, but it presents constraints and the results obtained on the hyperacuity problem are disappointing which might be related to the fact that the inverse filter/system utilised is unstable and used in a non-bijective algebraic application.

Although the discussion now is not about the specific method for the inverse problem – the method to be used for a complete restoration of the blurred image – we consider that the two dimensional IIR inverse filtering is an interesting and effective approach that should be taken into account because at this point we have successfully processed the images presented in this chapter. This time-space domain analysis is observed to suit better computational features of the inverse problem solved by the HVS (and depending on the specific implementation software implementation will as well be more computationally efficient) especially due to the linear model apparently carried out by the biological layout. Convolution-deconvolution schemes though do not appear to be the case, since there are several approaches and techniques involving non-linear and iterative features which are not credible to be happening in the brain, plus the immediate opposite procedure of the convolution – direct approach – has to face the issue of zeroes or NZV and does not facilitate any additional manipulation.

As of this thesis is written we believe that systems described by difference equations can give an answer to a definite solution to our inverse problem due to the simplicity and local nature of the way the problem is solved. Moreover, all methods exposed seem to yield a system of equations with an ill-posed inverse creating as well an unstable output except that of difference equations. We could additionally discuss on the suitability of an algorithm or method to carry out the hyperacuity test scheme where unlike the convolution (or even deconvolution) scheme, difference equations need not the whole input data array (blurred signal/image) to be processed and can return accurate values on a localised area by inverse filtering. This might look like an iterative approach but it is rather a sequential process because information data to compute are locally dependent, not globally. The FFT does not clearly suit the criteria exposed about its feasibility by the HVS but in case that computational costs are not a constraint it might well provide interesting results, which are shown in the following chapter.

In connection with this, there are two challenges left: to effectively inverse filter noisy images and improve inverse filtering of inaccuracies (rounding, interpolation).

Although we haven't shown any test result with neural networks we should notice that any of the methods tested and shown so far can be developed by mean of these. In this sense neural networks are very promising and interesting due to the similarity of the concept to that of the biological paradigm and open possibilities for real-time implementations. In fact, it is known that the information processing in the human visual system is performed by biological neural networks, but again, we remark that complexity and still unexplained features of these neural configurations make these approaches uncertain. There are already efforts to imitate this biological paradigm.

As a last remark, visual inspection remains as the most reliable technique to measure details related to angular resolution, which means that PSNR measurements usually

provided in scientific papers reporting comparisons of image processing techniques are not necessarily meaningful. In contrary to this, PSNR can be meaningful for the comparison of different interpolation techniques because there are allegedly some reference unchanged static points and the rest can be more or less modified, so the degree of approximation – as long as the position is unchanged – can be representative.

Regarding the applications of this novel paradigm, we should take into account that degree of enhancement makes especially sense for some fields where the information present in an image is extremely important, such as MRI, Terahertz imaging applications, seismology… And a factor of 10 as shown in this chapter means that an MxN pixel image would become a $10Mx10N$ size image, that is to say, an image of 100 times higher resolution.

Chapter V. Technological Applications of the Hyperacuity Paradigm

A. Introduction

Up to this chapter, we have shown the hyperacuity existing in the eye, and how the diffraction hyperacuity could be used to obtain 'unsampled' data so as to compose a higher-resolution image.

There are still many challenging issues wherever any sampling or discretisation of data is performed. One of these is the maximum number of samples captured at a sampling sweep imposed by physical restrictions. This is not an important concern in digital regular photo-cameras but there are novel imaging systems where this is very constraining, as for example in Terahertz imaging. Here, the size of the antennas is a physical preset that precludes any handy system configuration due to the size of the antenna array required for a minimum resolution. This is especially important whenever embedded solutions are necessary – aircrafts – or security non-collaborative schemes – handy-cams – are considered for use.

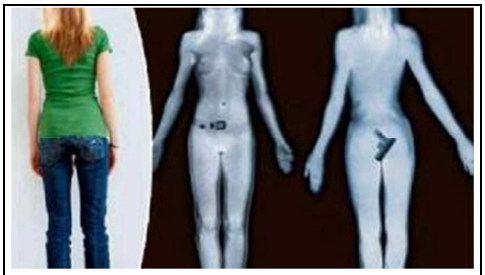

Figure V.1. Terahertz full-body scanner

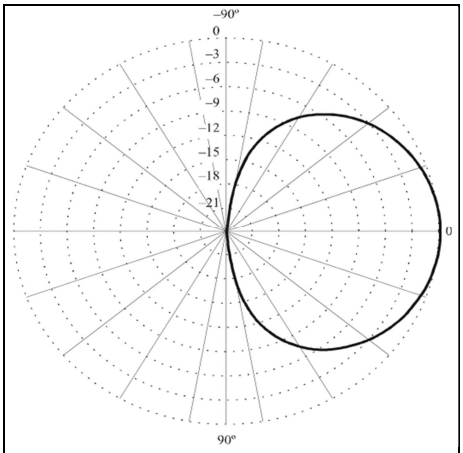

Figure V.2. Vertical pattern for a half-wave dipole in vertical polarization

Imaging systems are probably the most known systems having to face this kind of problems, but there are others such as antenna measuring field-metre probes which have to deal with similar sampling limitation issues.

We will first give a brief outline of an overview of current antenna systems, where the eye's resolving capabilities are analysed from the perspective of antennas giving an idea of what it can be expected from this new concept.

Next, we deal with some systems where the hyperacuity model could provide a novel paradigm and could lead to powerful solutions, i.e. how hyperacuity could leverage a solution to some of the existing limitations.

B. Antenna imaging systems

An imaging system could be understood from the point of view of antennas as a multi-beam system. Usually, each specific application with antenna systems handles a specific solution.

In many applications where acquisition time is not a critical issue, the illusion of a multi-beam could be created by electronically scanning a single beam through all the field of interest (using hopping spot beam techniques). The Synthetic Aperture Radar (SAR) systems are a clear example of that, but there are also many communication satellites that create coverage spot maps just hopping a single spot beam sequentially onto different locations (Campuzano, Montesano et al. 2010, Alvarez, Peña et al. 2011, Alvarez, Montesano et al. 2011, Montesano, de la Fuente et al. 2012, Snoeij, Attema et al. 2009). In both cases, the aim is to draw a certain coverage map over the earth's surface.

All astronomical observation systems could be classified inside this category, since even though some of them are not array outfitted, a high directivity beam is created to obtain an image of the sky profiting from the movement of the earth. In the same sense, the HFI and LFI experiments of PLANCK (Mandolesi) – and other similar systems – are capturing images through high directivity beams, i.e. scanning the field of interest using some kind of movement.

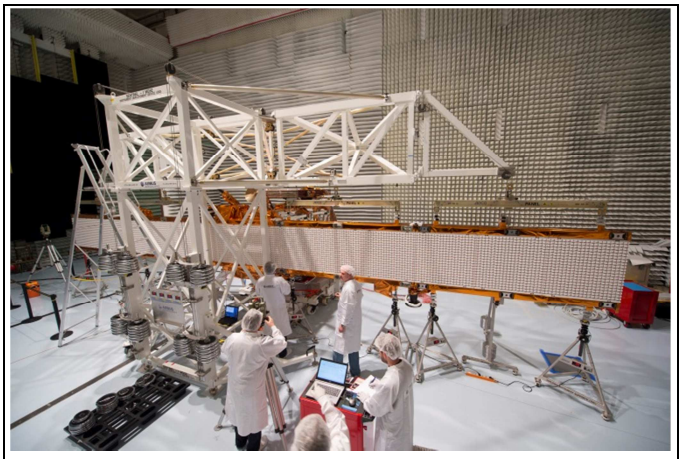

Figure V.3. Tests with the array antenna for the Sentinel-1A satellite (courtesy of ESA).

From the antenna perspective, all the antenna elements in these systems are devoted to create a single spot beam, defining the resolution, mainly, by the beamwidth. These systems could also be considered as cooperative imaging systems, since all the elements are working together to create a unique resulting image or coverage map.

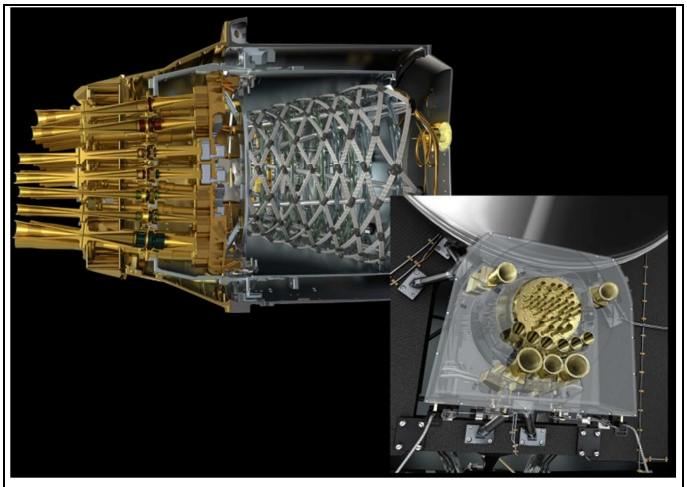

Figure V.4. Planck's Low Frequency and High Frequency Instruments. (courtesy of ESA).

Besides, there are applications where the beams are created by individual radiating elements, including the possibility to be magnified by a lens system. The classical parabolic reflector antenna and low directivity feeder could be an excellent example of this type of systems, as well as the multi-feed reflector antenna configuration (D'Amico 2011, O'Connor , Kramer). The antenna satellite systems have used this multiple feed configuration at multiple frequencies illuminating a reflector system to create the desired coverage map on the surface of the earth (O'Connor).

The resolution issue rises up due to the limit imposed by the minimum distance between the radiating elements, which is fixed by its aperture dimensions. This limitation often forces the use of several reflector antennas on the same satellite aiming to generate adjacent beams on the earth's surface (O'Connor).

Additionally, the number of beams per lens is limited by the distortion-free area nearby the focal point of the lens. Normally, the bigger the magnification of the lens, the smaller the area free of distortion would be.

Figure V.5. Arecibo Observatory.

In short, these limitations prevent from extending endlessly the number of detectors per lens, so the only option left would be to iterate the whole system, leading to some kind of a multi-focus array system such as the ALMA (Marcelino) and VLA (Kogan) experiments (Figure V.6), which are well known by the scientific community. These configurations

though, resemble as well the compound eye of some insects, as in CCD sensors of digital cameras, where each sensor or detector works independently from the neighbouring elements.

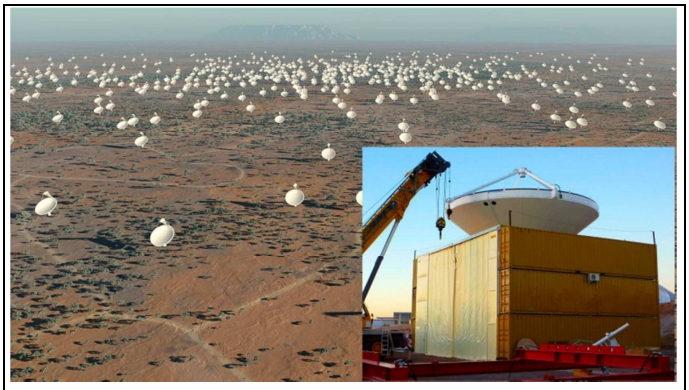

Figure V.6. ALMA installation (ESA) and SKA antenna layout.

Although the behaviour of these systems could be understood as non-cooperative, the final result is usually a composition of different signals received from different sensors which may compose some kind of image.

Back to the human hyperacuity paradigm, we know at this point that the angular resolution achieved by the eye is surprisingly high, but let's before take a look on other visual systems existing in the wild-life.

Some examples of these different technological approaches could be found in nature too. For instance, the typical fly's eye – actually a compound eye – is a multiple-lens system allowing the detection of subtle signal variations from almost all directions around (Figure V.7).

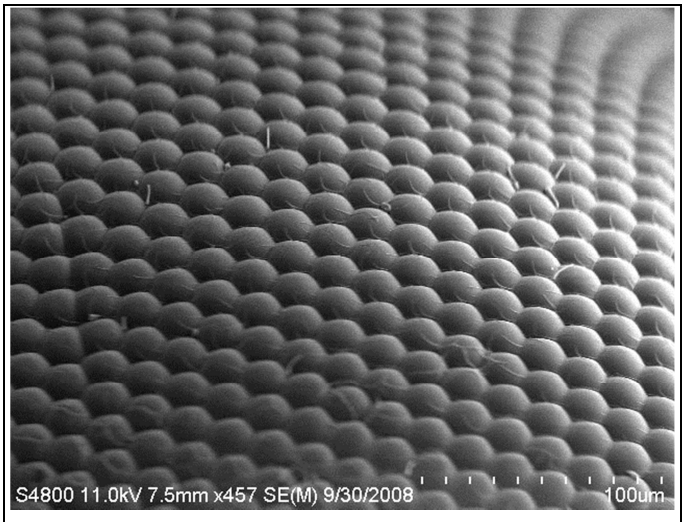

Figure V.7. Augmented area of a real fly's eye.

Under the point of view of antenna systems, we could say that it will be a non-cooperative multi-beam system. Each one of the lenses creates a high directivity beam, which is separated angularly from the neighbouring beams because of the physical separation between lenses.

The previous system is more than enough for insects that intend to be aware of possible dangers that could stalk from almost any direction. Resolution is a minor issue for them.

On the other hand, there are visual systems rather oriented to improving the resolution of the captured image. For instance, many predators need to distinguish among possible preys from long distances, or vice versa. But this is also the case of the human eyes, which are able to automatically focus objects at different distances and see under low light conditions –they can control the entrance of the light to prevent any possible

saturation of the photoreceptors –. But maybe the most surprising feature is the high resolving angle with an amazing low number of detectors – as seen in the first chapter –.

Morphologically, the human eye is composed by a unique lens significantly bigger than the lenses of insects, which means, that the area free of distortion is also bigger. Therefore, it is capable to locate a higher number of sensors.

Initially we could assume that each sensor creates a beam as the insects' do, with the only difference that now a unique lens is used to increase the directivity of all the beams, in the same way as conventional digital cameras do. The surprise arises when the number of beams capable to explain the resolution is compared to the number of sensors. This number is much higher than the number of sensors, as we will see later on.

In contrast to the invertebrates' eye, the human eye does not detect motion from 360°, but it reaches the known hyperacuity, that is to say, acuity beyond the capacity provided by its own sampling, giving the impression to surpass the Nyquist limit.

But along with the classical resolving ability (1 min of arc), again we remind the hyperacuity, which permits capturing images of objects as small as even an arc of a second (Klein, Levi 1985) and is a proof of the decoupling between the number of beams and the number of sensors.

The explanation for the hyperacuity from the perspective of antennas is that the human eye is using several sensors to create high directivity beams and the effective areas as we have already seen, they are strongly overlapped. In this sense, the directivity of individual beams is enhanced. By overlapping the effective areas we could keep all beams close together in angle, improving the resolution. It would be an intermediate strategy between the two presented above: cooperative and non-cooperative techniques.

In both paradigms the captured image resolution improvement can be achieved. In the case of the first, this can be done by artificially introducing some blur and taking advantage of the radiation pattern itself. It should in both cases be ensured that the blur remains constant throughout the image, has a more or less uniform phase in its central part, and that we can somehow control the noise input at the system.

C. Non-cooperative antenna systems

Non-cooperative systems are understood as those in which the different sensors work independently and the information intended to be captured by each is different. One of its main features is that the resolution is usually limited by the size and separation of the sensors. Different applications can be found among these: conventional digital cameras, more modern imaging systems, and even other high frequency multiple feeder systems – such as in satellite applications intended for cellular coverage –.

So that results in such systems can be similar to that of the achieved by the human eye, a common aperture prior to detection must be introduced; in the case of transmission systems, smaller feeders combined with beam forming networks of the type of CORPS could be used (Southall, Mcgrath 1986, Mailloux 1974, Hrycak 1982, Betancourt, Del-Rio-Bocio 2007a, Betancourt, Del-Rio-Bocio 2008, Betancourt, Del-Rio-Bocio 2007b, Schneider, Hartwanger et al. 2009). Thus, we may get the blur/overlap required in reception/transmission, respectively, aiming to improve performance in terms of angular resolution.

1. Terahertz imaging

Depending on the detection paradigm implemented on a Terahertz imaging device, the system can be cooperative or non-cooperative.

Terahertz imaging systems are currently riding highest in terms of complexity and potential. Its features show a variety of possible future – and current – applications.

Figure V.8. Possible applications of Terahertz imaging systems

Airport full body scanners are maybe the most lately popular of these imaging systems as shown in Figure V.1 and Figure V.8 (centre). But thanks to the way electromagnetic waves behave at these frequencies, there are many new featured examples important applications, such as imaging under poor visibility conditions (transportation, aircraft,...), detection of skin cancer, different types of medical imaging, etc.

In turn, due to the nature of terahertz frequencies, this technology still has to face some challenges. An important limitation is related to the dimensions of the antenna which can be understood with a simple overview at the electrical features of waves at those frequencies. This constraint affects the total number of sensing antennas. Therefore a typical – and practical – configuration is using a single sensor – or limited number of sensors – but assisted by a beam scanning.

Figure V.9. Terahertz imaging device using a mirror sweeping technique.

Thus, one of the ways the problem of spatial resolution is solved is mechanically, with a mirror based sweep. Nevertheless, the performance is so slow that capturing an image in a single shot becomes unfeasible; it actually demands a scanning time that typically exceeds a minute. This could be overcome with an electronic beam scanning, but this possibility is still under research; more specifically phase shifters which could work at these frequencies.

Apparently, the only way of capturing an image in real-time is by means of a sensor array that equals the number of elements to that of the pixels. But in this case, on a

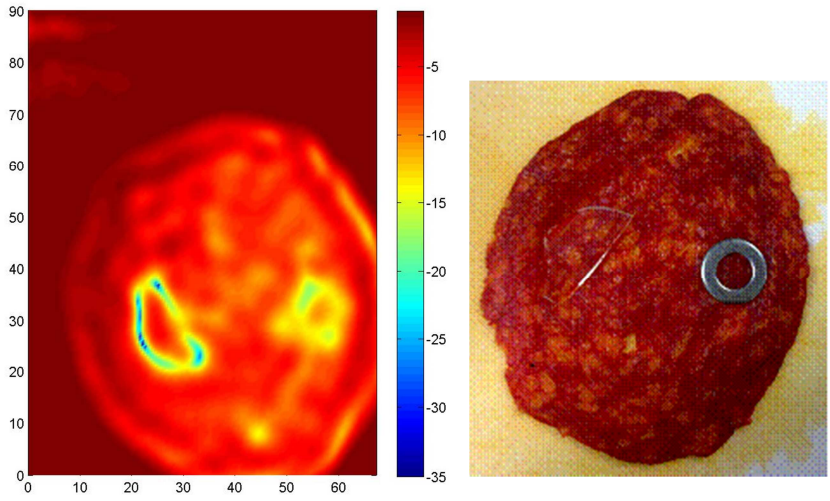

Figure V.10. A slice of chorizo with conductor materials on its surface. Regular photograph taken with visible light (left). Image taken at 140 GHz.

configuration of an array of sensors – such as in a digital camera – we would have to deal with a poorly featured array, of very few sensors due to its dimensions.

The amorphous shapes shown in the terahertz image from Figure V.10 shows clearly the lack of resolution points.

On another hand – as already said – so far each of the terahertz sensors captured an area of an image avoiding any overlap with contiguous ones, that is, one sensor per pixel, exactly the same way as any other digital cameras do.

Now, we could use the hyperacuity paradigm to improve the spatial diversity as exposed along this document, and so, instead of trying to get rid of distortion, use to extract the information and improve the acuity such as the human visual system is doing.

2. Hyperacuity and overlapped beams

In connection with previous chapters, as well as with the entire work presented in this document, as may be understood at this point, overlapping beams could be once more contributing to spatial diversity instead of just mixing and distorting the information or signal captured.

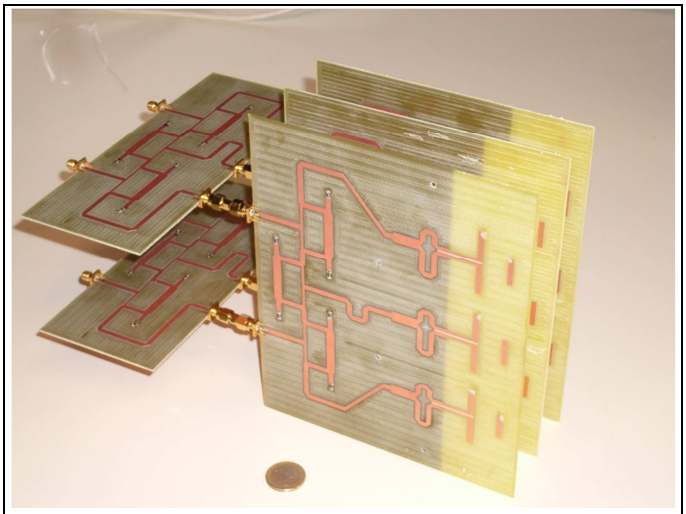

Figure V.11. Antenna system with overlapped beams (Betancourt, Del-Rio-Bocio 2007b).

Figure V.11 shows an example of beam forming networks where beams are overlapped: CORPS-BFN. This is a structure that can smartly spread different signals into it, in a way that each signal introduced to the system is driven into a specific set of outputs shared between signals; all this without losing information due to couplings or other associated effects.

The difference in this case is that the role of blurring is performed by the antenna system due to its radiation pattern instead of by an aperture as happens in the eye.

Thus, the virtual sources generated by a CORPS-BFN system can be put with separations of a wavelength or even less and generate beams that are closer in angle than the ones generated by independent horn antennas which separation is limited by their size. We should notice that when working with clusters of horns the minimum distance is fixed by the diameter of the single-horn aperture which results in a spot spacing greater than the one required, whereas with a CORPS-BFN combined with electrically smaller radiating elements, the spatial step is the physical size of a single radiator, much smaller than the effective radiation area of one beam.

D. Cooperative antenna systems

Cooperative systems can be defined as those where different radiating elements work together towards creating a single beam which can be potentially moved angularly, either electronically or by physically moving the entire system. These are often very large groups of more or less small antennas (slots, patches, apertures, etc.) amongst, ranging from conventional radar systems to the latest generation ASAR type radar.

In this type of systems the resolution limit is defined by the width of the most directive beam that can be generated, as it defines the minimum angular interval for subsequent – and independent – intervals where information is captured, i.e. preceding and following angular positions. It would be a very similar criterion to that used in non-cooperative systems but on radiation. This is usually translated as a limit in the angular sampling beamwidth interval, or intersection of 3dB. Thus, most of the energy received entering the main lobe, can be attributed to a specific direction, in an unambiguous manner.

The improvement proposed here consists in breaking that rule and sweeping as fine as technologically possible, knowing that the result will be blurred because of the radiation diagram of the array or radiating element. If the radiation meets a series of conditions such that the phase in the main lobe is as flat as possible and the levels of the side lobes stay below a certain value, the effect of the blur generated in the signal can be reversible. This will redound in images (signals) of much higher angular resolution but captured with a relatively wide radiation beam, or what comes to be the same, with physically smaller groupings.

There are different systems or applications where we may encounter this issue. In a few cases the consequences of the lack of beam resolution can be critical. We will hence illustrate a couple of them.

1. Field-probe antenna measurements

There are different scenarios where the radiation of antennas is measured. Free space would probably be the ideal context if there were no interference from other sources, but since this case is ideal – and often unfeasible – more practical approaches lead to measurements in enclosed and isolated spaces such as GTEM cells or anechoic chambers. Here, absorbent materials and geometries are used in order to prevent reflections – including a few exceptions –. So in general, the use of a specific scenario is important and the response of these chambers is modelled and known before any test is carried out.

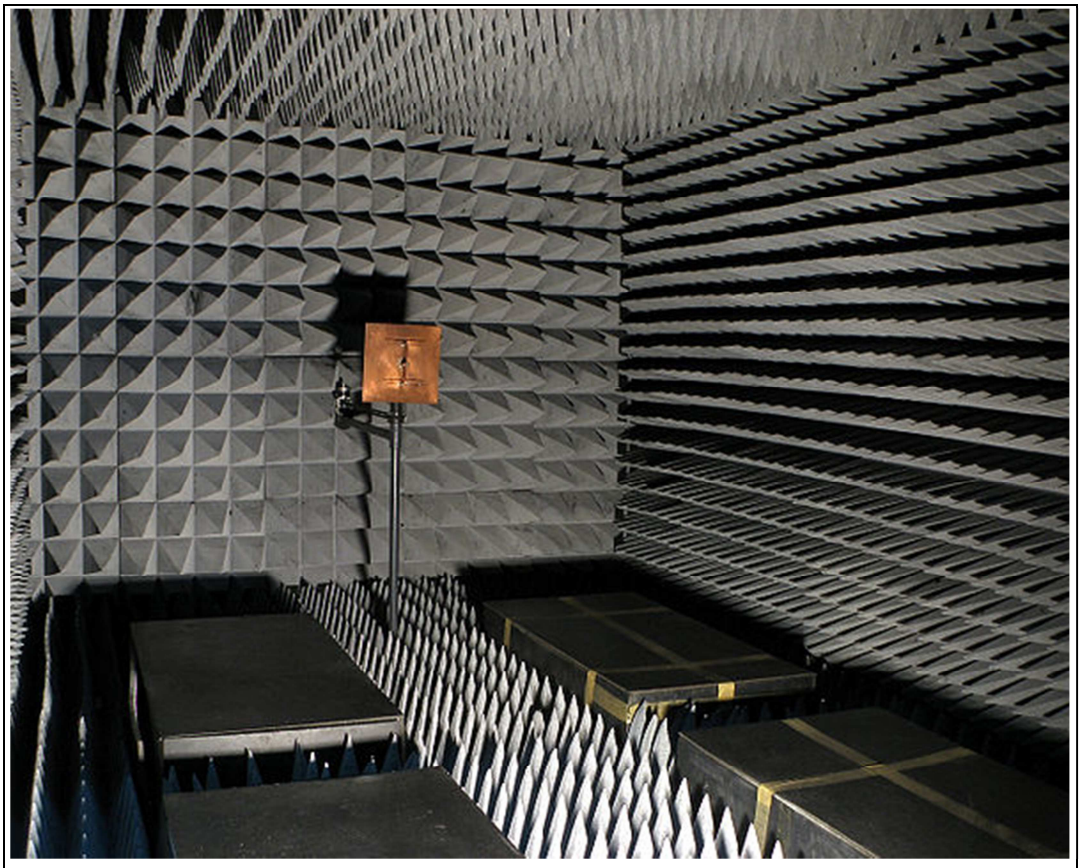

Figure V.12. Radio-frequency anechoic chamber. Credits: Adamantios

One of the most seemingly basic applications often performed in anechoic chambers, is measuring antenna parameters. The typical layout consists of the AUT (Antenna Under Test) intended to be measured and placed at a strategic location whereas the field probe is usually located at a fixed venue.

In connection with this, the characterisation of the far-field pattern is a major concern within the testing procedure, because of the generally reactive near field detected by the probe due to the short distances. In this regard, ideally the far field condition should be observed at

$$d = \frac{2D^2}{\lambda} \tag{5.1}$$

So, in order to get a fair radiation diagram of the antenna it is necessary to compensate the effects of the measuring probe, also known as *probe correction* and intends to correct the consequences of the probe's radiation diagram as well as some response to cross-polarisation on measurements. The use of high directivity probes is rather common and is justified when in far-field environments due to the increase of the dynamic range and reduction of the effects of reflexions. In near-field measurements though, it is important to avoid any null which may appear since it would be impossible to recover the information at these points so lower directivity probes – usually a maximum of 10 dB – are used. Therefore, the probe correction is performed, increasing the directivity of the radiation pattern – narrowing as well the main lobe –. This is a process consisting in an inverse problem widely accepted by the scientific community which reminds that carried out in our hyperacuity model where the information can be processed in the transform domain.

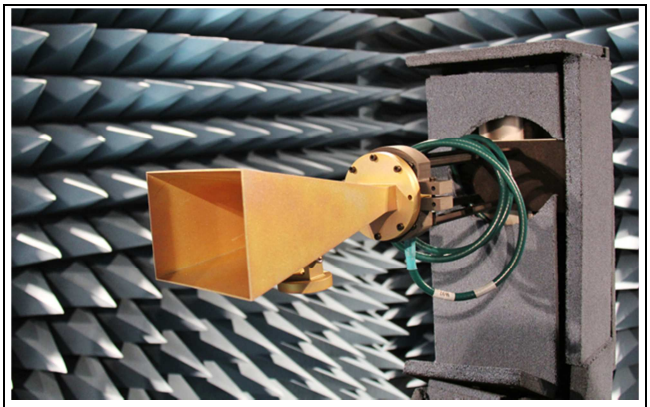

Figure V.13. EM field-test probe. Source: University of Alberta.

Antenna measuring field-metre probes have to deal with the issue of a limit related to the sampling of the received electromagnetic field, because the directivity of the probes is not as an ideally infinitesimally narrow delta-like pattern permitting to capture spatially unlimited independent samples, because the probe must be small to prevent distortion of the field intended to measure. Thus, probes receive the signal from many directions which overlap with the desired one. In this sense, we could provide this application with the inverse technique used in our model to avoid the effects of zeroes on the radiation diagram given that we can recover the information even when zeroes are present in the system.

In all, the conclusion at this point should be that the process inversion such as the probe-correction is possible and is a common and widely extended regular practice performed in near-field radiation measurements which consequence is getting the radiation pattern enhanced.

The deblurring process is in general performed in the frequency and the probe effect is generally removed in the transform domain by simple division with the theoretical near-field pattern of the probe. This is just the same procedure proposed to improve the resolution by means of the hyperacuity paradigm for cooperative systems: a finer scanning first and deblurring afterwards.

2. Radar measurements

In the recent years modern signal encoding techniques have leveraged radar imaging and more accurate systems. SAR (Synthetic Aperture Radar) type radars are a sample of this advance.

But radars in general have to deal with several problems related to the reception of the echoes amid resolution. As mentioned in the introduction of this section, the lack of resolution here can be an issue, since the radar antenna's beam is swept and sampled at a distance of equal beamwidth (3 dB), because otherwise the beams would be overlapped and the information from each direction would be mixed with its neighbours'.

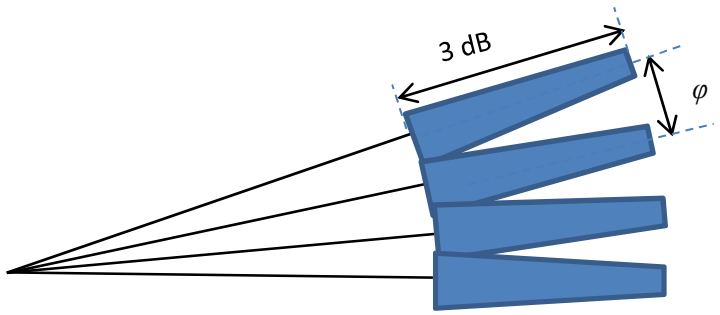

Figure V.14. Radar sweeping at an angle of a beamwidth.

The beam sampling is a typical problem arising from the field or radar. In connection with this, the hyperacuity paradigm could be used to obtain more points than initially captured. Thus, our hyperacuity model could again assist to increase the angular resolution of the area covered by the radar.

Weather forecasts are an application of radars where the detection of masses of water is of special interest. Detection of tornados is a particular challenging issue in these systems where this is often hindered by the rotation and movement of irregular masses. As in all radar systems, resolution is crucial for the detection of any kind of atmospheric anomalies.

Nowadays, when considering the effects of radar sampling, the protocol considered most beneficial is to display views from several radars simultaneously.

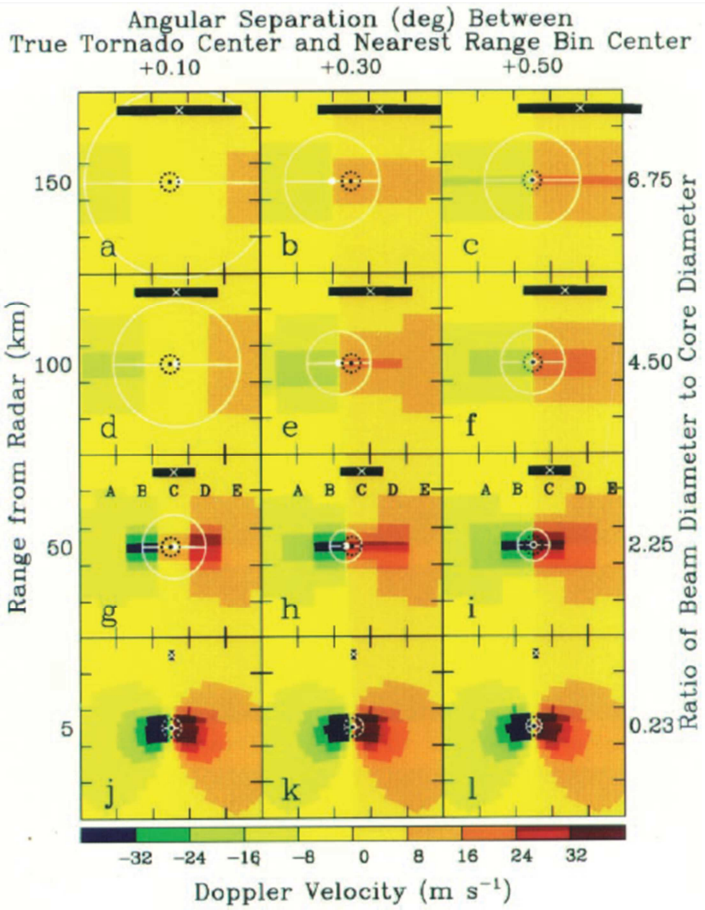

Figure V.15. Plan views of simulated Doppler velocity tornado signatures measured by a radar located at 50, 100, 150 and 200 km from a Rankine combined vortex centre (Wood, Brown 1997)

In this figure, the discrete azimuthal sampling may coincide or not with the peak rotational velocities in the vortex. As a result of that, strength and location of the vortex will seem to vary and often cause circulations to appear weaker than they really are.

The improvement proposed in this case consists in breaking the beam sweeping sampling rule – the 3 dB separation rule – and carry out the sweeping as fine as it is technologically possible, noticing that the result will be blurred by the antenna's radiation diagram.

If the radiation pattern meets a series of conditions such as certain flatness in the main lobe and the power level of secondary lobes stays below a given value, the effect of blur on the image can be reversed. This will ultimately enable to obtain images of much greater angular resolution with relatively wide radiation beams, in other words, with physically smaller groupings.

E. Conclusions

Current trends on electrical engineering show some approaches that resemble mechanisms existing in nature, such as cooperative antenna systems and the lens paradigm, but none of these use diffraction or just some mechanism of spatial diversity to improve resolution. Among the existing constraints, we may find that lack of resolution is the major issue, which is related to the dimensions and distance between the sensing antennas In Microwave-THz imaging systems.

The parallel between the human eye and an imaging device presented in this chapter shows a clear conclusion: the eye performs better and its paradigm is more beneficial.

As we know at this point, the clear advantage of the diffraction paradigm is that information in classic architectures would be received by a single detector that in the hyperacuity model is present in several ones. This may also be understood as spatial diversity which is commonly used to improve the signal to noise ratio of a communication system, which in classic image applications reduces resolution because the image is blurred. This fact increases the robustness of the entire system by making it in some way fault tolerant, something that occurs naturally in the eye.

Radar systems still have to deal with the beamwidth limit. The hyperacuity model could help by providing spatial diversity to the classical radar layout.

Chapter VI. Final comments

A. Contributions

1. Technical contributions

The theory of diffraction enhanced hyperacuity has many implications. We have shown that diffraction is not a limiting factor but in the contrary, is a source of spatial diversity.

We have introduced an unprecedented idea about the human eye's diffraction scheme, the fact that it works as a low-pass filter beyond an anti-aliasing one – with a much lower cut-off frequency–.

In addition, we have provided a novel working model of the hyperacuity by means of diffraction and have defined the technical steps involved: diffraction, sampling, interpolation and inversion.

Besides, although the idea of two dimensional IIR filters is not new, we have developed an uncommon way to solve the inverse by making use of only filter's coefficients and process the data matrix locally instead of the whole ensemble of data. We have additionally proposed the idea of using alternative 2D-IIR filtering equations instead of those followed by the regular expression.

2. Conference publications

[Published]

Dominguez O., Lizarraga J. and Del-Rio-Bocio C. 2011. An approach to explain the human hyper-acuity: Applied to THz imaging. Cyber-enabled distributed computing and knowledge discovery (CyberC), 2011 international conference on. 551 p.

Del-Rio-Bocio C., Crespo G., Lizarraga J. C. and Dominguez O. 2011. Discrete lens for multibeam applications. Microwave conference (EuMC), 2011 41st european. 1011 p.

Dominguez O., Lizarraga Juan C., Teniente Jorge and Del-Rio-Bocio C. 2012. Measurement campaign of the ka-band discrete lens antenna for multibeam applications. Antennas and propagation (EUCAP), 2012 6th european conference on. 2989 p.

Dominguez O. and Del-Rio-Bocio C. 2012. Hyper-acuity through inverse filtering: Application to terahertz cameras. Antennas and propagation (EUCAP), 2012 6th european conference on. 3268 p.

[Accepted]

C. del Río, O. Domínguez, D. Moneo, A. Lagunas. 2015. Applications of Hyperacuity in antenna systems. 36th ESA Antenna Workshop

3. Journal publications

[Submitted for publication]

Dominguez O, Martinez-Conde S, Macknik S.L, Lagunas A, Del-Rio C. 2015. Pupil Diffraction Can Enable Human Hyperacuity. Proceedings of the National Academy of Sciences

Dominguez O, Lagunas A, Del-Rio-Bocio C. 2015. The human eye as a novel paradigm for antenna systems. Antennas and Propagation Magazine

Dominguez O, Lagunas A, Del-Rio-Bocio C. 2015. Localised filtering with 2D-IIR for a hyperacuity model for antenna imaging systems. Radioengineering.

B. Conclusions

Nature has shown amazing engineering solutions to questions often even nowadays unanswered by science. The human eye, as an imaging system might be a clear example of that, as it is in a sense still unbeaten by any artificial device.

The HVS has been studied – especially in the last year – in many ways and forms: from theory to practical dissections, implants and probes, but it is and will still be at least for some time an enigma from the computational point of view due to the complexity of the neural connections involved. Anyway, we believe that the robust and efficient solution existing in the human eye must be simple and it is probably performed in few neural network stages. Following this rule of simplicity, we have carried out several tests which have led to the foundation of our approach to the two dimensional inverse filtering scheme explained.

The inverse problem is maybe the most important challenge related to the hyperacuity model explained in this document. The inverse problem itself constitutes a field of research; the number of different techniques developed by this scientific community is almost endless, but this does not mean our model does not work or does not efficiently work. In fact, the performance of our approach is outstanding but there are still issues which affect the outcome of the process, such as the sensitivity to noise and in some cases the phase. Besides, the interpolation technique can also be itself a topic of deep study, but we have just done a practical overview of different methods of interpolation which will yield best results in our scheme.

On another hand, we have exposed the possibilities hyperacuity may provide to other fields where limited sampling is in particular challenging. The overall picture and conclusion of this technique is that a limited sampling scheme should not necessarily be understood at an extent as resolution limited – as proven by nature – so we could apply the same paradigm to obtain high resolution signals or acuities.

Due to the multidisciplinary nature of this work, we have shown along this document different aspects of our theory of hyperacuity which reporting has sometimes been challenging because of the difficulty to address in proper terms to any of the scientific communities potentially interested or involved in these topics.

C. Future work

After completing the different tasks within this research, we should say that regarding the optimal applicability of our model there is still a way to go.

a) Noise and irregularities at the signal capturing process

Although our hyperacuity model considers a natural noise elimination process by means of diversity, photo-chemical high sensitivity (good SNR) and an optimal sensitivity threshold, a method which could allow eliminating noise should be considered, because any irregularity on an image included the moiré style noise we get with our method, should be removed. The methods proposed in this document are very sensitive to any disturbance of the picture and it is clear that the human visual system is more robust to the possibly existing noise. Therefore, it could be interesting to research a method to simulate this in order to achieve such good results.

Restoration of spatially irregular distortions in the blurred image could be another of the ideas which could be interesting to develop. This problem is related to the real-world problem of irregular, non-linear optics and surfaces, where the distortion is far from being homogeneous and is different at each point or area of an image. This could be tackled by means of a varying IIR two-dimensional inverse filtering technique which would consist in modifying its coefficients in function of the pixel's location on the picture. In other words, we could think of a context or location-aware filter which could inverse-filter/restore with great accuracy the distortion, since as long as the direct filter or distortion is modelled the corresponding non-linear inverse filter could be applied.

b) From realistic procedures to real-world models

Another idea could be the development of techniques based on more realistic practices. One of them could be to capture a blurred image using a pinhole camera. Next, we would proceed to recover the image using Matlab software in a similar manner as done with the tests described in previous chapters. The major difficulty of this method is to exactly model the inverse filter in order to accurately reverse the diffraction produced by the camera lens, as the PSF is not precisely known.

Another line of work could be the development of biological neural networks. This is an approach still at a very early stage in the scientific community due – among other reasons – to the often lack of accurate values and models. The complexity of these neural networks can be extremely high because of the several factors and parameters to take into account, and the additional fact that most part of the neural system itself is still full of unknowns. Nevertheless, ninety-five percent of what is known about the brain has been discovered in the last twenty years which gives an idea of the exponentially increasing progress done on neuroscience, where modern analysis techniques provide data of great value. So this method could be more faithful to the processing performed by the HVS which could be of great interest but we ignore at this time its feasibility.

Non-linear systems could also be an interesting field of study. Even though the hyperacuity model we present is linear, we could think of some non-linear approach

possibly computed with ANN or other methods found in the extensive literature of inverse methods.

Regarding the algorithms that model the human eye there is still a very long way to go. As an example of this is the fact that no eye motion blur was considered in this research.

c) 2D IIR inverse filtering paradigm in the HVS

A novel proposal we present in this research is that the visual system might be performing some kind of equation difference processing in two dimensions. The particular method we suggest is a modification of the explained 2D IIR filtering which we speculate, could be implemented by the eye.

This signal processing ongoing in the visual system would consist in using the output deblurred (inverse filtered signal) in previous frames.

As we saw in chapter III the order imposes that the output will not reach any value making sense until MxN samples have been processed.

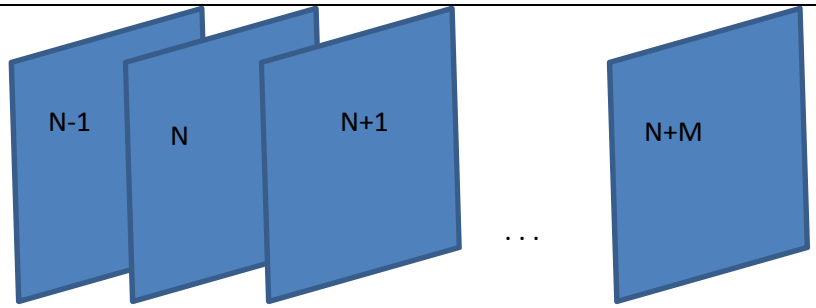

Figure VI.1. Frames allegedly processed by the HVS

Although the fact of capturing the image signal by the photoreceptors in the retina is a discretisation process (such as in digital imaging devices), the information is captured and processed by the HVS continuously. This means that discrete points on a captured image are processed which are discrete only in space, not in time. Therefore the samples change continuously in time and as they are updated the output is updated as well reaching the correct values after some stabilisation time. This is illustrated as an example of discrete frames in the sequence shown above in Figure VI.1.

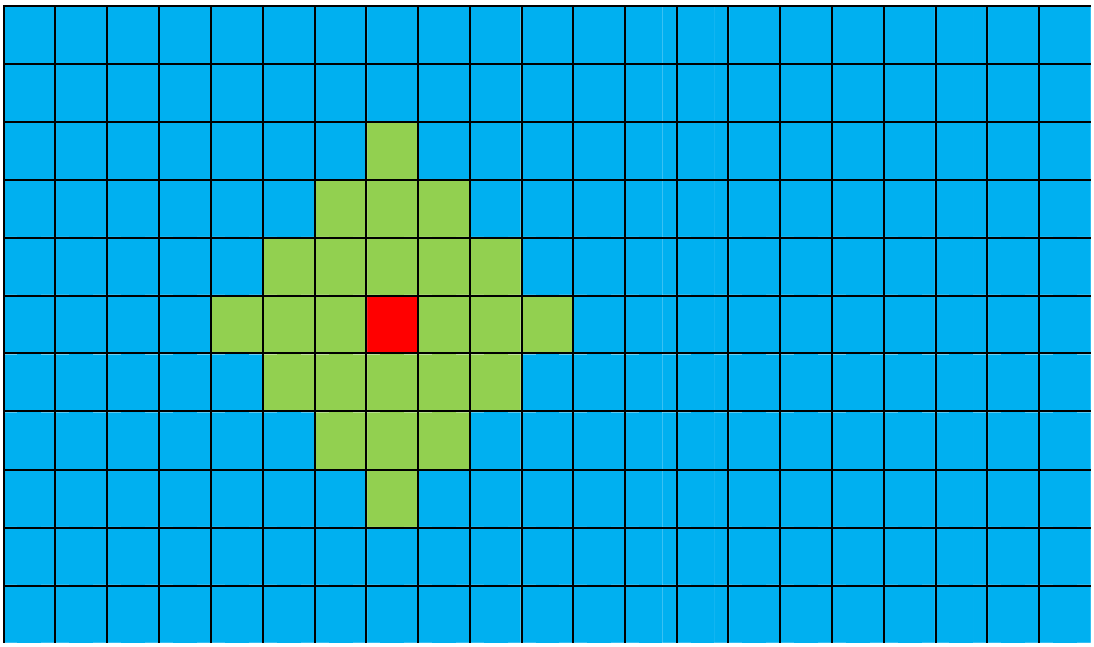

Figure VI.2. Two-dimensional equation difference filtering. Each sample needs MxN previous output samples.

A signal to be filtered by means of difference equations – as already seen in chapter III – needs a given previous (in space) number of samples – let's give MxN – corresponding with the order of the filter. Above is shown how each of the samples (as the one marked in red) could also be processed using the output of its MxN surrounding positions (marked in green and including the red one) matching the pattern of the distortion filter, and thus processing the two-dimensional IIR (Infinite Impulse Response) layout.

We could imagine a similar scheme but combined with samples corresponding with different time frames instead of just in space. Even though this is pure speculation, we may think of a valid value for the output (starting from the zero value) that can be reached as it is calculated after MxN samples have been processed in time. As we say, the HVS does not process samples in a discrete scheme in time, but as we understand, as information is processed by the HVS it will necessarily take a period of time to process the information regarding those samples.

On the other hand, there are some structural problems with the IIR inverse filtering, related to causality. As it arises from (3.68) when calculating the initial values of the estimated signal, previous values of the blurred signal are needed but these, do not exist, so zero values are required, thus, imposing causality restrictions at image boundaries, which can be solved by zero-padding.

The issue of phase, that is to say, filter phase mismatches can be minimised by means of a filter pre-test adjust. In case the phase mismatch was high the result would be a suboptimal deblurred output. As stated earlier, any imprecision with the phase may lead to an unstable system, which can be fixed by readjusting it.

d) Other approaches

Another topic connected to the hyperacuity of the human eye could be the human ear's acoustic FDT (Frequency Discrimination Threshold). Apparently, a similar issue happens

in this organ which could be comparable to the hyperacuity in the eye. The literature reports an FDT that can reach 3% at 100 Hz (in consequence 3 Hz) and 5% at 2 kHz (10 Hz) and it is achieved by approximately 20,000 outer hair cells and 3,500 inner cell hairs. As such, these numbers do not seem so spectacular if it weren't because a frequency spacing of 5 Hz along the audible 20,000 Hz would require a minimum of at least 4,000x2 (8,000) inner cell hairs just to apparently fulfil the requirements of the sampling theorem and be able to discriminate frequencies at that level, which gives an idea of the low number of detectors present in the ear. Thus, we could use our knowledge background to contribute with our progress in other fields of neuroscience.

Following to this work, more ideas and methods will probably emerge but these have been the potential future lines of research that arise from this research.

Index of Abbreviations

ANN
Artificial Neural Networks, 112, 113
CCD
Coupled Charged Device, 38, 41, 136, 145, 152
DF-I
Direct Form I, 116
DF-II
Direct Form II, 116
DFT
Discrete Fourier Transform, 102, 133
FFT
Fast Fourier Transform, 102, 133, 143, 144
FIR
Finite Impulse Response, 117, 118
HVS
Human Visual System, 25, 36, 37, 54, 58, 73, 82, 88, 112, 133, 139, 168, 169
IIR
Infinite Impulse Response, 116, 117, 118, 122
ISO
International Organization for Standardization, 40
LGN
Lateral Geniculate Nucleus, 34, 35, 73, 81
LTI
Linear Time Invariant, 118
MRI
Medical Resonance Imaging, 84, 95, 124
NZV
Near Zero Values, 145, 146
PRE
Pigmented Retinal Epithelium, 29
PSD
Power Spectral Density, 30
PSF
Point Spread Function, 70, 88, 89, 109, 110, 111
PSP
Post-Synaptic Potentials, 36
PU
Processing Unit, 113
RE
Resolution Enhancement, 42
RGB
Red Green Blue, 40, 128
RMS
Root Mean Square, 97, 101
ROC
Region of Convergence, 119
SR

References

AHNELT, P.K., KOLB, H. and PFLUG, R., 1987. Identification of a Subtype of Cone Photoreceptor, Likely to be Blue Sensitive, in the Human Retina. *Journal of Comparative Neurology,* **255**(1), pp. 18-34.

ALVAREZ, D., MONTESANO, A., ZORNOZA, A., MARTÍN-POLEGRE, A., F. DE LA FUENTE, L., ARENAS, S., BUSTAMANTE, M., CAMPUZANO, J., TRASTOY, A.M., HERRERA, I., GONZALEZ, E., MORENO, T., MIQUEL, C. and VILLETE, E., 2011. Hispasat AG1 DRA-ELSA active antenna: RF design and performance, *Proceedings of 33rd ESA Antenna Workshop on Challenges for Space Antenna Systems* 2011.

ALVAREZ, D., PEÑA, D., MONTESANO, A., ZORNOZA, A., RUBIO, A., ACEVEDO, D., LOPEZ-MATEOS, J., F. DE LA FUENTE, L., ARENAS, S., MIQUEL, C. and VILLETE, E., 2011. Hispasat AG1 DRA-ELSA active antenna: thermo-mechanical design and control aspects, *Proceedings of 33rd ESA Antenna Workshop on Challenges for Space Antenna Systems* 2011.

ARSENAUL.H and GENESTAR, B., 1971. Deconvolution of Experimental Data. *Canadian Journal of Physics,* **49**(14), pp. 1865-&.

ASHTARI, A., NOGHANIAN, S., SABOUNI, A., ARONSSON, J., THOMAS, G. and PISTORIUS, S., 2010. Using a priori Information for Regularization in Breast Microwave Image Reconstruction. *Ieee Transactions on Biomedical Engineering,* **57**(9), pp. 2197-2208.

AVERILL, H.L. and WEYMOUTH, F.W., 1925. Visual perception and the retinal mosaic II The influence of eye-movements on the displacement threshold. *Journal of Comparative Psychology,* **5**(2), pp. 147-176.

BARLOW, H.B., 1979. Reconstructing the visual image in space and time. *Nature,* **279**(5710), pp. 189-190.

BARNES, C.W., 1966. Object Restoration in a Diffraction-Limited Imaging System. *Journal of the Optical Society of America,* **56**(5), pp. 575-&.

BENSON, J.B., LUKE, G.P., WRIGHT, C.H.G. and BARRETT, S.F., 2009. *Pre-Blurred Spatial Sampling can Lead to Hyperacuity.*

BETANCOURT, D. and DEL-RIO-BOCIO, C., 2008. Multi-beam applications of CORPS-BFN: Reflector Antenna Feeding System, *30th ESA Antenna Workshop* 2008.

BETANCOURT, D. and DEL-RIO-BOCIO, C., 2007a. A novel methodology to feed phased array antennas. *Ieee Transactions on Antennas and Propagation,* **55**(9), pp. 2489-2494.

BETANCOURT, D. and DEL-RIO-BOCIO, C., 2007b. Using CORPS-BFN to feed Multi-beam antenna systems, *29th ESA Antenna Workshop* 2007b.

BILLE, J.F., HARNER, C.F.H. and LOESEL, F.H., 2004. *Aberration-Free Refractive Surgery: New Frontiers in Vision.* Springer Verlag.

BIRCH, K.G., 1972. Spatial Filtering in Optical Data-Processing. *Reports on Progress in Physics,* **35**(11), pp. 1265-&.

BRACEWELL, R.N. and ROBERTS, J.A., 1954. Aerial Smoothing in Radio Astronomy. *Australian Journal of Physics,* **7**(4), pp. 615-640.

CAMPBELL, F.W. and GREGORY, A.H., 1960. Effect of size of pupil on visual acuity. *Nature,* **187**, pp. 1121-1123.

CAMPBELL, F.W. and GREEN, D.G., 1965. Optical and Retinal Factors Affecting Visual Resolution. *Journal of Physiology-London,* **181**(3), pp. 576-&.

CAMPBELL, F.W. and GUBISCH, R.W., 1966. Optical Quality of Human Eye. *Journal of Physiology-London,* **186**(3), pp. 558-&.

CAMPUZANO, J., MONTESANO, A., F. DE LA FUENTE, L., TRASTOY, A.M., BUSTAMANTE, M. and ÁLVAREZ, D., 2010. EADS CASA Espacio DRA-ELSA Patterns and G/T Predicted Performances, *ESA Conference 2010 - ESA/ESTEC, NOORDWIJK, THE NETHERLANDS* 2010.

CANBAY, C. and UNAL, I., 2008. Electromagnetic Modeling of Retinal Photoreceptors. *Progress in Electromagnetics Research-Pier,* **83**, pp. 353-374.

CARNEY, T. and KLEIN, S., 1997. Resolution acuity is better than vernier acuity. *Vision research,* **37**(5), pp. 525-539.

CARPENTER, R.H.S., 1977. *Movements of the eyes.* London: Pion.

CURCIO, C.A., SLOAN, K.R., PACKER, O., HENDRICKSON, A.E. and KALINA, R.E., 1987. Distribution of Cones in Human and Monkey Retina - Individual Variability and Radial Asymmetry. *Science,* **236**(4801), pp. 579-582.

D'AMICO, N., 2011. The Sardinia Radio Telescope, M. BURGAY, N. D'AMICO, P. ESPOSITO, A. PELLIZZONI and A. POSSENTI , eds. In: *American Institute of Physics Conference Series*, aug 2011, pp. 317-324.

DEMB, J.B., STERLING, P. and FREED, M.A., 2004. How retinal ganglion cells prevent synaptic noise from reaching the spike output. *Journal of neurophysiology,* **92**(4), pp. 2510-2519.

DI FRANCIA, G.T., 1955. Resolving Power and Information. *Journal of the Optical Society of America,* **45**(7), pp. 497-501.

DITCHBURN, R.W., 1980. Function of Small Saccades. *Vision research,* **20**(3), pp. 271-272.

DONNELLY III, W.J. and ROORDA, A., 2003. Optimal pupil size in the human eye for axial resolution. *Journal of the Optical Society of America A,* **20**(11), pp. 2010-2015.

ELIAS, P., GREY, D.S. and ROBINSON, D.Z., 1952. Fourier Treatment of Optical Processes. *J.Opt.Soc.Am.,* **42**(2), pp. 127-132.

ESKICIOGLU, A.M. and FISHER, P.S., 1995. Image quality measures and their performance. *IEEE Transactions on Communications,* **43**(12), pp. 2959-2965.

FINKELSTEIN, M.A. and HOOD, D.C., 1984. Detection and discrimination of small, brief lights: Variable tuning of opponent channels. *Vision research,* **24**(3), pp. 175-181.

GEISLER, W.S., 1984. Physical limits of acuity and hyperacuity. *Journal of the Optical Society of America A (Optics and Image Science),* **1**(7), pp. 775-82.

GELIUS, L. and ASGEDOM, E., 2011. Diffraction-limited imaging and beyond - the concept of super resolution. *Geophysical Prospecting,* **59**(3), pp. 400-421.

GERCHBERG, R.W., 1974. Super-resolution through error energy reduction. *Optica acta,* **21**(9), pp. 709-20.

HADAMARD, J., 1923. *Lectures on Cauchy's problem in linear partial differential equations.* New York; London: Yale university press; H. Milford, Oxford university press.

HANSEN, P.C., 2002. Deconvolution and Regularization with Toeplitz Matrices. *Numerical Algorithms,* **29**(4), pp. 323-378.

HARRIS, J.L., 1964. Diffraction + Resolving Power. *Journal of the Optical Society of America,* **54**(7), pp. 931-&.

HARTRIDGE, H., 1922. Visual acuity and the resolving power of the eye. *Journal of Physiology-London,* **57**(1/2), pp. 52-67.

HECHT, S., 1924. Intensity Discrimination and the Stationary State. *The Journal of general physiology,* **6**(4), pp. 355-373.

HENNIG, M. and WOGOTTER, F., 2004. Eye micro-movements improve stimulus detection beyond the Nyquist limit in the peripheral retina. *Advances in Neural Information Processing Systems 16,* **16**, pp. 1475-1482.

HIRSCH, J. and HYLTON, R., 1982. Limits of spatial-frequency discrimination as evidence of neural interpolation. *JOSA,* **72**(10), pp. 1367-1374.

HIRSCH, J. and HYLTON, R., 1985. Spatial-frequency discrimination at low frequencies: evidence for position quantization by receptive fields. *Journal of the Optical Society of America A (Optics and Image Science),* **2**(2), pp. 128-35.

HRYCAK, P.D., 1982. The theoretical and experimental investigation of a constrained feed totally overlapped subarray antenna system. *1982 APS International Symposium Digest.Antennas and Propagation,* , pp. 695-8 vol.2.

IPSEN, I.C.F. and MEYER, C.D., 1998. The idea behind Krylov methods. *American Mathematical Monthly,* **105**(10), pp. 889-899.

ITU, 2004. *Objective perceptual assessment of video quality: Full reference television.* 2014.

JAMES DREVER, M.C., 1972. *Experimental Psychology.* Methuen.

JANSSON, P.A., 2012; 1979. *Deconvolution of images and spectra.* 1 publ edn. Mineola NY: Dover Publications.

KAMITANI, Y. and SAWAHATA, Y., 2010. Spatial smoothing hurts localization but not information: Pitfalls for brain mappers. *NeuroImage,* **49**(3), pp. 1949-1952.

KARA, P., REINAGEL, P. and REID, R.C., 2000. Low response variability in simultaneously recorded retinal, thalamic, and cortical neurons. *Neuron,* **27**(3), pp. 635-646.

KAUFMAN, P.L., ALM, A. and ADLER, F.H., 2003. *Adler's physiology of the eye.* 10th edn. St. Louis, Missouri: Mosby.

KLEIN, S.A. and LEVI, D.M., 1985. Hyperacuity thresholds of 1 sec: theoretical predictions and empirical validation. *Journal of the Optical Society of America A (Optics and Image Science),* **2**(7), pp. 1170-90.

KO, H., POLETTI, M. and RUCCI, M., 2010. Microsaccades precisely relocate gaze in a high visual acuity task. *Nature neuroscience,* **13**(12), pp. 1549-1553.

KOGAN, L.R., 02/17/2014, , NRAO Website.

KOLB, H., 2/3/2015, Photoreceptors by Helga Kolb – Webvision . Available: http://webvision.med.utah.edu/book/part-ii-anatomy-and-physiology-of-the-retina/photoreceptors/ [2/3/2015, 2015].

KOUDELKA, V., DEL RIO BOCIO, C. and RAIDA, Z., 2013. Diffracted image restoration: A machine learning approach, *Electromagnetics in Advanced Applications (ICEAA), 2013 International Conference on* 2013, pp. 931-934.

KRAMER, M., 2014, May 22, , Effelsberg continuum mapping [Homepage of Max Planck Institute for Radio Astronomy], [Online].

LOUER, D., WEIGEL, D. and LOUBOUTI.R, 1969. A Direct Method of Correction of X-Ray Diffraction Line Profiles .1. Numeric Deconvolution Method. *Acta Crystallographica Section A-Crystal Physics Diffraction Theoretical and General Crystallography,* **A 25**, pp. 335-&.

MAILLOUX, R.J., 1974. Overlapped Subarray for Limited Scan Application. *Ieee Transactions on Antennas and Propagation,* **AP22**(3), pp. 487-489.

MANDOLESI, N., 07/11/2012, , Planck Telescope, ESA.

MARCELINO, N., 01/21/2014, , NRAO ALMA/NAASC Website.

Marcos S. Calidad óptica del ojo. Investigación y ciencia. 2005 JUN 2005;345:66-74.

MARSHALL, W. and TALBOT, S.A., 1942. Recent evidence for neural mechanisms in vision leading to a general theory of sensory acuity. .

MARTENS, J.B. and MEESTERS, L., 1998. Image dissimilarity. *Signal Processing,* **70**(3), pp. 155-176.

MARTINEZ-CONDE, S., MACKNIK, S.L. and HUBEL, D.H., 2004. The role of fixational eye movements in visual perception. *Nature reviews. Neuroscience,* **5**(3), pp. 229-240.

MARTINEZ-CONDE, S., MACKNIK, S.L. and HUBEL, D.H., 2000. Microsaccadic eye movements and firing of single cells in the striate cortex of macaque monkeys. *Nature neuroscience,* **3**(3), pp. 251-258.

MCLELLAN, J.S., MARCOS, S., PRIETO, P.M. and BURNS, S.A., 2002. Imperfect optics may be the eye's defence against chromatic blur. *Nature,* **417**(6885), pp. 174-176.

MOJABI, P. and LOVETRI, J., 2009. Enhancement of the Krylov Subspace Regularization for Microwave Biomedical Imaging. *IEEE Transactions on Medical Imaging,* **28**(12), pp. 2015-2019.

MOLLER, F., LAURSEN, M.L., TYGESEN, J. and SJOLIE, A.K., 2002. Binocular quantification and characterization of microsaccades. *Graefe's archive for clinical and experimental ophthalmology = Albrecht von Graefes Archiv fur klinische und experimentelle Ophthalmologie,* **240**(9), pp. 765-770.

MONTESANO, A., DE LA FUENTE, L.F., BUSTAMANTE, M., ALVAREZ, D., CAMPUZANO, J., TRASTOY, A.M. and ARENAS, S., 2012. EADS CASA Espacio RX DRA: IRMA heritage in X band and ELSA development in KU band, *Antenna Technology and Applied Electromagnetics (ANTEM), 2012 15th International Symposium on* 2012, pp. 1-9.

O'CONNOR, V., May 27, 2014, , Europe's first High Throughput Satellite.

ØSTERBERG, G., 1935. *Topography of the layer of rods and cones in the human retina.* Levin & Munksgaard.

PAPOULIS, A., 1975. New Algorithm in Spectral Analysis and Band-Limited Extrapolation. *Ieee Transactions on Circuits and Systems,* **22**(9), pp. 735-742.

PITKOW, X., SOMPOLINSKY, H. and MEISTER, M., 2007. A neural computation for visual acuity in the presence of eye movements. *Plos Biology,* **5**(12), pp. 2898-2911.

RATLIFF, F. and RIGGS, L.A., 1950. Involuntary Motions of the Eye during Monocular Fixation. *Journal of experimental psychology,* **40**(6), pp. 687-701.

RIGGS, L.A. and RATLIFF, F., 1951. Visual Acuity and the Normal Tremor of the Eyes. *Science,* **114**(2949), pp. 17-18.

RIGGS, L.A., RATLIFF, F., CORNSWEET, J.C. and CORNSWEET, T.N., 1953. The Disappearance of Steadily Fixated Visual Test Objects. *Journal of the Optical Society of America,* **43**(6), pp. 495-501.

ROBERTS, N.W., 2006. The optics of vertebrate photoreceptors: Anisotropy and form birefringence. *Vision research,* **46**(19), pp. 3259-3266.

RUBAEK, T., MEANEY, P.M., MEINCKE, P. and PAULSEN, K.D., 2007. Nonlinear microwave imaging for breast-cancer screening using Gauss-Newton's method and the CGLS inversion algorithm. *Ieee Transactions on Antennas and Propagation,* **55**(8), pp. 2320-2331.

RUCCI, M., IOVIN, R., POLETTI, M. and SANTINI, F., 2007. Miniature eye movements enhance fine spatial detail. *Nature,* **447**(7146), pp. 852-855.

SCHNEIDER, M., HARTWANGER, C., SOMMER, E. and WOLF, H., 2009. The multiple spot beam antenna project "Medusa", *Antennas and Propagation, 2009. EuCAP 2009. 3rd European Conference on* 2009, pp. 726-729.

SCHOBER, H., 1938. New inquests on the acuity and the resolution of optical instruments, particularly of the human eye. *Physikalische Zeitschrift,* **39**, pp. 934-936.

SCHULZ, J.M., REDGRAVE, P. and REYNOLDS, J.N.J., 2010. Cortico-striatal spike-timing dependent plasticity after activation of subcortical pathways. *Frontiers in Synaptic Neuroscience,* **2**(23),.

SNOEIJ, P., ATTEMA, E., PIETROPAOLO, A., MASTRODDI, V., L'ABBATE, M. and BRUNO, C., 2009. *Analysis of Sentinel-1 Mission Capabilities.*

SOUTHALL, H.L. and MCGRATH, D.T., 1986. An Experimental Completely Overlapped Subarray Antenna. *Ieee Transactions on Antennas and Propagation,* **34**(4), pp. 465-474.

SPAUSCHUS, A., MARSDEN, J., HALLIDAY, D.M., ROSENBERG, J.R. and BROWN, P., 1999. The origin of ocular microtremor in man. *Experimental Brain Research,* **126**(4), pp. 556-562.

STEVENS, J.K., EMERSON, R.C., GERSTEIN, G.L., KALLOS, T., NEUFELD, G.R., NICHOLS, C.W. and ROSENQUIST, A.C., 1976. Paralysis of the awake human: visual perceptions. *Vision research,* **16**(1), pp. 93-98.

WEI, L., 2004. A theory on constructing a hyper-acuity electronic device. *Electronics Letters,* **40**(23), pp. 1464-1466.

WESTHEIMER, G. and MCKEE, S.P., 1977. Spatial Configurations for Visual Hyperacuity. *Vision research,* **17**(8), pp. 941-947.

WESTHEIMER, G., 2009. Ch4. Visual Acuity and Hyperacuity. In: M. BASS, J.M. ENOCH, C. DECUSATIS, V. LAKSHMINARAYANAN, V.N. MAHAJAN, G. LI, E. VAN STRYLAND and C. MACDONALD, eds, *Handbook of Optics: Vision and vision optics.* McGraw-Hill, .

WESTHEIMER, G., 1976. Diffraction Theory and Visual Hyper-Acuity. *American Journal of Optometry and Physiological Optics,* **53**(7), pp. 362-364.

WHITHAM, E.M., FITZGIBBON, S.P., LEWIS, T.W., POPE, K.J., DELOSANGELES, D., CLARK, C.R., LILLIE, P., HARDY, A., GANDEVIA, S.C. and WILLOUGHBY, J.O., 2011. Visual Experiences during Paralysis. *Frontiers in human neuroscience,* **5**, pp. 160.

WOOD, V.T. and BROWN, R.A., 1997. Effects of Radar Sampling on Single-Doppler Velocity Signatures of Mesocyclones and Tornadoes. *Weather and Forecasting,* **12**(4), pp. 928-938.

YARBUS, A.L., 1967. *Eye movements and vision.* Plenum Press.

ZHANG, Z.Q. and LIU, Q.H., 2004. Three-dimensional nonlinear image reconstruction for microwave biomedical Imaging. *Ieee Transactions on Biomedical Engineering,* **51**(3), pp. 544-548.

ZHOU WANG, BOVIK, A.C. and LIGANG LU, 2002. Why is image quality assessment so difficult? *Acoustics, Speech, and Signal Processing (ICASSP), 2002 IEEE International Conference on* 2002, pp. IV-3313-IV-3316.

ZOZOR, S., AMBLARD, P. and DUCHENE, C., 2009. Does eye tremor provide the hyperacuity phenomenon? *Journal of Statistical Mechanics-Theory and Experiment,* , pp. P01015.